Magnetostriction of superconductors (a review)

V. V. Eremenko and V. A. Sirenko

*B. Verkin Institute for Low Temperature Physics and Engineering, National Academy of Sciences of the Ukraine, 310164 Kharkov, Ukraine**

H. Szymczak and A. Nabialek

*Institute of Physics, Polish Academy of Sciences, 02-668 Warsaw, Poland***

(Submitted September 27, 1998; revised December 12, 1998)
Fiz. Nizk. Temp. **25**, 311–332 (April 1999)

The results of magnetostriction studies of different superconducting compounds made during the last several years are presented. Special attention is paid to giant magnetostriction and ''superconducting background'' against which it emerges. The results are compared with the traditional magnetostriction components in magnetic materials. Possibilities of using magnetostriction measurements for analysis of the mixed state in hard superconductors and practical applications of the results of such measurements are considered. © *1999 American Institute of Physics.* [S1063-777X(99)00104-8]

INTRODUCTION

The phenomenon of magnetostriction (MS) consists in the deformation of a solid during magnetization. Experimentally, MS has been studied mainly in materials with ferro- and antiferromagnetic ordering. In strongly magnetic materials, MS attains values $\Delta L/L \sim 10^{-5}-10^{-2}$. A quite comprehensive phenomenological description has been developed for such materials. In diamagnetic and paramagnetic materials, the values of MS vary between 10^{-7} and 10^{-5}.

The striction of superconductors (SC) in a magnetic field ($\Delta L/L \sim 10^{-8}$) was first measured in Kharkov in 1940's.[1] Subsequent studies were undertaken by several groups of experimenters in different countries possessing adequate experimental facilities for measuring elastic deformations at low temperatures under the action of a magnetic field (see the review by Brändli[2] and the literature cited therein). These groups mainly employed highly sensitive dilatometric technique using the optical lever (Kerr cell) and the capacitive cell method. Their studies culminated in the review article by Brändli[2] and a description in terms of the Ginzburg–Landau expansion.[3] In spite of the unambiguous interpretations of nature of the striction of metallic SC, uncertainties appeared in terminology, and stimulated discussions concerning the possible use of the magnetic terminology for SC. This is due to the differences in the nature of striction in magnets and in SC in a magnetic field, associated with the peculiar features of their magnetization. A characteristic feature of magnets undergoing second-order phase transition to the magnetically ordered state is the spontaneous magnetization which is their vector order parameter, while the magnetic permeability may attain values equalling several thousands. For SC in the Meissner state, the magnetic permeability is equal to zero while the order parameter is a scalar (but complex wave function) connected with the concentration of electrons which combine to form Cooper pairs.

The interest in striction was revived by the discovery of nontraditional SC containing magnetic ions, especially high-temperature superconductors (HTSC) which provided the most interesting results associated with values of MS ($\sim 10^{-4}$) that are enormous for SC. Hence to analyze the problem concerning the modern state of striction of superconductors, it is expedient to separate the superconducting subsystem and its characteristic elastic response to the magnetic field from the specific magnetocrystalline background against which it is formed. Hence, in spite of the fact that the striction of superconductors and magnets is identical in most respects and the term ''magnetostriction of superconductors'' has become conventional in the description of these phenomena, we shall use the term ''suprastriction''[3] to discuss the elastic response of the superconducting system to the applied magnetic field. The presence of magnetic ions presumes the contribution from the traditional MS. Since the magnetic ions (atoms) are in the paramagnetic state under conditions corresponding to the superconductivity of these compounds, their contribution to the total MS will be called parastriction (PS), and the striction observed in the general case will be termed as magnetostriction.

1. MAGNETOSTRICTION COMPONENTS

Magnetostriction is the reaction of a magnetic material to the change in its free energy associated with magnetization in accordance with the thermodynamic relation

$$\frac{1}{V}\left(\frac{\partial V}{\partial \mathbf{H}}\right)_{P,T} = -\left(\frac{\partial \mathbf{M}}{\partial P}\right)_{\mathbf{H},T}, \tag{1}$$

where $\mathbf{M}$ is the magnetization, P the pressure, $\mathbf{H}$ the external magnetic field, T the temperature, and V the volume. Assuming that the magnetization has a linear dependence on the magnetic field, i.e., $M=\chi H$, where χ is the magnetic susceptibility, we can present Eq. (1) in the form

$$\left(\frac{\delta V}{V}\right)_{P,T} = -\frac{1}{2}\left(\frac{\partial \chi}{\partial P}\right)_T H^2. \quad (2)$$

Depending on the sign of the derivative on the right-hand side of this equation, MS may be positive or negative.

In magnetism, one encounters bulk MS and linear MS. Bulk MS is the result of exchange interaction and contributes towards spontaneous MS caused by spontaneous magnetization of the sample in the vicinity of the disorder–order type second-order phase transition temperature as the sample is cooled to the Curie temperature T_C. Such a transition also takes place in zero magnetic field and is predominantly isotropic since the exchange energy depends only on the magnitude M of magnetization[4] although the exchange integral may have different values in different directions. Linear MS is associated with a change in the shape without a change in the volume. It is determined by relativistic magnetic interactions (magnetic anisotropy energy) and is anisotropic in nature. The anisotropy is inherent in *induced* MS associated with a change in the value of **M** for the sample in the magnetically ordered state upon a change in **H**. In the general case, MS is the strain tensor u_{ik} obtained by differentiating the Gibbs thermodynamic potential $\Phi(T,P,\mathbf{M})$ containing magnetoelastic terms that depend on the elastic stress tensor σ_{ik} and on the direction of **M**, with respect to the components of σ_{ik}:[4]

$$u_{ik} = -\frac{\partial \Phi}{\partial \sigma_{ik}}. \quad (3)$$

The ratio of contributions from bulk and linear MS to spontaneous and induced MS of a magnet is determined by the ratio of the exchange energies to the magnetic spin–spin and orbital (spin–orbit, orbit–crystal field) interactions.

In low-symmetry crystal structures containing paramagnetic ions of elements with incomplete electron shells, anisotropic magnetic interactions may make a dominant contribution to the magnetoelastic properties. This is due to the fact that low-lying electrons do not play an active role in exchange processes and may control structural rearrangements during spontaneous magnetization. For low anisotropy energies, this leads to astonishingly large values of MS (10^{-2} for some actinides). The contribution to MS from such ions, including rare-earth (RE) ions and actinides, may be significant in new superconducting compounds with large thermodynamic characteristics, i.e., HTSC and heavy-fermion SC. In HTSC compounds, such ions are in the low-symmetry oxygen environment which should facilitate the emergence of MS effects associated with quadrupole interactions of $4f$ electrons.

The participation of *d*-electrons from the Jahn–Teller copper ion in the processes of pairing in HTSC is an important topic of discussion. Investigation of spontaneous MS by structure-sensitive methods may provide valuable information for such an analysis.

In addition, it should be mentioned that electron paramagnetism with high critical parameters is observed in strong magnetic fields.[5] Spontaneous paramagnetic component of magnetization was also detected in the Meissner state of granular HTSC.[6,7]

The theory of MS of paramagnetic ions was developed for magnets with different types of magnetic ordering, i.e., ferromagnets (FM), ferrites, and antiferromagnets (AFM).[8,9] To analyze the results of measurements of MS in new SC, we made use of the conclusions drawn for AFM since they include rare-earths, and antiferromagnetic ordering in them is the only type of long-range magnetic ordering compatible with superconductivity. We shall discuss this case by considering the example of heavy-fermion superconductors. The MS of rare-earth ions in HTSC will be analyzed in the paramagnetic limit.

The Jahn-Teller effects were studied by measuring the magnetization and thermal expansion in the region of second-order phase transitions in superconducting and manganese perovskites. A number of common features were observed for these materials.[10,11]

The irreversibility of MS is another striking resemblance between antiferromagnets and SC. The irreversibility of MS in magnets is observed in the region of fields corresponding to the displacement of domain walls. Identical features of the magnetic structures of AFM and SC were detected and discussed by Dudko *et al.*[12,13]

In the light of the above analogies, it should be quite interesting to compare the strictional properties of superconducting compounds of transition elements. The use of concepts developed for the MS of paramagnetic ions seems to be quite promising.

2. SUPRASTRICTION

The superconducting transition is a second-order phase transition, and hence the bulk variations accompanying this transition can be associated with spontaneous striction as in ferromagnetic transition.[3] The striction associated with the variation in the magnetic field from zero to the critical value below the superconducting transition temperature is induced; it is determined by the magnetic field pressure on the SC, and contains components associated with the penetration of the magnetic field into the sample.

2.1. Spontaneous suprastriction and peculiarities of thermal expansion coefficients during *NS*-transition

A change in the volume during NS-transition in a magnetic field was first observed by Lazarev and Sudovtsov[1] in type I superconductors. The temperature dependence of this ΔV-effect was studied by White,[14] Andres *et al.*,[15] and Rohrer,[16] while the magnetic field dependence was studied by Brändli *et al.*[2,17] For a thermodynamic (TD) analysis of spontaneous suprastriction, we introduce volume $V_S(H_e)$ as a variable below T_{SN}, and V_N as the volume in the normal (N) state. The *NS*-transition is accompanied by a decrease in the free energy of the superconductor by an amount equal to the condensation energy. Considering that the magnetic field decreases the condensation energy, the condensation energy for the *NS*-transition in a magnetic field can be presented for all values of the magnetic field $H_e \leqslant H_c$ in the form

$$F_S(H_e) - F_S(0) = \frac{V_S}{8\pi} H_c^2. \quad (4)$$

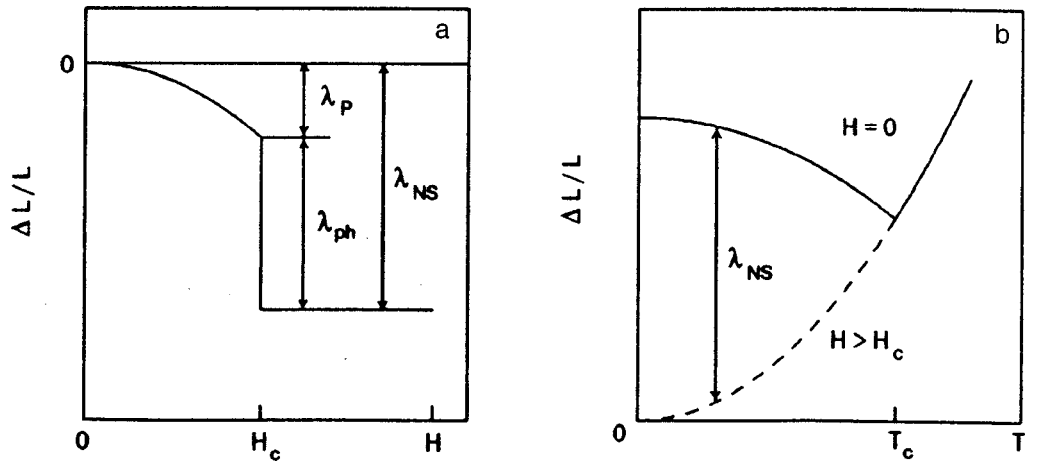

FIG. 1. Suprastriction components: induced by magnetic field (a) and spontaneous (b).

Using the TD relation

$$V=\left(\frac{\partial\Phi}{\partial P}\right)_{T,H}, \tag{5}$$

we obtain (see, for example, Ref. 18)

$$V_N-V_S(0)=V_S\frac{H_c}{4\pi}\left(\frac{\partial H_c}{\partial P}\right)_T+\frac{H_c^2}{8\pi}\left(\frac{\partial V_S}{\partial P}\right)_T. \tag{6}$$

The change in the linear dimension along the crystallographic direction i can be presented in the form

$$l_{Ni}-l_{Si}(0)=l_{Si}\frac{H_c}{4\pi}\left(\frac{\partial H_c}{\partial\sigma_i}\right)_T+\frac{H_c^2}{8\pi}\left(\frac{\partial l_{Si}}{\partial\sigma_i}\right)_T, \tag{7}$$

where σ_i is the uniaxial stress in the direction i.

Taking the relation $\partial M/\partial H=\chi$ into account, we obtain the ''thermodynamic'' components of suprastriction (disregarding the field penetration into the sample) which are determined by the magnetic field pressure on the SC in the Meissner state and by the pressure dependence of the condensation energy (direct spontaneous phase suprastriction) λ_P and $\lambda_{\rm ph}$, respectively:

$$\left(\frac{\Delta L}{L}\right)_{NS}=\lambda_{NS}=\lambda_P+\lambda_{\rm ph}. \tag{8}$$

For SC based on metals and their alloys, $\lambda_{NS}\sim10^{-7}-10^{-6}$.

Spontaneous suprastriction can be analyzed by the Ginzburg–Landau phenomenological theory taking into account the dependence of the energy expansion parameters on elastic strains u_{ij} of the medium. This deformation dependence is associated with the changes in the density of electron states in the vicinity of the Fermi surface, phonon spectrum, and electron–phonon interaction.[3]

Size effects in the vicinity of T_{SN} can be determined experimentally by dilatometric measurements below T_{SN} in zero field, in a field exceeding the upper critical field and by removing the applied field, as well as from measurements of temperature dependences in the region of the transition temperature (Fig. 1). These measurements can be used to determine the pressure derivatives of the thermodynamic critical field and temperature of superconducting transition, which are required for studying spontaneous suprastriction. The analysis is based on the Ehrenfest relation for second-order phase transitions:

$$\frac{d\ln T_c}{dP}=\frac{\Delta B(T_c)}{\Delta C_P(T_c)}, \tag{9}$$

where C_P is the heat capacity at constant pressure, and β the volume coefficient of thermal expansion (CTE). Testardi[19] generalized the results of such investigations for $A15$ compounds.

The above relations can be transformed for estimating the TD contribution to MS from the results of measurements of thermal and physical characteristics. For the first term in Eq. (6), we obtain[20]

$$V_S\frac{H_c}{4\pi}\left(\frac{\partial H_c}{\partial P}\right)_T\simeq\frac{V_S}{T_{SN}}\frac{H_c^2}{4\pi}3\alpha(T)\frac{T}{\Delta C_P(T)},$$

where α is the linear coefficient of thermal expansion, and $\Delta C_P(T)$ is the change in heat capacity during *NS*-transition. The second term in Eq. (6) has the form

$$\frac{H_c^2}{8\pi}\left(\frac{\partial V_S}{\partial P}\right)_T\simeq V_S\frac{H_c^2}{8\pi}\frac{3}{E}.$$

In this case, we have

$$\frac{\Delta V}{V_S}=3\frac{\Delta L}{L}\simeq3\frac{H_c^2}{8\pi}\left(\frac{2\alpha}{C_V}\frac{T}{T_{SN}}-\frac{1}{E}\right).$$

The TD analysis of the data on thermal expansion of superconductors near T_{SN} is based on the relations for free energy F in the N and S-states taking into account its dependence on deformation.[21–23] Interesting results are obtained in this case. For example, a change in T in the compound $A15$ leads to a jump in the deformation near T_{SN} which compensates considerably for the deformation increase associated with structural transformation. In other words, the emergence of superconductivity retards further evolution of structural transformation at T_{SN}.

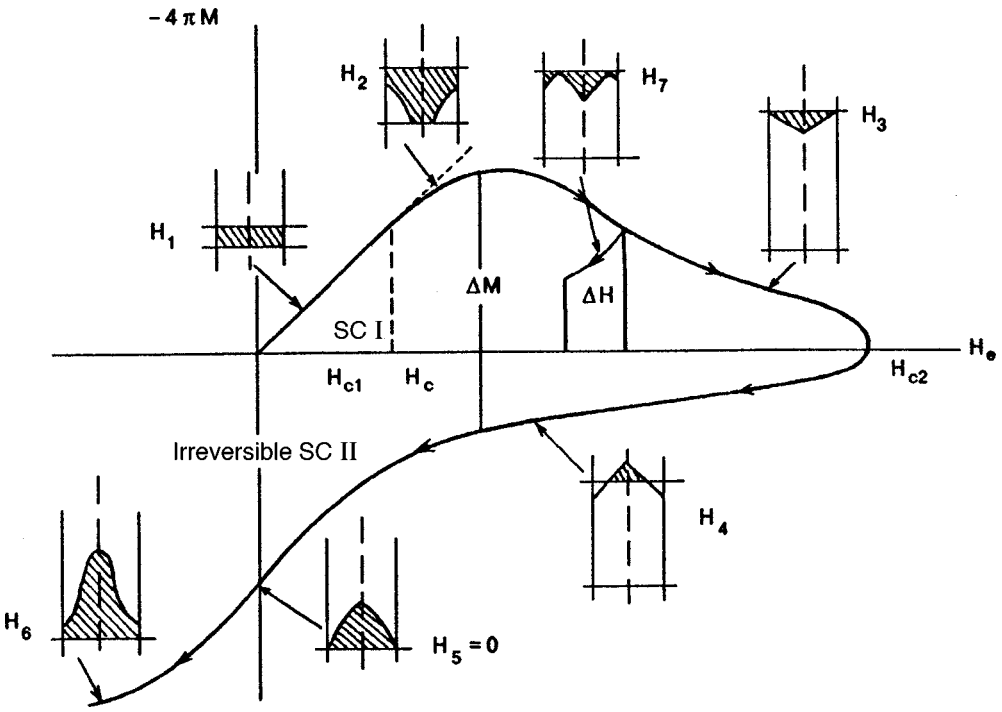

FIG. 2. Magnetization curves for an infinitely long type I superconductor plate and irreversible type II superconductor. The insets show schematically the distribution of the magnetic flux density in the irreversible type II superconductor with increasing and decreasing magnetic field oriented along the long axis of the plate.

2.2. Induced suprastriction

The effect of the magnetic field on the size of a superconductor at temperatures below T_{SN} is associated with the pressure of the magnetic field. We shall consider below the relations determining the magnitude of induced suprastriction in field intervals corresponding to complete expulsion of magnetic flux from the SC (Meissner state), as well as upon partial penetration of the magnetic field into the sample due to demagnetization effects and in the mixed state of type II superconductors. Induced suprastriction of type I superconductors is considered in detail in Ref. 2.

2.2.1. Magnetic field pressure

In order to derive the relations for SC in the Meissner state (magnetic induction $\mathbf{B}=0$ inside the SC), we consider a bulk SC and disregard in the initial approximation the penetration of magnetic field even in a thin layer near the surface.[4] The normal component of induction at the boundary between any two media must be continuous on account of the relation $\mathrm{div}\,\mathbf{B}=0$ which is always true. Since $\mathbf{B}=0$ inside the SC, the normal component of the external field at its surface must also be equal to zero, i.e., the field outside an SC is always directed along the tangent to its surface, and the magnetic field lines envelope the superconductor.[4] Taking this circumstance into consideration, we can easily determine the forces acting on the SC in a magnetic field. The force per square centimeter of the surface is defined as $\sigma_{ik}n_k$, where

$$\sigma_{ik}=\frac{2H_iH_k-\delta_{ik}H^2}{8\pi} \tag{10}$$

is the Maxwell stress tensor for magnetic field in vacuum. Since $nH_e=0$ in this case ($\mathbf{H}_e$ is the field at the surface of the body from outside), we obtain

$$\mathbf{F}_P=-\mathbf{n}\frac{H_e^2}{8\pi}, \tag{11}$$

i.e., the surface of the body is subjected to a compressive force whose magnitude is equal to the energy density of the field. This pressure determines the induced component of spontaneous suprastriction λ_P considered in Sec. 2.1 from TD point of view. Penetration of the field into SC means that we must consider both components in Eq. (10) determining the additional components of the induced suprastriction.

2.2.2. Penetration of magnetic field in a superconductor

Peculiarities of Magnetization of SC. Correlation of strictional and magnetic properties of SC indicates that magnetization peculiarities of SC must be considered in detail for a better understanding of the nature of striction in SC. When cooled to the superconducting transition temperature in zero magnetic field, all SC undergo a second-order phase transition. As the magnetic field is increased, the process of magnetization below T_{SN} occurs in different ways in type I and type II superconductors (Fig. 2). The colored insert shows the distribution of magnetic induction and the modulus of induction gradient, obtained by computer image processing and corresponding to the trapping of magnetic flux. These two types of SC have different ratios of the main parameters of the SC state defined by the electron mean free path, viz., the penetration depth of the external magnetic field into the superconductor in the Meissner state (λ) and the Cooper pair coherence length (ξ). The ratio $\lambda/\xi=\varkappa$ is called the Ginzburg–Landau parameter ($\varkappa<1/\sqrt{2}$ corresponds to type I superconductivity and $\varkappa>1/\sqrt{2}$ to type II superconductivity). The parameter $\varkappa$ determines the relation between the upper critical field H_{c2} of a type II SC and its thermodynamic critical field H_c ($H_{c2}=\sqrt{2}\varkappa H_c$). The quantities H_c and $\varkappa$

TABLE I. Energies of elementary elastic interactions of flux lines with crystal lattice defects (according to Freyhardt[24]).

Defect	Defect parameters	Elastic interactions	
		I kind	II kind
Edge dislocation ∥ FL	b_0-Burger's vector	$(\Delta V/V)\xi\mu\mathbf{b}_0\mathbf{c}$ per unit length	[3]
Screw dislocation ⊥ FL	ΔC_{44} during *NS* transition	No contribution, β—parameter in GL expansion	$(1/4)\Delta C_{44}\xi(\mu\beta)^2$
Precipitation of Phase II	R—radius, δ_0—nonconformity parameter	$16\pi(\Delta V/V)\mu R^3\delta_0$, $R\leqslant\xi$	$4\pi\Delta S_{44}(\mu\delta_0)^2$, $R\cong\xi$
Pores	R—radius, γ_{eff}—surface tension, δR variation of R, $\Delta\mu$—variation of μ during *NS* transition, $V=4/3\pi R^3$	$16\pi(\Delta V/V)\mu R^3\delta R$, $R\ll\xi$	$2\pi\gamma_{\text{eff}}^2 R/\mu^2\Delta\mu$, $R<\xi$

have a fundamental physical meaning since they determine the sign of the energy δ of the interface between the normal and superconducting phases of SC, and hence the peculiarities of their magnetization.

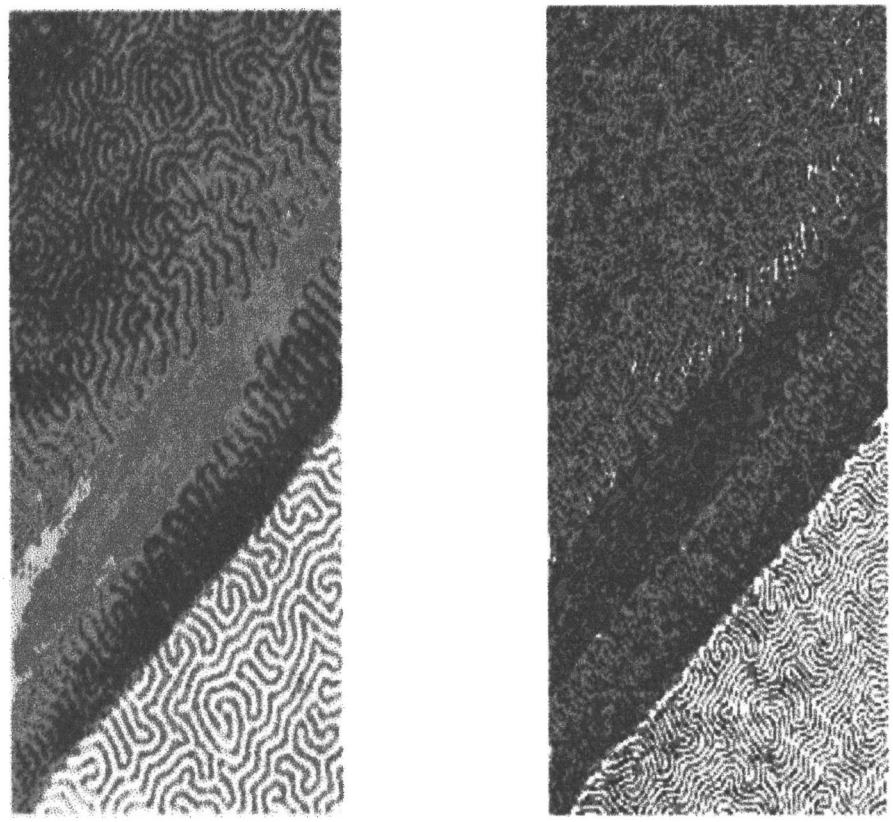

Distribution of magnetic induction, T

Distribution of the modules of the induction gradient, mT/m

In type I superconductors, $\delta>0$ and hence an intermediate state corresponding to the minimum total area of plane Landau domain type boundaries emerges in a magnetic field. In type II superconductors, a mixed state is formed with normal regions of cylindrical geometry (magnetic flux lines). Such a situation is analogous to the behavior of antiferromagnets with positive[12] and negative[13] energies of grain boundaries in a magnetic field. The analogy becomes even closer for highly correlated layered HTSC in which ξ is of the order of atomic spacing. For $\varkappa<1/\sqrt{2}$, the emergence of normal regions is associated with the sample geometry or, to be more precise, with demagnetization effects. The induced suprastriction associated with it was studied in detail by Brändli.[2] In the case $\varkappa>1/\sqrt{2}$, the suprastriction is induced by the interaction of surface currents at the interface with the magnetic field and was also studied in detail by Brändli.[2] To analyze the case of irreversible type II superconductors, we must consider the interaction of the magnetic structure of SC with crystal lattice defects.

Interaction of Magnetic and Defect Structures in SC. The fact that the characteristic size of normal regions in the mixed state of type II superconductors is comparable with the size of crystal lattice defects suggests that the magnetic and defect structures might interact with each other. The forces of interaction of magnetic flux with inhomogeneities of the crystal structure are called pinning forces. These forces are due to the difference in elastic and SC characteristics of the defect and the crystal lattice matrix, which creates conditions for energetically advantageous spatial arrangement of normal regions carrying the magnetic flux.

Elastic interaction is associated with the fact that elastic constants of a material have higher values in the normal state as a rule. For low-temperature metallic SC, the relative variation in volume is $\Delta V/V\simeq 10^{-7}$, while the corresponding variation in the tensor of elastic moduli $\Delta C_{ik}/C_{ik}\sim 10^{-5}-10^{-4}$. Table I shows the parameters of elastic interactions of flux lines (FL) with different types of defects.[24]

The interaction mechanism associated with the difference in the SC characteristics of the defect and the matrix is determined by the size of the defect. The change in the SC parameters at the defect core having a size of the order of ξ leads to a local variation of the condensation energy $H_c^2/8\pi$ in this region, which determines the energetically advantageous position for magnetic flux lines and leads to core interaction. For defects whose size exceeds λ, the equilibrium value of induction may differ from its value in the matrix. This leads to the emergence of a barrier obstructing the motion of magnetic flux across the phase boundary (magnetic interaction). Grain boundaries and twins as well as walls of dislocation cells can be treated as such interfaces.

Many peculiarities of interaction between the magnetic and defect structures of HTSC are connected with the small values and a strong anisotropy of ξ.

Let us consider in detail the interactions in a system of magnetic flux lines and crystal lattice inhomogeneities since the latest data point towards their dominating role in the induced suprastriction of irreversible superconductors. Singularities of magnetic structure in the mixed state of type II superconductors determine the local field distribution $\mathbf{h}(\mathbf{r})$ in the sample. Spatial averaging of $\mathbf{h}(\mathbf{r})$ leads to the magnetic induction $\mathbf{B}$ which is associated with the external magnetic field $\mathbf{H}_e$ through the simple relation

$$\mathbf{B}=\mathbf{H}_e+4\pi\mathbf{M}. \tag{12}$$

The interaction of magnetic flux lines with the crystal lattice obstructs their movement in the sample. Hence a gradient of B from the surface to the inner region of the SC appears in an increasing magnetic field. The situation is reversed in a decreasing magnetic field. To prevent the demagnetization effects, the interaction of magnetic flux with crystal lattice defects is considered in the geometry of an infinitely long cylindrical SC in an external magnetic field in the direction of the long axis z of the cylinder. In the state of thermodynamic equilibrium, the density of flux lines (FL) is the same at all points of the sample and is equal to $B(H)/\Phi_0$, where Φ_0 is the magnetic flux quantum. In the metastable case, when the induction B varies from point to point, e.g., along the z-axis, the density of FL is not constant in space, and a microscopic current of density

$$j=\frac{c}{4\pi}\frac{\partial B}{\partial x} \tag{13}$$

flows along the y-axis. The forces acting in the system of FL can be divided into two groups. Under the action of the repulsive forces between FL, regions with higher FL density (higher values of B) tend to expand at the expense of regions with a lower FL density. This effect is described by introducing the pressure P in the two-dimensional FL system, disregarding the tensor properties of the quantity P. In this case, the force acting per unit volume is equal to $-\partial P/\partial x$. On the other hand, the motion of FL is obstructed by their pinning at structural defects. The pinning force cannot assume large values indefinitely, and is restricted to a certain threshold value f_p. The necessary condition for mechanical equilibrium is the inequality

$$\left|\frac{\partial P}{\partial x}\right|\leqslant f_p. \tag{14}$$

If $|\partial P/\partial x|>f_p$ at a certain point of the sample, the movement of FL begins, and is accompanied by energy dissipation which continues until condition (14) is satisfied once again. In real situation, the density of FL automatically acquires a value $B(x)/\Phi_0$ for which the threshold condition [the sign of equality in (14)] is satisfied at all points of the sample. Such a SC state was first considered by Bean[25] and was called the *critical state*. In this case, transformation of (14) leads to the following equation for the critical state:

$$\left|\frac{B}{4\pi}\frac{\partial B}{\partial x}\right|=\left|\frac{Bj_y}{c}\right|=f_p \quad \text{for} \quad H\gg H_{c1}. \tag{15}$$

In the general form, this equation can be written in terms of the average pinning force $\mathbf{p}_v$:

$$\mathbf{B}\times\mathrm{curl}\mathbf{H}=\mathbf{B}\times\mathbf{j}_c=\mathbf{p}_v(\mathbf{B}). \tag{16}$$

Various models that have been proposed for the critical state differ in the form of dependence of the pinning force f_p on induction, i.e., on the FL density. It is assumed in Bean's

model[25] that this dependence is linear, and the current density j_y in the critical state has a constant value over the sample. In the model proposed by Kim,[26] f_p is independent of B. The model with exponential dependence[27,28] was developed after the discovery of HTSC since it provides a satisfactory explanation for many experimentally observed results. It will be shown that studies of induced suprastriction in type II hard superconductors allow us to carry out a comparative analysis of the applicability of various models of the critical state.

Using the critical state model, we obtain the following estimate for the bulk pinning force:[29]

$$p_v(\mathbf{B}) = j_c B = \frac{\Delta M(\mathbf{B})}{kR} B, \tag{17}$$

where ΔM is the difference in magnetizations in increasing and decreasing magnetic fields, R the characteristic size of the sample in a direction perpendicular to the external magnetic field, and k a constant depending on the sample geometry. The bulk pinning force calculated from magnetic or resistive measurements can be connected with the microscopic parameters by using the empirical scaling relation:[30]

$$p_v = A B_{c2}^n(T) f(b), \tag{18}$$

where $f(b) = b^l(1-b)^m$, $b = B/B_{c2}$ is the reduced induction (normal phase concentration) in the sample, $l = 1/2, 3/2$; $m = 1-2$, A is a constant independent of T and H, and l, m, n are parameters depending on the microstructure.

Effects Associated with SC Geometry in a Magnetic Field. The model of the critical state was developed for the ideal case of an infinitely long cylinder in a longitudinal magnetic field. In accordance with Eq. (10), the penetration of field in an SC generates additional components of the stress σ_{ik} exerted on the SC in a magnetic field. In turn, this leads to additional deformation of the sample in a magnetic field, i.e., to additional components of MS of the superconductor. The magnetic field penetration may be due to the demagnetizing factor g determined by the sample geometry. i.e.,

$$\lambda_\varphi(\mu) = \frac{2\pi\mu^2}{E}(1-g), \tag{19}$$

where $\lambda_\varphi \in (0-10^{-9})$, circulation of the superconducting currents in the surface layer of the superconductor, i.e.,

$$\lambda_{\text{surf}}(H) = \frac{H\Delta\mu}{E}\{-2\nu + (1-\mu)g\} - \frac{2\pi\Delta\mu^2}{E}(-2\nu + g) \sim 10^{-7}. \tag{20}$$

and the peculiarities of the mixed state of a type II superconductor in the intermediate field interval.

These components were studied and analyzed in detail by Brändli[2] for type I and reversible type II superconductors in intermediate and mixed state respectively.

2.2.3. Induced suprastriction in type II superconductors in the mixed state

The effect of magnetic field on the size of an SC was studied in the interval between H_{c1} and H_{c2} in polycrystalline and monocrystalline superconducting metallic alloys, intermetallic compounds, alloys based on transition elements from the iron (V_3Si)[31] and palladium (NbTi)[32] groups in which filling of $3d$ and $4d$ shells respectively takes place, and complex compounds with rare-earth elements La, Y, Eu, Sm, Gd, Dy, Ho, Er, Tm (see Ref. 33 and the literature cited therein) and actinides (U)[34] in which filling of $4f$ and $5f$ shells, respectively, takes place. Moreover, the symmetry of the crystal structure is lowered in the above-mentioned series from bcc to orthorhombic. In all cases, a correlation of the striction characteristics of the superconductor with the parameters of irreversible magnetization curve is observed.

Superconducting Alloys. Alloys PbIn, TaNb and InTl with concentrations corresponding to type II superconductors were studied.[2] The observed values of striction $\sim 10^{-8}$ were attributed to irreversible changes in length associated with a decrease in the condensation energy in the magnetic field superimposed by the deformation caused by the interaction of screening currents at the interfaces with the external magnetic field. Since the main results were obtained for HTSC, we shall follow Braden *et al.*[35] and consider the conclusions[2] that are significant for HTSC in the mixed state. In fields below H_{c1}, the magnetic flux is expelled from the SC having a magnetization $-(1/4\pi)H$. This leads to suprastriction associated with the interaction between the magnetic field and surface currents, and also to deformation by demagnetizing currents. Both mechanisms result in a striction peak at H_{c1}. For HTSC, $H_{c1} < 1$ kOe as a rule, and these mechanisms cannot explain the field dependence of striction in fields of the order of 10 kOe. In fields higher than H_{c1}, the magnetic field penetrates the SC and lowers its condensation energy. This effect is associated with a change in the volume leading to strictional deformations. If the condensation energy decreases to zero, the suprastriction is determined by formula (9), but the upper critical fields are practically unattainable for HTSC under actual experimental conditions (at $T = 4.2$ K). The irreversible striction was attributed in Refs. 2 and 35 to the interaction of surface currents with the magnetic field. It was mentioned above that in fields $H_{c1} < H < H_{c2}$ (i.e., in the Shubnikov phase whose existence was first demonstrated by Shubnikov *et al.*[36]), the magnetic flux penetrates a type II superconductor in the form of normal filaments surrounded by current loops circulating in the SC regions. Upon an increase in the external field, the screening current increases until the flux pinning obstructs the attainment of equilibrium magnetization. This leads to a nonequilibrium magnetization of the sample and striction caused by the Lorentz force exerted by the external magnetic field on the screening current:[35]

$$\left(\frac{\Delta L}{L}\right)_{\parallel,\perp} = \frac{H\Delta M}{E} C_{\parallel,\perp}, \tag{21}$$

where E is the Young's modulus, ΔM the nonequilibrium part of the magnetization curve, and $C_{\parallel,\perp}$ are the constants associated with the Poisson's ratio. For superconducting alloys, the striction in the mixed state was of the order of 10^{-7}, while the elastic constants calculated by using Eq. (21) are in good accord with the experimental results.

Striction of the polycrystals of hard SC alloy NbTi was measured for studying the crystal lattice deformation caused by the action of FL on the crystal lattice through pinning centers.[32] The change in the length of the sample in a magnetic field was measured in a capacitive dilatometer at right angles to the applied magnetic field. The quantity $\Delta L/L$ was found to be of the order of 10^{-6}. A singularity in the field dependences of striction and magnetization was observed in the vicinity of H_{c2}. No anomaly in the critical current was observed. Considering that the macroscopic pinning force P_v is proportional to the elastic constants $C(b)$ in the *S*-state, which are proportional for B_{c2} to the elastic constants $C_0(b)$ in the *N*-state $[C(T,B)=C_0(b)B_{c2}^{-2}$, where B_{c2} is the induction in the sample corresponding to the upper critical field],[37] and $\mathbf{p}_v=[B_{c2}(T)]^{2.5}f(b)$ for NbTi, we find that $\Delta L/L$ obeys scaling, i.e., $\Delta L/L=B_{c2}(T)]^{4.5}f(b)$. Comparing the above relations and considering that there is no anomaly in the direct measurements of the critical current (i.e., there is no pinning force in the region of H_{c2}), we can conclude[32] that the singularity of $\Delta L/L$ is rather associated with an abrupt softening of elastic constants, and not with the peak of the pinning force. Indeed, the densities of electron states of NbTi have a peak near the Fermi surface. According to Wyder *et al.*,[32] if the field applied along and across the sample has a different effect on its electron properties, the field variation results in more than double degeneracy of ground state, which must lead to the Jahn–Teller effect. In this case, the sample is deformed in the direction of the emerging forces, which can be attributed to the peculiarities of suprastriction, magnetization, and critical current. Hence Wyder *et al.*[32] concluded that the peculiarities of suprastriction in the mixed state of NbTi are associated with the elastic constant anomaly caused by the degeneracy of the ground state in a magnetic field.

Intermetallic Compounds. Isino *et al.*[31] studied the structural instability and its relation with the high values of T_{SN} in single crystals of the intermetallic compound V_3Si having the *A*15 structure and various degrees of purity. In the mixed state, the measured values of $\Delta L/L$ were found to be of the order of 10^{-6}, which is much larger than the corresponding values in metallic alloys (10^{-8}). The field dependences of striction and magnetization are completely in accord with the peculiarities of the pinning force. The large values of $\Delta L/L$ may be due to the fact that the pinning forces change the orientation of tetragonal domains left in the crystal structure by the martensite structural transformation suppressed by the NS transition.

HTSC Based on Copper Oxides with Bi and RE Ions. It should be noted at the very outset that a considerable magnetostriction was observed earlier in Bi and RE (Dy, Tb, Er) samples. For the RE samples, it attained values up to 10^{-2} along the hexagonal axis, while Bi serves as an exception among diamagnetic metals.

$Bi_2Sr_2CaCu_2O_y$. The results of measurements of giant striction distinguished by a large hysteresis in a magnetic field ($\Delta L/L\sim10^{-4}$) were first reported[38] for HTSC containing Bi. The first increase in the field led to a compression of the sample, and the quantity $\Delta L/L<0$ decreased monotonically (its absolute value increased), passing through zero at $B\approx4.3$ T upon a decrease in the field. This was followed by an expansion of the sample beyond the initial size, attaining the maximum value at $B\approx2$ T. After this, $\Delta L/L$ decreased but remained positive in zero field. The above data pertain to transverse MS: the field was applied along the crystallographic axis *c* while the change in the length was measured in the *ab* plane. The dependence of MS in negative fields was completely symmetric to MS in positive fields with the exception of the initial stage of magnetization. The MS curves for the same sample at various temperatures show that an increase in temperature lowers the value of MS for the same external field. The shape of the curves also changes. Upon an increase in the value of the field, a minimum is observed for positive fields at 20 K. The linear CTE along *a* and *b* axes in $Bi_2Sr_2CaCu_2O_8$ does not exceed $1.5\cdot10^{-5}$ at room temperature[39] and decreases upon cooling in zero magnetic field. The observed variation $\sim10^{-4}$ in the length corresponds to a more than 10 K variation in temperature and cannot be attributed to temperature fluctuations.

Y123. The correlation of the magnetic induction and MS can also be illustrated by considering the example of the texturized HTSC compound $YBa_2Cu_3O_{7-x}$.[40] Size variations with huge values for SC were observed in texturized as well as ceramic SC samples in fields up to 12 T, in contrast to the results obtained by Braden *et al.*[35] in fields up to 5 T that do not exhibit any giant values of MS. Such a disparity indicates that attainment of fields corresponding to total penetration is important. However, significant compressions of *texturized* Y123 were observed even in increasing fields of the order of 5 T. Studies of the effect of Josephson vortices on MS in granular SC are in their initial stage only.[41] No significant striction was observed in oxygen-deficient Y123 samples.

$La_{1.85}Sr_{0.15}CuO_4$. Another interesting manifestation of correlation between magnetic and strictional characteristics in the mixed state of LaSrCuO was observed by Nabialek *et al.*[42] They found a correspondence between the magnetic flux jumps and the jumps on the MS curve in accord with the critical state model. It need not be reiterated that a correlation between striction and magnetization exists in these compounds, and the value of $\Delta L/L$ is of the order of 10^{-4}.

RE123. De la Fuente *et al.*[33] measured MS in strong fields (up to 12 T) in single crystals of $RE\,Ba_2Cu_3O_{7-x}$ (RE=Dy, Ho, Er) in paramagnetic and superconducting phases between 3.8 and 100 K. They discovered a low-temperature component of induced MS, which is associated with the pinning of magnetic flux lines and is manifested in the form of a strong hysteresis of MS isotherms. At certain temperatures $T<T_{SN}$ and in an increasing field *H*, the MS isotherm displays a strong field dependence with a broad peak for a certain value of the field that increases with decreasing temperature in accordance with the behavior of the critical current. Figure 3a shows the isotherms of the hysteresis loops of deformation $\lambda(\mathbf{c},\mathbf{a})$ as functions of the applied magnetic field for the compound $HoBa_2Cu_3O_{7-x}$. The lower branches correspond to increasing field and the upper branches to decreasing field. Reversible behavior is observed only above ~20 K since the maximum attainable field is equal to 12 T. These data are presented in the section

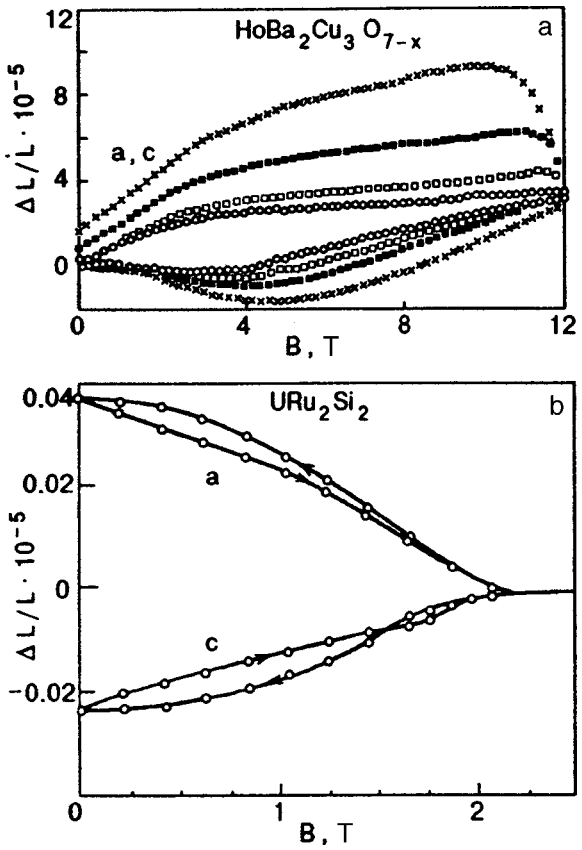

FIG. 3. Magnetostriction of superconducting compounds containing paramagnetic ions with unfilled $4f$- (a) and $5f$- (b) shells at various temperatures T, K: 30 (○), 25 (□), 20 (■), 15 (×) (see Ref. 33) (a) and 0.5 K (see Ref. 34) (b).

devoted to suprastriction in order to illustrate the universal nature of the hysteresis of striction curves in the mixed state of SC. The results for compounds with paramagnetic ions will be considered in detail in connection with the crystal field and magnetic interaction effects.

Superconducting Actinides. Van Dijk *et al.*[34] studied the heavy-fermion uranium SC compound URu_2Si_2, whose suprastriction is of the order of 10^{-7}. In a magnetic field, it exhibits a hysteresis which is apparently associated with magnetic flux pinning (Fig. 3b). The NS of these compounds will be considered below in detail from the point of view of separation of supra and magnetic components.

2.2.4. Phenomenological description of striction induced by magnetic flux pinning

The large body of experimental data accumulated to date indicates that the critical state model can be applied to HTSC (see, for example, Ref. 43). The induced suprastriction in the mixed state of traditional SC does not exceed 10^{-7}. However, latest measurements in HTSC with high j_c reveal that the striction for the sample in the mixed state of an SC has very large values $\sim 10^{-4}$. For an infinitely long cylinder or thin plate in a longitudinal field, this result can be explained by using the model of the critical state. Since the magnetic flux lines are subjected to the action of the pinning force, an equal but opposite force must act on the crystal. Thus, the length of the sample varies in the applied field, and MS must be observed in the case of a quite strong pinning.

As the applied field is increased, a compressive force acts on the crystal, since the movement of magnetic flux lines is obstructed by pinning. A decrease in field results in a tensile force acting on the crystal through the same mechanism. The trapped magnetic flux leads to extension in zero field. A decrease in temperature causes an increase in MS with the pinning force. In order to simplify the quantitative description, we consider the one-dimensional flux penetration while disregarding the demagnetization effects. It is also assumed that reversible magnetization is a small part of the total magnetization, and that the critical state sets in. Let f_p (in units of N/m) be the pinning force per unit length of the flux line. In this case, the flux line exerts a force $-f_p$ on the sample. If there are n flux lines in an area element, the force acting on the sample is equal to $-nf_p$ [N/m^3]. In this case, the following equilibrium condition is satisfied (see Ref. 38):

$$\frac{\partial \sigma(x)}{\partial x} + [-n(x) f_p] = 0, \tag{22}$$

where $\sigma(x)$ is the local internal stress, and the local pinning force is defined as

$$f_p = \Phi_0 \mu^{-1} \frac{\partial B(x)}{\partial x}.$$

Here, Φ_0 is the magnetic flux quantum, and $B(x) = \Phi_0 n(x)$ is the local magnetic flux density. The quantity $\sigma(x)$ is obtained by integration:

$$\sigma(x) = -\frac{B_e^2 - B^2(x)}{2\mu_0}; \tag{23}$$

B_e being the induction at the sample surface. Assuming elastic isotropy of the plane *ab*, we arrive at the following expression for the relative variation in length in an experiment with the above geometry:

$$\frac{\Delta L}{L} = \frac{1}{L} \int_{-L/2}^{L/2} \frac{\sigma(x)}{C} dx \sim 10^{-4}. \tag{24}$$

Here, C is the elastic modulus, and L the sample length.

If the distribution $B(x)$ is known, say, from Bean's model,[25] we can obtain the MS curve, taking into account the fact that the critical current density j_c is a rapidly decreasing function of T and H.[30] The peak in the field dependence of the pinning force and its displacement towards higher values of H upon a decrease in T were observed in type II superconductors[5] and HTSC of the type $REBa_2Cu_3O_{7-x}$ and $Bi_2Sr_2CaCu_2O_{8+y}$.[44,45] Following Refs. 30 and 33, we obtain for the pinning-related MS the following expression for the diagonal component of the strain tensor:

$$\overline{\langle \varepsilon_{xx} \rangle} = K \left(\frac{L}{2C_{11}} \right) (H^*(T))^{2,5} f(h). \tag{25}$$

In increasing and decreasing fields, the branches of MS isotherms in Fig. 3 must contain contributions from the MS of paramagnetic ions and from pinning. In order to isolate the contribution of pinning to the deformation, we equate the difference $\lambda^{\downarrow}(\mathbf{c},\mathbf{a}) - \lambda^{\uparrow}(\mathbf{c},\mathbf{a})$ to $\overline{\langle \varepsilon_{xx} \rangle}$. We disregard the flux

creep[46] which is significant for HTSC.[47] Ikuta *et al.*[48] have presented the results of computer simulation of pinning-induced MS using three versions of the critical state model, viz., Bean's model,[25] Kim's model,[26] and the model proposed by Karasik *et al.*[27] In the latter model, an exponential dependence of the critical current density on the flux density is assumed. Analytic expressions were obtained for the change in the length of samples in the form of an infinite plate in a longitudinal magnetic field under the assumption that the reversible part of total magnetization is negligible. The obtained results were used for computer simulation and hysteresis loops were calculated over a wide range of variation of the corresponding parameters. Since the striction induced by pinning is a direct manifestation of the pinning force, the hysteresis loops have different shapes in different models. A meticulous analysis[48] speaks in favor of the model presented in Ref. 27 According to the preliminary data obtained by Ikuta *et al.*,[48] the exponential model is in good agreement with the experimental results for $(La_{1-x}Sr_x)_2CuO_4$ single crystals with a low concentration of Sr. It is shown that the pinning force can be obtained directly from the width of the MS hysteresis loops. The results of simulation reveal a satisfactory agreement with the experimental results.

However, the results of numerical simulation differ significantly (by more than an order of magnitude) from the experimental results. It is also hard to explain the lower values of the HTSC striction characterized by the same values of the critical current densities. The assumption concerning the isotropy of the elastic modulus may be one of the reasons behind the experimental and theoretical results. The estimates presented below are based on the values of the Young's modulus calculated for the main crystallographic symmetry directions for the investigated materials. The phenomenological model also disregards the peculiarities of the HTSC magnetic structures that are mainly associated with the formation of layers in such structures,[49] as well as inhomogeneities of magnetic flux within a unit cell.[50]

In all probability, the huge values of striction of HTSC can also be associated with the peculiarities of their crystalline and magnetic states. The obvious peculiarities are associated with a sharp anisotropy of their structure and the presence of paramagnetic ions of *f*- and *d*-transition elements. We shall consider below their effect on the MS of complex SC compounds.

2.2.5. Effect of anisotropy on the suprastriction of SC

A Thin Plate in a Transverse Magnetic Field. The phenomenological description of suprastriction in the mixed state presented so far has been based on the assumption that the experimental geometry is close to the ideal case of an infinitely long cylinder in a longitudinal magnetic field. The actual situation is quite different even for the longitudinal geometry of the experiment. Moreover, under actual conditions of investigation of spatial distribution of magnetic flux in an SC (for example, in direct optical observations of magnetic flux distribution in the sample using various indicators), the situation corresponds to that of a plane superconductor in a transverse magnetic field. In this case, which is also significant for studying giant magnetostriction in HTSC, an analytic solution can be obtained by making certain assumptions. Earlier, Brandt *et al.*[51] obtained for a thin superconducting strip an analytic solution for current and field distribution in a sample placed in a transverse magnetic field. The corresponding magnetostriction effects can also be determined for this geometry.[52] It is assumed that the sample in the form of an infinitely long narrow layer of thickness d and halfwidth a occupies the halfspace $|x| \leqslant d/2$, $|y| \leqslant a$, $|z| < \infty$, and is placed in an external magnetic field H_e at right angles to the direction of measurement of magnetostriction. The spatially uniform magnetic field H_e, which is directed along the x-axis, induces along the z-axis a superconducting current of density $j(x,y)$ which screens the inner part of the plane sample from the applied field. The quantity $j(x,y)$ is limited by the value j_c which does not depend on the applied field. The integral current density $J(y)$ over the sample thickness, expressed in field units, is connected with the field $\mathbf{H}(x,y)$ at the sample surface through the Ampere law. The longitudinal and transverse components of the field are defined as

$$H_y(d/2,\ y) = -H_y(-d/2,\ y) = \tfrac{1}{2} J(y)$$

and

$$H_x(d/2,\ y) = H_x(-d/2,\ y) \approx H_x(0,\ y) = H(y).$$

The transverse component corresponds to the magnetic flux density $H(y)\mu_0 B(y)$. From Maxwell's relations, we obtain

$$H(y) = \frac{1}{2\pi} \int_{-a}^{a} \frac{J(u)\,du}{y-u} + H_e. \tag{26}$$

This expression allows us to calculate first the distribution of screening currents and magnetic flux over the sample width as a function of H_e, and then the striction also.

The results of numerical simulation of MS were compared with the results of measurements in a $La_{1.85}Sr_{0.15}CuO_4$ single crystal (Fig. 4).[52] Calculations were made by using the results of measurement of elastic moduli.[53]

A comparison of the measured values of MS with the results of computer simulation reveals a similarity in the plotted curves and a closeness of the absolute values for size variations.[52] Thus, the concepts on which the model is based do not contradict reality. Obviously, the finite size of the real sample must lead to a discrepancy between the experimental and theoretical results. However, the MS along the short face of the sample which presumes the existence of only screening currents may be an indication of the ''induced'' critical state which is widely discussed at present (see, for example, Ref. 54 and the literature cited therein). For more profound physical conclusions, we must use the data of local measurements of magnetic flux distribution and elastic distortions in the sample under the action of a magnetic field.

Effect of Layered Structure on Suprastriction in SC. The compound $Ba_{1-x}K_xBiO_3$,[55–62] which does not have many distinguishing features of HTSC cuprates but has the highest superconducting transition temperature $T_{SN} \approx 30$ K among

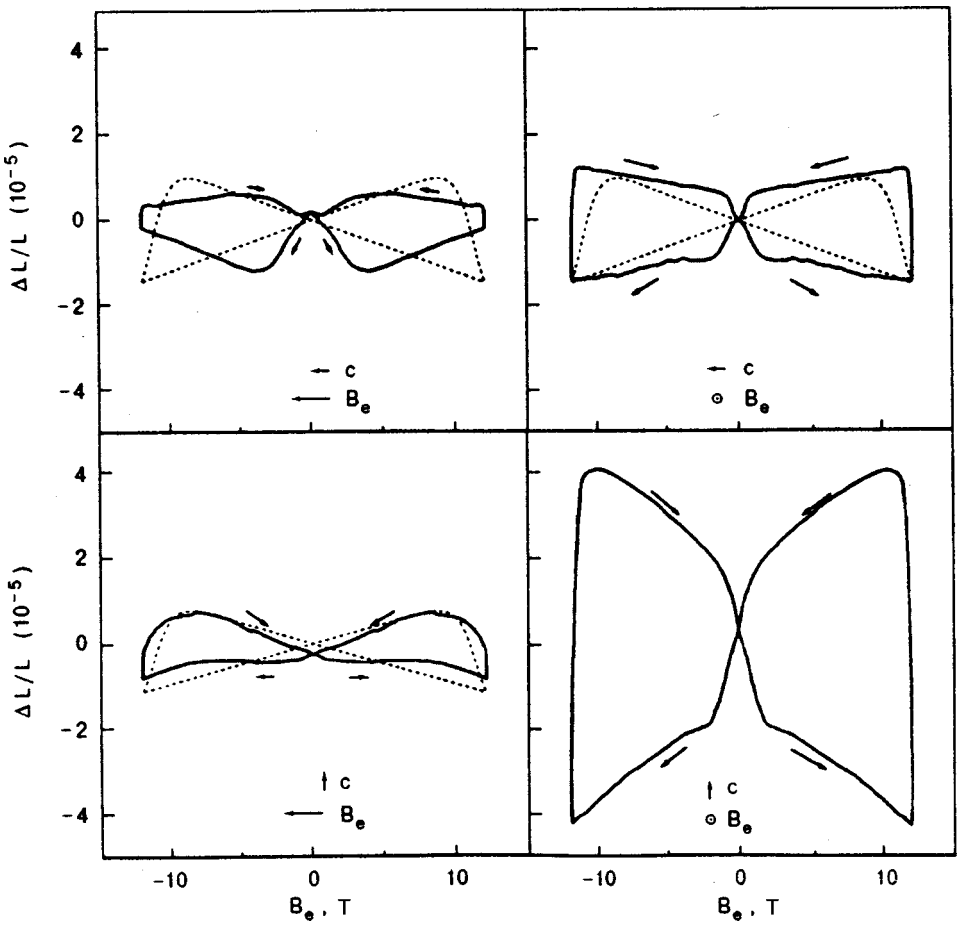

FIG. 4. Results of experiments (solid curves) and numerical simulation (dashed curves) of magnetostriction in $La_{1.85}Sr_{0.15}CuO_4$ single crystals for various orientations of applied magnetic field relative to the crystallographic axis *c*.

non-cuprate superconductors (close to LaSrCuO with $T_{SN} \approx 35$ K), is a convenient object for determining the contribution of characteristic structural peculiarities in the formation of superconducting state and characteristics of HTSC based on copper perovskites. Unlike cuprate HTSC, this compound does not contain any two-dimensional metal–oxygen planes which are considered to be an important factor determining the high-temperature superconductivity. It also does not have any magnetic moments, and this rules out the mechanism of magnetic pairing. Several experimental facts like a strong isotopic effect and the width of the superconducting gap indicate that the superconductivity of BaKBiO is associated with the phonon mechanism. However, superconductivity emerges near the metal–insulator transition of this compound, as in cuprate HTSC, only in the cubic phase ($x > 0.3$) and vanishes during a transition to the semiconducting phase upon a decrease in potassium concentration. In view of the above, we used the cubic modification[20] of the compound BaKBiO for studying magnetostriction and comparing the analogous experimental results with those obtained for high- and low-temperature superconductors while considering the effect of magnetic field on their size. Measurements were made on monocrystalline samples of $Ba_{0.66}K_{0.34}BiO_3$ with $T_c = 32.5$ K, obtained by electrochemical sputtering in a flow of KOH (see Ref. 57 and the literature cited therein). The temperature dependences of lattice parameters and structural deformations in a magnetic field were obtained on an x-ray diffractometer with a low-temperature attachment in fields between 0 and 5 T. The magnetostriction was measured by strain gauges in the crystallographic direction [100] at right angles to the applied magnetic field in the interval between 0 and 12 T with the field varying at a constant rate of 1 T/min. Simultaneously, the field dependence of the sample magnetization was measured by using the ballistic technique. The critical current density j_c in zero field attained values of 1.7×10^8 A/m^2 at 4.2 K and 0.67×10^8 A/m^2 at 10 K. The absolute values of striction were found to be $\approx 10^{-6}$ which is an order of magnitude lower than the values obtained for cuprate SC and an order of magnitude higher than for low-temperature SC. It was found that the main contributions to the magnetostriction of SC are determined by the pressure of the magnetic field on the sample at temperatures lower than the *NS*-transition temperature and by the pressure dependence of H_c. Our estimates[20] are for $T = 10$ K, which corresponds to $T/T_{SN} = 0.31$ for the compound under investigation. Using the thermodynamic analysis presented in Sec. 2.1, we obtain for the TD component of the MS of the investigated BaKBiO compound[20] for $T/T_{SN} = 0.31$ the value $\Delta L/L \approx 8 \times 10^{-6}$, which is slightly higher than the measured values of MS. Calculations were made by using the data obtained by Batlogg *et al.*[63] which led to estimates $H_c^2 \approx 10$ J/mole and $C \approx 0.5$ J/mole. The x-ray data lead to the value $\alpha \simeq 0.9 \times 10^{-6}$ which was obtained by using the following expression for the Young's modulus E of a cubic crystal:[64]

$$\frac{1}{E}=\frac{c_1+c_2}{(c_1+2c_2)(c_1-c_2)}+\left(\frac{1}{c_3}-\frac{2}{c_1-c_2}\right)\times(n_x^2n_y^2+n_x^2n_z^2+n_y^2n_z^2), \quad (27)$$

where **n** is a unit vector in the direction of deformation, $c_1=\lambda_{xxxx}$, $c_2=\lambda_{xxyy}$, and $c_3=\lambda_{xyxy}$ (λ_{iklm} are the components of the elastic moduli tensor). The values of the elastic moduli used were obtained from dispersion curves showing the results of measurements of inelastic neutron scattering.[65]

The measured field dependences of the magnetostriction of noncuprate isotropic HTSC are irreversible and correspond to the irreversibility of the magnetization curves. The values of magnetostriction are more than an order of magnitude higher than for low-temperature metallic superconductors. However, giant magnetostriction characterizing layered cuprate superconductors was not observed. A comparison of the experimental and theoretical results reveals an enhanced value of the thermodynamic contribution. This is due to the fact that the estimate was made under the assumption of a complete transition of the sample to the superconducting state upon removal of the magnetic field. In actual practice, the quantity V_S appearing in the thermodynamic relation under consideration characterizes only a part of the sample volume that has undergone an *NS*-transition following the trapping of magnetic flux. The part of the sample volume with trapped magnetic field that has not undergone a superconducting transition can be estimated from the experimental $B(H)$ dependence as the ratio of the trapped magnetic flux to the quantity B_{c2} corresponding to the upper critical field. A comparison of the experimental results with the theoretical values of the thermodynamic components reveals a satisfactory agreement between them. This is also true for the results of numerical simulation of pinning-induced magnetostriction. Thus, the results of macroscopic analysis do not allow a separation of the dominating contribution to the effect. The obtained results also indicate that both types of components reflect the contributions associated with the magnetic field pressure as well as the contributions induced by magnetic flux pinning. The latter is responsible for the irreversible nature of the field dependence of magnetostriction. The difference between the obtained results and the data of low-temperature SC is explained by a higher sensitivity of H_c of the investigated compound to pressure. The disparity between the measurements on cuprate HTSC and the absence of giant magnetostriction can be explained only after an analysis of the effect on microscopic level.

3. MAGNETOSTRICTION OF SC COMPOUNDS WITH PARAMAGNETIC IONS OF TRANSITION ELEMENTS

Latest achievements in the field of materials science, various experimental investigations, and the theory of superconducting state are associated with the synthesis of exotic superconducting compounds containing ions of elements with unfilled *d*- and *f*-shells in which superconductivity coexists in an astonishing manner with paramagnetism, and even with a long-range antiferromagnetic ordering. Investigations of MS in such compounds, aimed at an analysis of both supra- and para components have been quite scarce although they could help in analyzing the relation between transition parameters in various subsystems of these complex low-symmetry compounds and in determining the reasons behind the transitions.

3.1. Magnetostriction under conditions of coexistence of superconducting and antiferromagnetic ordering

Van Dijk *et al.*[34] studied in the temperature interval $0.3\,\mathrm{K}<T<1.5\,\mathrm{K}$ the magnetostriction (MS) of the monocrystalline heavy-fermion compound URu_2Si_2 with antiferromagnetic ordering temperature $T_N=17.5\,\mathrm{K}$ and $T_{SN}=1.2\,\mathrm{K}$. The AFM state of this compound is associated with the weakly ordered magnetic moment $(0.03\pm0.01)\mu_\beta$ at the uranium atom, oriented along the *c*-axis. The uranium atom is in a low-symmetry configuration ($^3H_4$), and its magnetic properties can be interpreted in the framework of the crystal-field model.

The coexistence of SC and AFM ordering in the temperature interval $0.3\,\mathrm{K}<T<1.5\,\mathrm{K}$ was confirmed in experiments on neutron diffraction. Measurements of longitudinal and transverse MS were made by using a capacitive dilatometer in fields up to 5 T, while $H_{c2}(T\to0)$ is equal to 3 T along the tetragonal *c*-axis, which is the easy magnetization axis, and equal to 14 T in the basal plane. This made it possible to isolate the supra- and parastriction components. The latter depends on the field as H^2. Suprastriction is of the order of 10^{-7}. Its behavior in a magnetic field is characterized by hysteresis which is associated in all probability with the magnetic flux pinning discussed above. A characteristic feature of hysteresis is that its sign is reversed in fields close to the upper critical field. This effect is apparently associated with the manifestation of AFM ordering since the hysteresis in ordering of moments, which may reflect the hysteresis of parastriction, is observed just in this interval of fields.

The relative volume variation is $(\Delta V/V)_{NS}=0.48\times10^{-6}$ at 0.5 K and 0.17×10^{-6} at 1 K. Spontaneous MS can also be estimated by subtracting the term bB^2 for MS in the *N*-state (where *b* is determined by MS measured at $H>H_{c2}$) from MS in the *S*-state. In this case, the relative variation in length for $H=0$ corresponds to spontaneous MS. The derivatives of the critical thermodynamic field H_{c2} are estimated from the heat capacity jump during *NS*-transition:[34]

$$\Delta(C/T)=\frac{V_m}{\mu_0}\left(\frac{\partial H_c}{\partial T}\right)^2, \quad (28)$$

where V_m is the molar volume, μ_0 the magnetic permeability of the vacuum, and $dH_c/dt=37\,\mathrm{mT/K}$. Van Dijk *et al.*[34] observed a sharply manifested hysteresis in the linear MS of the heavy-fermion compound URu_2Si_2 during measurements in a magnetic field at temperatures below $T_{SN}=1.18\,\mathrm{K}$ (see Fig. 3b). The hysteresis loop closes at H_{c2}. Interestingly, it

was observed experimentally that the sign of hysteresis is reversed at the lowest temperatures as H_{c2} is approached. The hysteresis of the flux profile may be accompanied by the hysteresis of the paramagnetic MS and ordered moments.

3.2. From phenomenological to microscopic description

An analysis of MS in the perovskite-like compounds containing ions with unfilled *f*-shells (*f*-ions) of rare-earth elements as well as actinides is based on the following conclusions drawn from an analysis of MS in *f*-magnets in the paramagnetic limit.[8,66] The crystal structure of these compounds may be described in the tetragonal symmetry approximation. Orthorhombicity, which is inherent in these compounds, is characterized by a small difference between the *a* and *b* axes in the basal plane. In the paramagnetic limit, which is observed in HTSC, the *f*-ions are separated by quite large distances, and hence their interaction can be disregarded (single-ion approximation). The deep electrons in the unfilled $4f$-shells are screened from exchange interactions and the effect of electric crystal field on their orbital angular momentum, which makes the latter more mobile in a magnetic field. This may give rise to a considerable MS. The screening of *f*-electrons by filled outer shells lowers the possibility of their participation in exchange as well as dipole interactions. An analysis of the magnetic properties of *f*-magnets is usually carried out under the assumption that spin-orbit interaction dominates over the crystal field (CEF) effects, i.e., in the weak field approximation.[67] The same assumptions also form the basis of the theory of MS of RE compounds in the paramagnetic limit.[8] For some RE ions, however, the splitting of the fundamental multiplet in CEF exceeds the Zeeman splitting in an external magnetic field.[66] Moreover, the MS models were developed mainly for high symmetries (fcc and hcp) which lead to less significant crystal field effects and admit a smaller number of model parameters, besides offering greater promise for obtaining giant MS in view of lower magnetic anisotropy energies. Thus, investigation of rare-earth MS in a low-symmetry surrounding characteristic of HTSC structures is interesting in itself in addition to the studies of mechanism of their extraordinary suprastriction and its relation to the main SC parameters. Assuming the lattice to be tetragonal, we can confine our analysis to the MS in a cylindrical symmetry. Let us denote the MS as $\lambda(\alpha,\beta)$. Here, $\boldsymbol{\alpha}\equiv(\alpha_x,\alpha_y,\alpha_z)$ are directional cosines of the field, and $\boldsymbol{\beta}\equiv(\beta_x,\beta_y,\beta_z)$ are cosines in the direction in which the deformation is measured. This makes it possible to determine the strictions $\lambda(\mathbf{a},\mathbf{a})$, $\lambda(\mathbf{a},\mathbf{b})$, and $\lambda(\mathbf{c},\mathbf{a})$ of crystals with Dy, Ho and Er. Here **a** and **b** are not orthorhombic axes, but only two arbitrary mutually orthogonal axes in the basal plane presumably with cylindrical symmetry. Four distortion modes are observed in the phenomenology of MS of axial systems:[8,9] bulk distortion λ_{1i}^{α}, the variation λ_{2i}^{α} in the ratio c/a, the violation λ^{γ} of cylindrical symmetry (tetragonal symmetry in the present case) in the basal plane, and shear strain λ^{ε} which tilts the *c*-axis. Phenomenological deformation modes λ_{ij}^{Γ} can be connected with strictions $\lambda(\boldsymbol{\alpha},\boldsymbol{\beta})$ as follows:

$$\lambda(\boldsymbol{\alpha},\boldsymbol{\beta})=\frac{1}{3}\lambda_{11}^{\alpha}+\frac{1}{2\sqrt{3}}\lambda_{12}^{\alpha}\left(\lambda_z^2-\frac{1}{3}\right)+\sqrt{3}\lambda_{21}^{\alpha}\left(\beta_z^2-\frac{1}{3}\right)+\frac{3}{2}\lambda_{22}^{\alpha}\times\left(\lambda_z^2-\frac{1}{3}\right)\left(\beta_z^2-\frac{1}{3}\right)+2\lambda^{\gamma}\frac{1}{4}(\alpha_x^2-\alpha_y^2)(\beta_x^2-\beta_y^2+\alpha_x\alpha_y\beta_x\beta_y)+2\lambda^{\varepsilon}(\alpha_y\alpha_z\beta_y\beta_z+\alpha_x\alpha_z\beta_x\beta_z). \tag{29}$$

In the present case, it is sufficient to isolate the mode $\lambda_{\Gamma}=\lambda(\mathbf{a},\mathbf{a})-\lambda(\mathbf{a},\mathbf{b})$ and a linear combination preserving the cylindrical symmetry of the crystal, i.e.,

$$\lambda(\mathbf{c},\mathbf{a})=\frac{1}{3}\left\{(\lambda_{11}^{\alpha}-\sqrt{3}\lambda_{21}^{\alpha})+\frac{1}{\sqrt{3}}(\lambda_{12}^{\alpha}-\sqrt{3}\lambda_{22}^{\alpha})\right\}.$$

For a rare-earth ion in the normal state inside a vortex, the Hamiltonian is analogous to the Hamiltonian of the ferromagnet:[68]

$$H=H_{CEF}+H_{ME}+H_z+H_{\rm ex}+H_Q+H_{\rm el}, \tag{30}$$

where H_{CEF} is the term associated with CEF in the unperturbed tetragonal symmetry:

$$H_{CEF}=B_2^0O_2^0+B_4^0O_4^0+B_4^4O_4^4+B_6^0O_6^0+B_6^6O_6^6. \tag{31}$$

Here B_n^m are CEF parameters (Ho,[69] Dy,[70] and Er,[71]), O_n^m are equivalent Stevens operators, and H_{ME} is the magnetoelastic coupling Hamiltonian. Retaining only the term associated with the violation of tetragonal symmetry in the basal plane, we can write

$$H_{ME}=-M^{\gamma}\epsilon^{\gamma}O_2^2, \tag{32}$$

where $\epsilon=(\epsilon_{xx}-\epsilon_{yy})/\sqrt{2}$ is the irreducible deformation, M^{γ} is the magnetoelastic coupling parameter, O_2^2 the Stevens operator: $O_2^2\sim(j_x^2-j_y^2)$; $\mathbf{J}=(J_x,J_y,J_z)$ is the total angular momentum of the RE element, and H_Q the two-ion quadrupole coupling component. According to the authors of Ref. 33, it is sufficient to consider just the term

$$H_Q=-k^{\gamma}\langle O_2^2\rangle O_2^2, \tag{33}$$

written in the mean field approximation, k^{γ} being the purely quadrupole coupling parameter, and $\langle ...\rangle$ the average over temperature obtained with the help of eigenvalues and wave functions diagonalizing the unperturbed Hamiltonian H_{CEF}. Finally, we retain in the elastic energy only the term[33]

$$H_{\rm el}=\frac{1}{2}C_0^{\gamma}(\epsilon^{\gamma})^2, \tag{34}$$

where C_0^{γ} is the elastic constant corresponding to the unperturbed case. Equations (32)–(34) provide a complete description of the Hamiltonian.[68] In the AFM state, which is realized for the compounds Dy and Er, the mean field acting on one of the magnetic sublattices, say *A*, can be presented in the form

$$\mathbf{H}_A=\lambda_{ii}\mathbf{M}_A-\lambda_{AB}\mathbf{M}_B+\mathbf{H}, \tag{35}$$

where **H** is the applied field, $\mathbf{M}_A$ and $\mathbf{M}_B$ are the magnetizations of the sublattices, and λ_{ii}, λ_{AB} are the mean-field constants describing the interaction within a sublattice and be-

TABLE II. Magnetic parameters of RE ions.[33]

RE ion	μ_{eff},μ_B	Θ, K	$c,\mu_B^2/k_B$	λ_{ii}	λ_{AB}	λ_{eff}
Dy^{3+}	11.87	27	46.96	0.55	0.60	1.15
Ho^{3+}	10.88	17	39.45	0.43	0.43	0.86
Er^{3+}	10.48	12	36.61	0.31	0.33	0.64

Remark: Values of mean field constants λ are given in units of k_B/μ_B^2.

tween sublattices, respectively. In the paramagnetic state, the field-induced sublattice magnetizations will be parallel to each other and to the field, and $M_A=M_B=M$. The mean field has the form $H_{\text{ex}}=-(\lambda_{ii}+\lambda_{AB})M\equiv-\lambda_{\text{eff}}M$ irrespective of the sublattice. In this case, the exchange and Zeeman Hamiltonians can be presented in the form

$$H_{\text{ex}}+H_Z=-g_jM_Bj(-H_{\text{ex}}+\mathbf{H}), \tag{36}$$

where

$$H_{\text{ex}}=-(\lambda_{ii}+\lambda_{AB})Ng_j\mu_B\langle\mathbf{j}\rangle; \tag{37}$$

N is the number of RE^{3+} ions per unit volume, g_j Lande's g-factor for rare-earths, and $\langle\mathbf{j}\rangle$ the temperature-averaged total angular momentum of the RE. The mean-field constants λ_{ii} and λ_{AB} can be estimated within the framework of Neel's theory of antiferromagnetism. It can be shown[72] that having presented the linear susceptibility in the form $\chi=c/(T+\Theta)$, where $c=\mu_{\text{eff}}^2/3k_B$ is the Curie constant (per ion) and μ_{eff} is the paramagnetic moment of an ion, we obtain

$$\lambda_{ii}=\frac{\Theta-T_N}{c};\quad \lambda_{AB}=\frac{\Theta+T_N}{c}. \tag{38}$$

In this case, $\lambda_{\text{eff}}=2\Theta/c$. In the latter equation, Θ is the paramagnetic Curie temperature. Table II contains the values of μ_{eff},Θ and c obtained from the paramagnetic susceptibility measurements;[73] λ_{ii} and λ_{AB} taken from Eq. (38), as well as the values of λ_{eff}. Minimization of the free energy $F=-k_BT\ln Z$ corresponding to the Hamiltonian (30) with respect to ϵ^γ,[33] we obtain the equilibrium deformation

$$\epsilon^\gamma=\left(\frac{M^\gamma}{C_0^\gamma}\right)\langle O_2^2\rangle. \tag{39}$$

Substitution of the equilibrium value ϵ^γ (39) into (32) together with H_Q (33), we obtain the effective Hamiltonian in the form $H_{ME}+H_Q=-G^\gamma\langle O_2^2\rangle O_2^2$, where the coefficient G^γ includes contributions from magnetoelastic and purely quadrupole interactions:

$$G^\gamma=K^\gamma+\frac{(M^\gamma)^2}{C_0^\gamma}. \tag{40}$$

In order to find the distribution function Z, we calculate $F|_{T>T_N}$ within the framework of the perturbation theory.[68]

Using the energy levels and wave functions of the Hamiltonian H_{CEF} with residual interactions as perturbations, we obtain F for irreducible deformations up to the second order and Stevens' quadrupole moments $\langle O_2^m\rangle$ up to fourth order in M and H. Assuming that $\mathbf{H}$ is parallel to $\mathbf{a}\equiv[100]$, we can determine ϵ^γ. This gives

$$\frac{H}{\sqrt{|\epsilon|^\gamma}}=\left(\frac{M^\gamma}{C_0^\gamma}\right)(1-\lambda_{\text{eff}}X_0^2)\left(\frac{1-G^\gamma\chi_\gamma}{\chi_\gamma^{(2)}}\right)^{1/2}, \tag{41}$$

where $\epsilon^\gamma\equiv\lambda^\gamma=\lambda(\mathbf{a},\mathbf{a})-\lambda(\mathbf{a},\mathbf{b})$, In Eq. (41), χ_0 is the conventional magnetic susceptibility of one-ion CEF, χ_γ the deformation susceptibility associated with the field induced moment $\langle O_2^2\rangle$, and χ_γ^2 the quadrupole field susceptibility. The susceptibilities are described by complex expressions for matrix elements $j_k, O_2^0\sim 3j_z^2-j(j+1)$ and O_2^2 in the range of wave functions $|ik\rangle$ of the CEF Hamiltonian. Thus, we have diagonalized H_{CEF} with CEF parameters borrowed from Refs. 69–71. According to Eq. (41), an antiferromagnet with two exactly equivalent sublattices in paramagnetic state is equivalent to a ferromagnet. A comparison of (41) with the values of $\epsilon^\gamma(H,T)$ measured in the paramagnetic state leads to the values of M^γ and C^γ.

3.3. Experimental studies of MS in perovskites $REBa_2Cu_3O_{7-x}$

These HTSC oxides are ordered antiferromagnetically at quite low temperatures in such a way that the paramagnetic and superconducting states overlap in the temperature interval between the Néel temperature T_N and T_{SN}. For $DyBa_2Cu_3O_{7-x}$, $T_N=1$ K and the magnetic moments ($7.2\pm0.6\mu_B$/ion) are aligned along the c-axis.[74] Antiferromagnetic ordering in the Er-based compound occurs in the basal plane with moments ($2.9\pm0.6\mu_B$/ion) along the b-axis at $T_N=0.61$ K.[75] These easy magnetization axes must be in good agreement with the magnitudes and signs of Stevens' coefficients α_j of the second kind, which are determined by the shape of the cloud (oblate or prolate). Only nuclear ordering can occur in Ho compounds below $T_N^*=0.17$ K, and the electron ground state is a singlet.[76,77] The presence or absence of low-temperature magnetic ordering is important for calculating MS in the paramagnetic limit.

Del Moral *et al.*[78] have presented the results of the first systematic investigations of thermal expansion and magnetostriction in $REBa_2Cu_3O_{7-x}$ compounds (RE=Eu, Sm, Gd, Dy, Ho, Er, Tm) in longitudinal and transverse fields up to 2.4 T. They studied the effect of substitution of rare-earth elements for yttrium. The anomaly associated with the phase transition at T_{SN} was not observed. All curves showing the temperature dependences of thermal expansion could be reduced to the curve for the unsubstituted alloy, which points towards the common origin of phonon contribution to the thermal expansion. The MS anisotropy was observed only for substitutions by Dy and Ho. For the remaining substitutions (Eu, Sm, Gd, Er, Tm), the MS is small as in nonmagnetic superconductors. It is possible that the MS is observed in the former case in N-regions inside the vortices, and does not emerge in materials in which the fields correspond to completely diamagnetic state.

Del Moral *et al.*[78] isolated an MS mode associated with CEF which lowers the symmetry of the basal plane ($\epsilon^\gamma\simeq-300\times10^{-6}$ at 10 K and 12 T for Dy and Ho compounds), and obtained the ratio $M^\gamma/C_0^\gamma=1.3\times10^{-4}$ for the Ho-based compound and $\simeq5\times10^{-4}$ for the Dy-based compound, where M^γ is the single-ion magnetoelastic coupling constant,

and C_0^γ is the elastic constant in the paramagnetic state. The obtained quadrupole coupling parameter G^γ for the Ho-compound is equal to -35 mK/ion.

Zvezdin *et al.*[79] measured the MS of SC polycrystals $HoBa_2Cu_3O_{7-x}$ in transverse and longitudinal fields. A comparison of the results of measurements with the results for unsubstituted Y123 (whose the MS is lower by two orders of magnitude) and with the data for nonsuperconducting $HoBa_2Cu_3O_{7-x}$ (whose the MS is close to that of a SC) leads to the conclusion that the field dependences of the MS of the Ho-substituted Y123 compound are determined by the paramagnetic component analogous to the paramagnetic garnets.[66] The longitudinal MS was described by taking only CEF into account.[79]

It should be remarked that the complex hierarchy (distribution) of critical fields has aroused special interest of researchers towards the SC components of MS in polycrystals of the SC compounds $HoBa_2Cu_3O_{7-x}$.[80]

3.4. Contribution of Jahn-Teller effects and magnetic-field-induced structural instability

The peculiarities of MS in low-symmetry SC can naturally be associated with their crystal structure. Anisotropy of spontaneous MS may serve as a unique instrument for studying the connection between the SC transition and the Jahn–Teller transitions in SC compounds containing ions with non-Kramers degeneracy of the ground state. Such compounds include HTSC perovskites in which RE ions as well as copper ions in low-symmetry D_{2h} surrounding of oxygen are Jahn–Teller ions. The mutual effect of *NS*- and structural phase transitions, which is associated with the spatial symmetry, was considered phenomenologically by Poluektov.[81] Experimental and theoretical studies reveal[77,82] that the crystal field acting on RE ions in HTSC compounds is strong (total splitting of the multiplet is 700 cm^{-1}). It is also known that the symmetry of the electron cloud of the RE ions undergoes severe distortions caused by quadrupole interactions leading to structural phase transition.[83,84] The manifestation of the Jahn–Teller effect itself can be expected primarily in copper ions since the degeneracy of RE ions is removed in all probability by quadrupole interactions. The transitions associated with the change in the electron structure of the Jahn–Teller Cu ion was observed experimentally in the HTSC compound $YBa_2(Cu_{1-x}{}^{57}Fe_x)O_{6+\delta}$.[85]

CONCLUSION

In this review, we have endeavored to generalize the results of MS investigations which completely reproduce the chronology of developments in the technology of superconducting materials, viz., type I and type II superconductors with fcc structure, alloys and intermetallic compounds based on $3d$- and $4d$-elements with tetragonal structure emerging as a result of structural transition from the fcc phase which is suppressed by the *NS*-transition, and lastly, orthorhombic (after structural transition from the tetragonal phase) HTSC compounds of $4f$ elements and heavy-fermion SC with AFM ordering containing $5f$-elements from the actinide group. The main aim of the authors was to highlight the results obtained for low-symmetry materials (starting from tetragonal ones) since the preceding investigations were discussed earlier in review articles, and also because the peculiarities of subsequent striction measurements of strongly correlated SC compounds are mainly associated just with the spatial anisotropy.

The strong hysteresis of MS isotherms led to the discovery of a low-temperature ($T<T_{SN}$) MS component which is unambiguously described by the mixed state models (called the critical state models), thus confirming its connection with the magnetic flux pinning at crystal lattice inhomogeneities. The MS caused by flux pinning displays temperature and field dependences that are in accord with the vortex lattice displacement model. The correctness of these concepts is confirmed by independent conclusions drawn by various authors on the basis of measurements made in different materials. Hence MS measurements can be used as a tool for studying the collective pinning mechanisms. Investigations of SC compounds with paramagnetic ions also revealed MS hysteresis in the region of mixed state of superconductivity which may be described in terms of the magnetic flux pinning. On the other hand, analogous dependences of giant MS ($\sim 10^{-4}$) were measured in manganites which are also oxides with a perovskite-type structure,[86] where superconductivity concepts are untenable. While studying SC compounds containing paramagnetic ions, we isolated an MS component with a quadratic dependence on the applied field, which is a characteristic feature for the paramagnetic limit. This component was found to be connected with the one-ion crystal electric field (CEF) lowering the symmetry of the basal plane. Such measurements make it possible to obtain the magnetoelastic interaction parameters for paramagnetic ions: $\epsilon^\gamma \simeq 300\times 10^{-6}$ at 10 K and 12 T for Dy- and Ho-based compounds.

Thus, the results of MS measurements reflect the elastic response of the superconducting phase to the applied magnetic field in pure form or together with para- and AFM response. In all the cases considered by us, we were able to separate the SC and magnetic response, and to analyze MS components in the framework of the concepts developed for each kind of material. It must be mentioned here that, while a universally accepted description exists for the induced MS of paramagnetic ions and has been tested for the results of macroscopic and local measurements, the phenomenology of induced suprastriction is based on the measurements of integral characteristics and provides only a qualitative, albeit effective, interpretation for the observed data.

Apart from the possibility of constructing the theory of magnetoelastic interactions in SC, MS measurements in superconducting compounds are found to be an effective tool for studying (1) the pressure dependence of thermodynamic characteristics of SC, (2) the relation between superconductivity with structural instability, (3) the mixed state, or the applicability of the critical state models and magnetic flux pinning mechanisms in SC, and (4) interaction of superconductivity and magnetism. Additional possibilities emerge during investigations of the dynamic striction in SC, but these have been little studied and have not been touched upon in this review.

Several applied aspects of strictional measurements in SC compounds have been revealed so far. Above all, this concerns the development and applications of SC magnetic systems based on prospective materials. Strictional data are required for estimating the elastic deformations of superconducting windings in strong magnetic fields, their effect on the current-carrying capacity, strength characteristics, and in the processes of training and degradation of hard superconductors. The direct connection between the induced striction and magnetic states in the Shubnikov phase makes these measurements as significant as visual observations using different indicators. It is also interesting to study the possibility of using high striction characteristics of some new superconducting materials, e.g., in magnetoacoustic transducers.

While studying the intrinsic nature of MS in superconductors, special attention should be paid to the ''giant'' induced striction in HTSC, which obviously cannot be explained just by the peculiarities of the mixed state of these compounds. The region connected with the magnetic field dependence of the elastic moduli tensor in a highly anisotropic medium has practically not been studied at all. The high values of the upper critical fields in the latest SC presume contributions made to MS due to electron paramagnetism and the splitting of degenerate levels. Considering the fact that ranges of all interactions in highly correlated superconducting copper oxides are of the order of atomic spacing, it can be stated that the peculiarities of the field dependences of MS in these compounds with different substitutions provide enormous possibilities (which have not been realized so far) of comparing the crystal field effects (change in the oxygen concentration and the resulting symmetry variation of the surroundings of the central atom), electron–phonon interactions (superconducting planes, Jahn–Teller copper ions) and quadrupole interactions (RE ions). The large values of MS in new SC materials make it possible to carry out measurements using less sensitive methods like strain gauge or x-ray technique. However, the creation of strong magnetic fields (over 10 T) is a problem. An analysis of the results of measurements of irreversible field dependences cannot be carried out with the help of thermodynamic relations and is confined to magnetoelastic and magnetic interactions leading to a global rearrangement of a highly correlated system in a magnetic field, including structural and electronic transitions. Thus, the problem of striction in SC is slipping rapidly from the realm of dilatometric measurements to magnetic investigations, including magnetic resonance and measurements in pulsed magnetic fields. The authors hope that this review will attract the attention of specialists in both fields towards this problem and will facilitate its solution by experimental and theoretical methods, resulting in specific practical applications.

*E-mail: sirenko@ilt.kharkov.ua
**E-mail: szymh@gammal.ifpan.edu.pl

[1] B. G. Lazarev and A. I. Sudovtsev, Dokl. Akad. Nauk SSSR **69**, 1345 (1949).
[2] G. Brändli, Phys. Kondens. Mater. **11**, 93 (1970).
[3] H. Kronmüller, Phys. Status Solidi **40**, 295 (1970).
[4] L. D. Landau and I. M. Lifshitz, *Electrodynamics of Continuous Media* [in Russian], Nauka, Moscow (1976).
[5] P. De Gennes, *Superconductivity of Metals and Alloys*, New York (1966).
[6] W. Braunisch, N. Knauf, V. Kataev *et al.*, Phys. Rev. Lett. **68**, 1908 (1992).
[7] F. N. Bukhan'ko, Fiz. Nizk. Temp. **22**, 701 (1996) [Low Temp. Phys. **22**, 539 (1996)].
[8] E. R. Callen and H. B. Callen, Phys. Rev. A **129**, 578 (1963); *ibid.* **39**, A455 (1965).
[9] A. E. Clark, B. F. De Savage, and R. Bozorth, Phys. Rev. A **138**, A216 (1965).
[10] Guo-meng Zhao, M. B. Hunt, H. Keller, and K. A. Müller, Nature (London) **385**, 236 (1997).
[11] Guo-meng Zhao, M. B. Hunt, and H. Keller, Phys. Rev. Lett. **78**, 955 (1997).
[12] K. L. Dudko, V. V. Eremenko, and V. M. Fridman, Sov. Phys. JETP **34**, 362 (1971).
[13] K. L. Dudko, V. V. Eremenko, and V. M. Fridman, Sov. Phys. JETP **41**, 326 (1975).
[14] G. K. White, Philos. Mag. **7**, 271 (1962).
[15] K. Andres, J. L. Olsen, and H. Rohrer, IBM J. Res. Dev. **84**, 6 (1962).
[16] H. Rohrer, Helv. Phys. Acta **33**, 675 (1960).
[17] G. Brändli and F. D. Enck, Phys. Lett. **26A**, 360 (1968).
[18] D. Shoenberg, *Superconductivity*, Cambridge University Press (1952).
[19] R. Testardi, in *Instability and Superconductivity in A15 Compounds* [Russian translation], Mir, Moscow (1982).
[20] V. V. Eremenko, V. A. Sirenko, H. Szymczak *et al.*, Fiz. Tverd. Tela (St. Petersburg) **40**, 1199 (1998) [Phys. Solid State **40**, 1091 (1998)].
[21] H. Svensmark and L. M. Falikov, Phys. Rev. B **40**, 201 (1989).
[22] V. G. Bar'yakhtar, V. N. Varyukin, and A. B. Nazarenko, Sverkhprovodimost: Fiz., Khim., Tekh. **3**, 1145 (1990).
[23] I. N. Nechiporenko, V. A. Sirenko, and D. N. Merenkov, Cryogenics **33**, 481 (1993).
[24] H. C. Freyhardt, in *Intern. Discussion Meeting on Flux Pinning in Superconductors*, Sonnenberg, Germany (1974).
[25] C. P. Bean, Phys. Rev. Lett. **8**, 250 (1962).
[26] V. B. Kim, C. F. Hempstead, and A. R. Strnad, Phys. Rev. Lett. **9**, 306 (1962).
[27] V. R. Karasik, N. G. Vasil'ev, and V. G. Ershov, Zh. Éksp. Teor. Fiz. **59**, 790 (1971) [Sov. Phys. JETP **32**, 433 (1971)].
[28] S. Senoissi, M. Ouss'ena, G. Collin, and I. A. Campbell, Phys. Rev. B **37**, 9792 (1988).
[29] W. A. Fietz and W. W. Webb, Phys. Rev. **B178**, 657 (1969).
[30] E. J. Kramer, J. Appl. Phys. **44**, 1360 (1973).
[31] M. Isino, T. Kobayashi, N. Toyota *et al.*, Phys. Rev. B **38**, 4457 (1988).
[32] U. Wyder, P. J. E. M. van der Linden, H. P. van der Meulen *et al.*, Physica B **211**, 265 (1995).
[33] C. de la Fuente, A. del Moral, J. I. Arnaudas, and J. S. Abell, Physica C **244**, 214 (1995).
[34] N. H. van Dijk, A. de Visser, J. J. M. Franse, and A. A. Menovsky, Phys. Rev. B **51**, 12 665 (1995).
[35] M. Braden, P. Böhm, H. Kalenborn, and D. Wohlleben, Z. Phys. B **79**, 173 (1990).
[36] L. V. Shubnikov, V. I. Khotkevich, Yu. D. Shepelev, and Yu. N. Ryabinin, Zh. Éksp. Teor. Fiz. **7**, 221 (1937).
[37] R. Labush, Phys. Rev. **170**, 470 (1968).
[38] H. Ikuta, N. Hirota, Y. Nakayama *et al.*, Phys. Rev. Lett. **70**, 2166 (1993).
[39] R. H. Arendt, M. F. Garbauskas, C. A. Meyer *et al.*, Physica C **182**, 73 (1991).
[40] V. V. Eremenko, I. N. Nechiporenko, and V. A. Sirenko, Physica C **282–287**, 1427 (1997).
[41] S. Sergeenkov and M. Ausloos, Phys. Rev. B **48**, 604 (1993).
[42] A. Nabialek, P. Komorowski, M. U. Gutowska *et al.*, Supercond. Sci. Technol. **10**, 786 (1997).
[43] A. P. Malozemoff and L. Krusin-Elbaum, Phys. Rev. B **38**, 6490 (1988).
[44] T. Nichizaki, T. Aomine, I. Fujii *et al.*, Physica C **181**, 233 (1991).
[45] R. A. Rose *et al.*, Supercond. Sci. Technol. **5**, S487 (1992).
[46] P. W. Anderson and Y. B. Kim, Rev. Mod. Phys. **36**, 39 (1964).
[47] D. Dew-Hughes, Cryogenics **28**, 674 (1988).
[48] H. Ikuta, K. Kichio, and K. Kitazawa, J. Appl. Phys. **76**, 4776 (1994).
[49] G. W. Crabtree and D. R. Nelson, Phys. Today April (1997).
[50] A. V. Bondar', S. M. Ryabchenko, and Yu. V. Fedotov, Fiz. Nizk. Temp. **20**, 95 (1994) [Low Temp. Phys. **20**, 77 (1994)].

[51] E. H. Brandt, M. V. Indenbom, and A. Forkl, Europhys. Lett. **22**, 735 (1993).
[52] V. V. Eremenko, V. A. Sirenko, H. Szymczak *et al.*, Superlattices Microstruct. **24**, 221 (1998).
[53] E. V. Bezuglyi, N. G. Burma, I. G. Kolobov *et al.*, Fiz. Nizk. Temp. **21**, 86 (1995) [Low Temp. Phys. **21**, 65 (1995)].
[54] E. H. Brandt, Phys. Rev. B **54**, 4246 (1996).
[55] P. Thalmeier and P. Fulde, Europhys. Lett. **1**, 367 (1986).
[56] S. Pei, J. D. Jorgensen, B. Dobrowski *et al.*, Phys. Rev. B **41**, 4126 (1990).
[57] S. N. Barilo, V. I. Gatalskaya, S. V. Siryaev *et al.*, Physica C **254**, 181 (1995).
[58] C. Paraechini, L. Romana, C. A. Bori, and M. Affronte, Physica C **260**, 147 (1996).
[59] T. Yamamoto, S. Suzuki, K. Takahashi, and Y. Yoshisato, Physica C **263**, 530 (1996).
[60] O. Navarro, Physica C **265**, 73 (1996).
[61] A. Ignatov, A. Menushenkov, and V. Chernov, Physica C **271**, 32 (1996).
[62] W. Herneit, T. Klein, C. Escribe-Filippini *et al.*, Physica C **267**, 270 (1996).
[63] B. Batlogg, R. J. Cava, L. W. Pupp, Jr. *et al.*, Phys. Rev. Lett. **61**, 1670 (1988).
[64] L. D. Landau and E. M. Lifshitz, *Theory of Elasticity* [in Russian], Nauka, Moscow (1987). [Trans. of 4th ed. Pergams. Oxford]
[65] M. Braden, W. Reichardt, W. Schmidbauer *et al.*, J. Supercond. **8**, 595 (1995).
[66] N. F. Vedernikov, A. K. Zvezdin, R. Z. Levitin, and 1978 A. I. Popov, Zh. Éksp. Teor. Fiz. **14**, 358 (1988) [*sic*].
[67] V. V. Eremenko, *Introduction to Optical Spectroscopy of Magnets* [in Russian], Naukova Dumka, Kiev (1975).
[68] P. Morin, J. Rouchy, and D. Schmitt, Phys. Rev. B **37**, 5401 (1988).
[69] A. Furrer, P. Brüesch and P. Unternäher, Phys. Rev. B **38**, 4616 (1988).
[70] P. Allenspach, A. Furrer, and F. Hullinger, Phys. Rev. B **39**, 2226 (1989).
[71] A. Podlesnyak, V. Kozhevnikov, A. Mirmelstein *et al.*, Physica C **175**, 587 (1991).
[72] A. Morris, *Physical Principles of Magnetism*, Wiley, New York (1965).
[73] J. M. Ferreira, H. Zhou, R. R. Hake *et al.*, J. Appl. Phys. **A47**, 105 (1988).
[74] A. I. Goldman, B. X. Yang, J. Tranqeada *et al.*, Phys. Rev. B **36**, 7234 (1987).
[75] H. D. Yang, H. C. Ku, P. Klavins, and R. N. Shelton, Phys. Rev. B **36**, 8791 (1987).
[76] A. P. Ramirez, L. F. Shneemeyer, and J. V. Waszczak, Phys. Rev. B **36**, 7145 (1987).
[77] A. Furrer, P. Bruesch, P. Unternahrer, Solid State Commun. **67**, 69 (1988).
[78] A. del Moral, M. Ibarra, J. Arnaudas *et al.*, J. Magn. Magn. Mater. **76–77**, 612 (1988).
[79] A. K. Zvezdin, A. M. Kadomtseva, N. P. Kolmakova *et al.*, Sverkhprovodimost: Fiz., Khim., Tekh. **2**, 87 (1989).
[80] N. N. Efimova, Yu. A. Popkov, N. B. Ustimenkova, and V. A. Finkel, Fiz. Nizk. Temp. **20**, 343 (1994) [Low Temp. Phys. **20**, 273 (1994)].
[81] Yu. M. Poluektov, Fiz. Nizk. Temp. **21**, 183 (1995) [Low Temp. Phys. **21**, 138 (1995)].
[82] V. Nekvasil, Solid State Commun. **65**, 1103 (1988).
[83] R. L. Rasera, B. D. Dunlap, and G. K. Shenoy, Phys. Rev. Lett. **41**, 1188 (1978).
[84] P. M. Levy, P. Morin, and D. Schmitt, Phys. Rev. Lett. **42**, 1417 (1979).
[85] V. V. Eremenko, D. V. Lukashev, K. M. Matsievskii, and V. L. Ponomarchuk, Fiz. Nizk. Temp. **22**, 1383 (1996) [Low Temp. Phys. **22**, 1048 (1996)].
[86] A. Asamitsu, Y. Moritomo, Y. Tomioka *et al.*, Nature (London) **373**, 407 (1995).

Translated by R. S. Wadhwa

QUANTUM LIQUIDS AND QUANTUM CRYSTALS

Static phenomena at the charged surface of liquid hydrogen

A. A. Levchenko, G. V. Kolmakov, L. P. Mezhov-Deglin,
M. G. Mikhailov, and A. B. Trusov

*Institute of Solid State Physics, Russian Academy of Sciences, 142432 Chernogolovka, Moscow Region, Russia**

(Submitted November 17, 1998)
Fiz. Nizk. Temp. **25**, 333–342 (April 1999)

Evolution of the shape of the equipotentially charged surface of the liquid hydrogen layer covering the lower plate of a horizontally arranged flat diode in increasing external stretching electric fields has been studied experimentally for the first time. Reconstruction of a flat charged surface (formation of a stationary hump) at voltages higher than a certain critical value U_{c1} is observed under conditions of total compensation of the electric field in the bulk of the liquid by a surface charge. It is shown that the transition of the flat charged surface to the reconstructed state is a phase transition close to a second-order transition. The height of the hump is found to increase with voltage, the reconstructed surface loses its ability at a voltage $U_{c2}>1.2U_{c1}$, and a streamed discharge is observed. Evolution of the shape of a charged droplet of constant volume suspended from the upper plate of a diode is studied with increasing electric field under the conditions when the forces of gravity and stretching electric field act in the same direction. © *1999 American Institute of Physics.* [S1063-777X(99)00204-2]

1. INTRODUCTION

Experiments[1] have revealed the possibility of creating a charge layer under the surface of liquid hydrogen, the sign and concentration of the charge being determined by the polarity and magnitude of the applied electric field E. In this work, we study the evolution of the shape of the positively charged equipotential liquid hydrogen surface under the action of a stretching electric field of intensity up to 10^4 V/cm in the temperature range 14–25 K.

It is well known that, if the charged flat surface of a liquid is subjected to an external electric field E applied at right angles to it (the surface), it loses its stability in fields stronger than a certain critical value.[2] The subsequent behavior of the charged surface depends on the conditions of observation.[3–8] For a fixed charge density lower than the maximum attainable in a given field, i.e., for $n<n_{\max}=E/4\pi$ (it is assumed that $e=1$), reconstruction may be observed in the form of static deformation at the surface. For a weakly charged surface $4\pi n \ll E$, $E^2>16.5\sqrt{\rho g \alpha}$, where α and ρ are the surface tension and density of the liquid and g is the acceleration due to gravity), multiply charged dimples[3] with characteristic size close to the capillary length $\lambda=\sqrt{\alpha/\rho g}$ are formed on the surface. Away from the center, the density of charges vanishes at the edges of the dimples. With increasing charge concentration, a different situation arises and a *crater crystal* is formed at the surface.[4]

To date, the reconstruction of the charged equipotential surface of liquid helium (in which the electrons are localized over the liquid surface) has been studied most extensively under the conditions when the thickness h of the liquid layer, i.e., the distance between the charged surface and the metallic control electrode at the bottom of the cell, is much larger than the capillary length λ, while the number of charges is fixed ($n<n_{\max}$) so that the compressing electric field is nonzero both in liquid and in gas. In this case, the liquid surface is reconstructed in a field higher than a certain critical field E_c, and a hexagonal structure with period $\sim\lambda$ and a finite depth of the dimple that depends on the extent of supercriticality (dimple crystal) is formed.[3–9] The charge density vanishes at the sites of the hexagonal lattice so that the surface is no longer equipotential. Reconstruction of the charged surface for a fixed number of charges $n<n_{\max}$ is a first-order phase transition in a state with individual multiply charged dimples, as well as in the dimple crystal state.

Reconstruction of the charged surface of a liquid was not observed earlier for complete compensation of the applied electric field by surface charges $n=n_{\max}$. It was found that the critical electric field E_c in which the flat surface of a thick liquid layer ($h\gg\lambda$) loses stability is independent of the value of h. For layer thicknesses $h\sim\lambda$, the value of E_c decreases with h,[10] while the variation for $h<\lambda$ is described by the dependence $E_c^2=4\pi\rho g h$.[11,12]

The possibility of observing the steady state of the reconstructed charged surface of a thin helium film of thickness $h\ll\lambda$ for a complete compensation of the applied electric field by charges was discussed recently by Shikin and Leiderer.[13] However, the stationary reconstruction of a charged liquid surface in the transient region of thickness $h\approx\lambda$ has not been studied earlier.

In the experiments discussed below, the situation differs

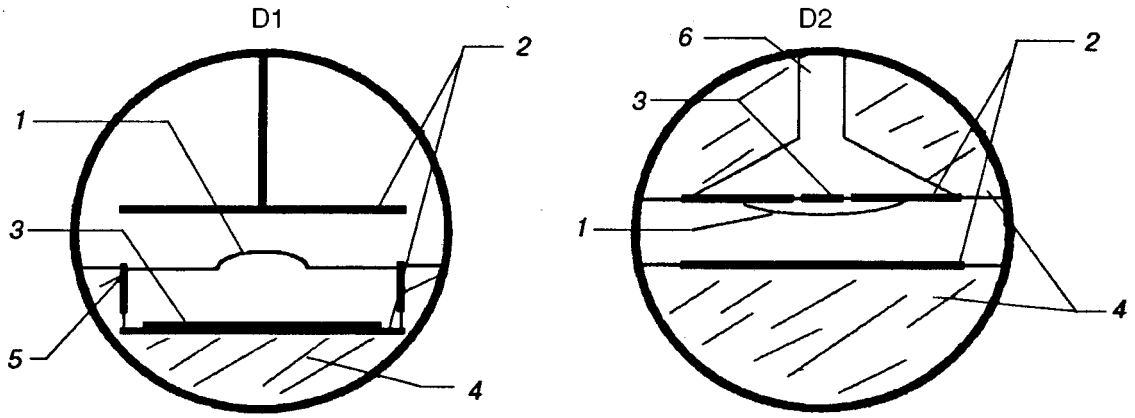

FIG. 1. Construction of the experimental cell with diodes D1 and D2: *1*—liquid hydrogen surface; *2*—copper plates of the diode; *3*—radioactive source; *4*—paper-based laminate; *5*—guard ring; *6*—copper finger.

radically from the one studied earlier: positive charges (clusters of diameter $\simeq 5$ Å)[1] are localized under the surface of the liquid hydrogen layer. The control electrode (collector) is situated in the vapor above the liquid surface at a distance $d \approx \lambda$, i.e., the liquid layer thickness h should be replaced by the distance d in theoretical calculations. The charge density $n = n_{\max}$ under the surface depends on the voltage U applied to the capacitor plates, so that $E = U/d$ in the steady state, and the charged layer completely compensates the electric field in the bulk of the liquid in fields lower as well as higher than the critical value E_c.

Our experiments show that the static reconstruction of the surface is possible under conditions $d \approx \lambda$ and $n = n_{\max}$. In an earlier work,[14] we reported on the observation of reconstruction of charged surface of liquid hydrogen as well as helium (electrons over the surface of a liquid layer of thickness $h \approx \lambda$). The investigation of evolution of the flat charged surface of the liquid hydrogen layer deposited on the lower plate of the diode was supplemented by that of evolution (in an increasing electric field) of the shape of a charged drop of constant volume formed during condensation of hydrogen vapor on the upper plate of the diode.

2. EXPERIMENTAL TECHNIQUE

Experiments were carried out in two types of cells (flat diodes D1 and D2) placed in an optical container (Fig. 1). The containers were put in the vacuum chamber of an optical helium cryostat and cooled by a copper finger in contact with liquid helium.

The charge sources were radioactive plates (targets) emitting β-particles with an average energy 5 keV and a maximum energy ~ 18 keV, which were located in the liquid and ionized a liquid layer of thickness $\sim 10\,\mu$m near the plate. The sign of charges pressed to the plate surface depends on the polarity of the voltage U applied between the diode plates. The current passing through the surface was measured by using an electrometer connected to the collector in vapor. We studied the properties of a positively charged surface since positive charges practically do not pass through the liquid hydrogen–vapor interface for voltages used in our experiments.[1]

A guard ring of diameter 25 mm and height 3 mm made of foil-clad paper-based laminate surrounded the radioactive plate in the diode D1 and prevented the leakage of charge from the liquid surface at the container walls. The guard ring and the radioactive target formed a cylinder in which hydrogen was condensed. The liquid layer thickness was 3 mm. A second metallic collector plate of diameter 25 mm was placed over the cylinder. The separation between the source and collector was 6 mm.

In diode D2, a target of diameter 3 mm was arranged on the specially cooled upper copper plate of the diode, on which hydrogen was condensed. The collector was at the bottom and the distance between the source and the collector was about 3 mm.

The shape of the charged surface was controlled visually and with the help of a telecamera. The variation in the curvature of the charged surface was determined from the deviation of a laser beam almost parallel to the surface and reflected at it.

Figure 2a shows the photograph of the reconstructed charge surface of liquid helium condensed on the lower plate of the diode D1 for a potential difference $U = 1620$ V between plates and at a temperature $T = 17$ K. The hump can be clearly seen in the middle of the photograph. It should be observed that the linear horizontal size of surface region shown in the photograph is 10 mm, which is two and a half times smaller than the diameter of the guard ring.

Using the heaters at the container walls and plates of diode D2, the temperature of the lower plate was raised above the temperature of the upper plate. Gaseous hydrogen was condensed mainly on the upper plate. Condensation took place for $U = 0$. As the thickness of the liquid layer increased, the shape of its uncharged surface changed from nearly flat for small volumes of the liquid in the layer ($V < 5$ mm^3) to a drop for larger volumes. On completion of condensation, the container was maintained for tens of minutes at a constant temperature for a total recondensation of the liquid from the container walls and the lower plate to the upper plate of the diode. Application of a potential difference between the diode plates led to the accumulation of charges under the liquid surface. In addition to the forces of gravity,

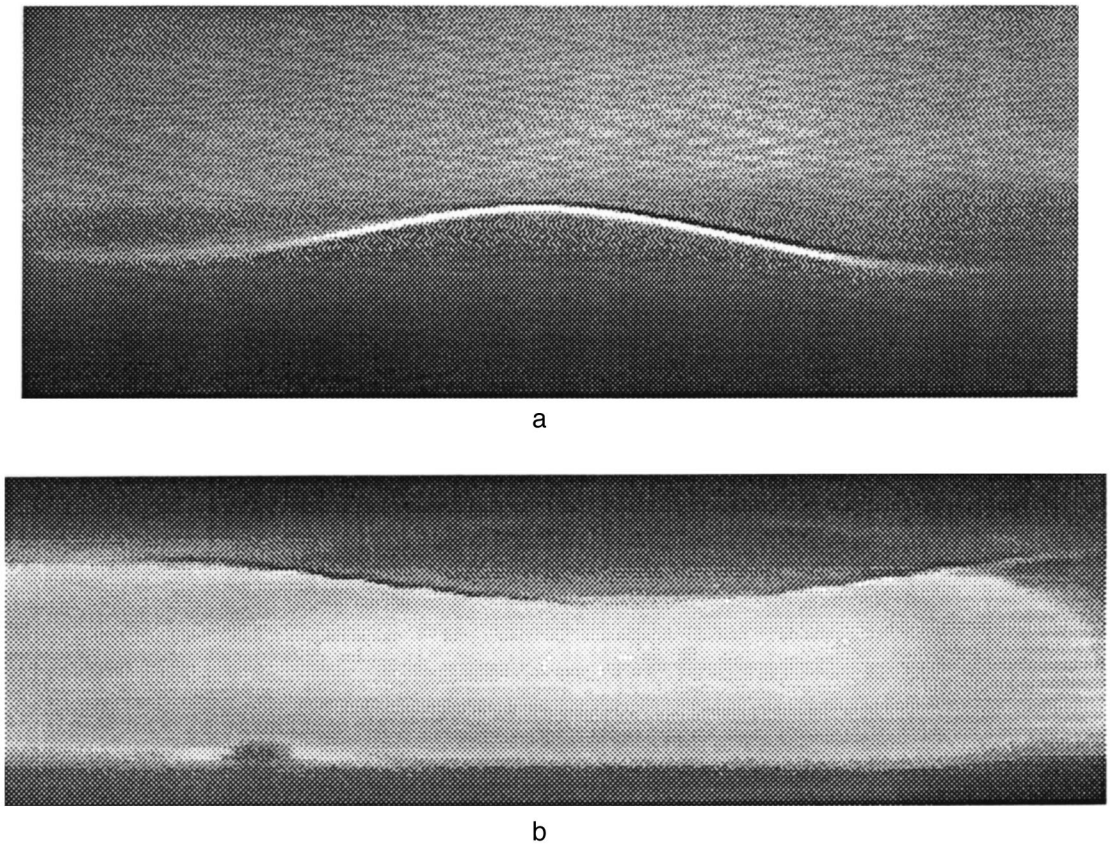

FIG. 2. Photograph of the charged surface of liquid hydrogen condensed on the lower plate of diode D1 (a) and the charged surface of a drop wetting the upper plate of the diode D2 (b). The linear horizontal size of the visible image is 10 mm.

the drop is also acted upon by electric forces in the same direction. This resulted in a change in the profile of the charged surface of the liquid hydrogen drop. Figure 2b shows the photograph of the equilibrium profile of the charged surface of the liquid hydrogen drop for a potential difference $U=500$ V between the plates of the diode. Measurements were made at a temperature 18.5 K.

3. EXPERIMENTAL RESULTS

Let us first consider the results of investigations of properties of an equipotentially charged surface of liquid hydrogen condensed on the lower plate of the diode D1.

For low potential differences between the plates of the diode, the equipotentially charged surface of the liquid is slightly bent towards the collector. As the applied voltage increases beyond a certain critical value U_{c1}, a macroscopic hump extending over several millimeters and having a height of the order of 0.1 mm is formed on the surface. This solitary hump can be displaced towards the center of the diode by slightly tilting the cell. Light circles in Fig. 3 were obtained by scanning the image of the hump profile. In a constant field, the shape of the profile remained unchanged during measurements over a period exceeding 10^3 s. while the current carried by the charges through the liquid surface, which was measured with the help of an electrometer connected to the upper plate of the diode, was less than 10^{-15} A. The height of the deformed region of the surface (hump) at the center of the diode can be controlled by varying the voltage applied between the plates of the diode. For voltages exceeding the lower critical voltage U_{c1} by about 20%, the hump on the charged surface became unstable and a pulse discharge (upper critical voltage U_{c2}) was observed. During the discharge, a charged stream (geyser) burst from the peak of the hump (see Fig. 4). The discharge at the collector involves about 10^8 charges. For a constant voltage, the surface reverted to the initial flat form after discharge, and the process was repeated. The observation of quasiperiodic current oscillations through the liquid hydrogen surface in fields $U>U_{c2}$ was reported by us earlier.[1] For voltages several times higher than U_{c2}, the surface became flat once again

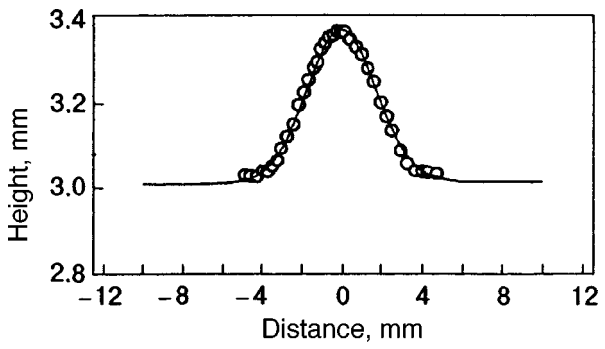

FIG. 3. Profile of a charged hump obtained by photograph scanning. The radius of the guard ring is 12.5 mm, $U=1620$ V, $T=17$ K.

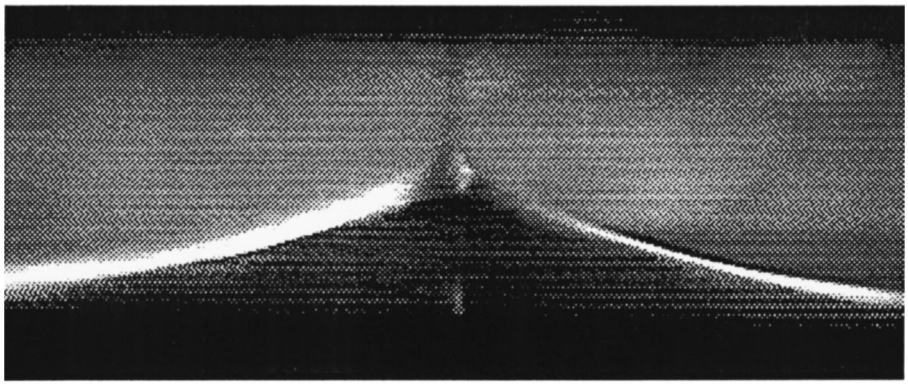

FIG. 4. Photograph of a charged surface at the instant of discharge for $U=1750$ V, $T=15$ K. The horizontal size is 5 mm.

and the electrometer recorded the flow of charges through the surface without the formation of any structure on it. The current flowing in the diode was smaller than the saturation current in the liquid, i.e., the electric field was weaker than the breakdown field in liquid or in gas. Apparently, a similar phenomenon was observed earlier by Boyle and Dahm[15] in their experiments on liquid helium and nitrogen.

Figure 5 shows the dependence of the maximum angle β of deviation of the laser beam reflected at the hydrogen surface on the applied voltage U at temperatures 15, 20 and 25.4 K. It should be emphasized that the experimentally observed point on the surface corresponds to the largest angle of reflection. The inset shows the derivative $\beta'(U)=d\beta/dU$ of the dependence $\beta(U)$ measured at 20 K. It can be seen that for low voltages $U<U_{c1}$, the angle β increases weakly with voltage. For voltages exceeding the critical voltage U_{c1} indicated by an arrow in the figure, the derivative β' depends much more strongly on U. It can be seen from the inset to Fig. 5 that the value of U_{c1} can be determined from the dependence $\beta'(U)$. Such dependences were used for determining the values of U_{c1} at various temperatures (Fig. 6). With increasing temperature, the value of U_{c1} decreases. The upper critical voltage U_{c2} at which a discharge of the reconstructed surface was observed decreases with the liquid temperature according to a nearly linear law (see Fig. 6).

Let us now consider the results of investigation of the evolution of an equipotentially charged surface of liquid hydrogen condensed on the upper plate of the diode D2.

For zero voltage, the shape of the surface of the initial liquid layer wetting the upper electrode was nearly flat for a liquid volume below 5 mm^3 and assumed the shape of a drop upon an increase in the volume of the liquid.

The profile of a charged drop of volume $V=30$ mm^3 is shown in Fig. 7 for a potential difference $U=350$ V between the plates of the diode. With increasing voltage, the amplitude of the drop increased and a discharge was observed for a certain voltage U_{c3}. This critical voltage depends on the volume of the liquid in the drop (amplitude for $U=0$). For the volume of the liquid in the drop considered by us, the discharge occurred at $U=800$ V. The volume of the liquid in the drop was estimated by integrating the profile of the drop. The absolute error in the volume estimate was $\pm 10\%$.

Figure 8 shows the dependence of the amplitude of a drop on the applied voltage. The volume of liquid in the drop was estimated at about 60 mm^3. Unlike the case of a flat layer in the diode D1, the amplitude of the drop increases under voltages much smaller than the lower critical voltage U_{c1} of surface reconstruction for a liquid layer on the lower plate of the diode D1. The amplitude A of the drop increases monotonically with increasing voltage according to a law $A \sim U^{\eta}$ that is stronger than linear ($\eta>1$).

For the sake of comparison, Fig. 9 shows the dependence of the amplitude A of a drop on the volume of the liquid in zero field (dark circles) and under a constant

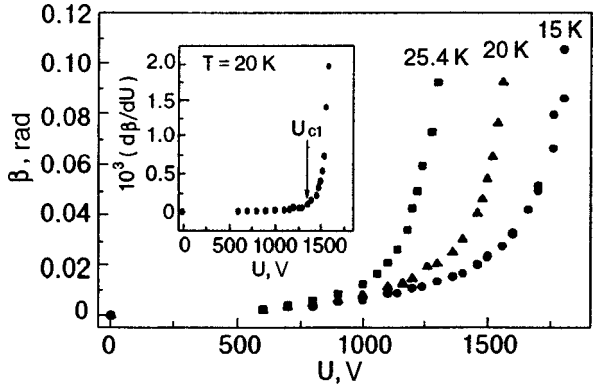

FIG. 5. Dependence of the laser beam reflection angle β on the applied voltage U. The inset shows the derivative $\beta'(U)$ with respect to voltage at 20 K. The arrow indicates the lower critical voltage U_{c1}.

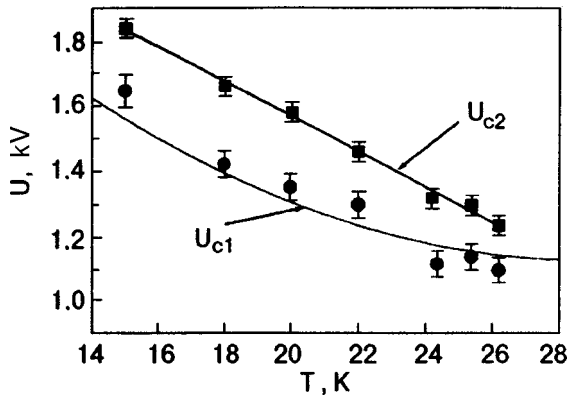

FIG. 6. Temperature dependence of the lower (U_{c1}) and upper (U_{c2}) critical voltages for the charged surface of liquid hydrogen: the points correspond to the experimental results, while the solid curves $U_{c1}(T)$ were obtained theoretically.

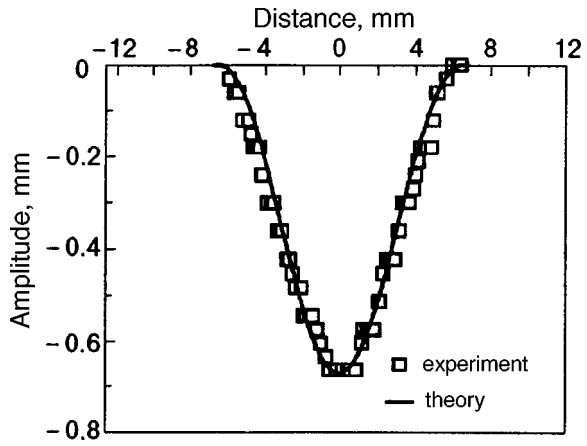

FIG. 7. Profile of the surface of a charged drop of volume 30 mm^3 at $U=350$ V and $T=15$ K. The diameter of the upper plate of the diode is equal to 25 mm.

voltage $U=630$ V between the plates (light squares). The volume of the liquid was varied by vaporizing at temperature 18.5 K. It can be seen that a decrease in the liquid volume leads to a monotonic decrease in the amplitude of the drop. Application of a potential difference between the diode plates leads to an increase in the amplitude of the drop and a change in the dependence $A(V)$.

4. DISCUSSION OF RESULTS

It should be remarked at the very outset that the situation in which the reconstruction of the flat charged surface of liquid hydrogen was observed in our experiments differs qualitatively from the situation studied by Leiderer *et al.*,[3] under which the total number of charges at the surface is fixed and the charge concentration away from the center of

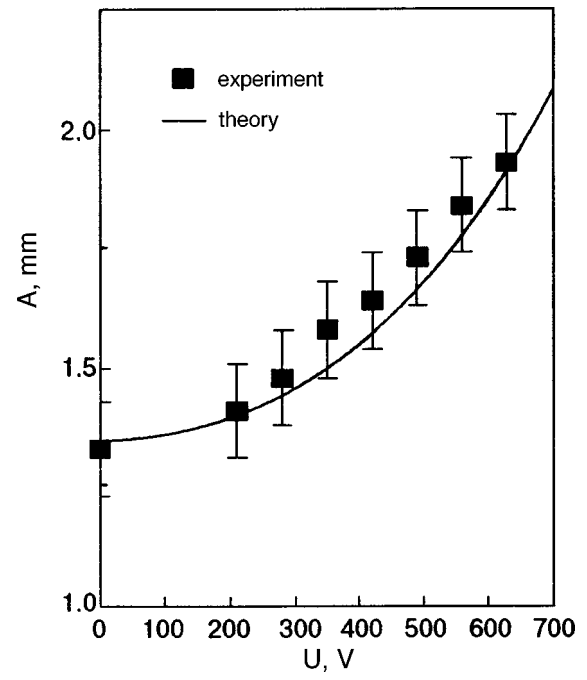

FIG. 8. Dependence of the amplitude A of a drop having a constant volume $V_0=60$ mm^3 on the applied voltage at the liquid temperature 19.3 K.

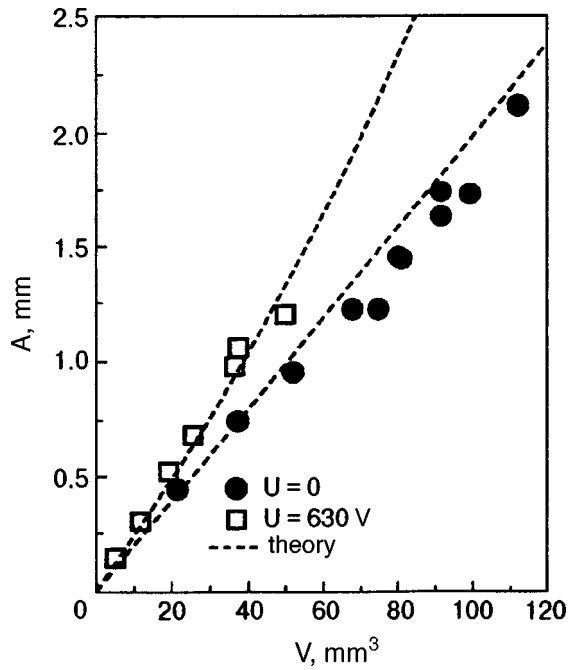

FIG. 9. Dependence of the amplitude A on the liquid volume V in an electric field (□) and in zero field (●) at a temperature 18.5 K of the liquid.

the reconstructed surface region and outside an individual multi-electron crater is equal to zero, so that the electric field near the surface is nonuniform and equipotentiality is observed only in the charged core of the dimple. In our experiments, the charge density under the surface is not equal to zero away from the deformed region (hump), and is determined by the voltage applied between the diode plates. The entire reconstructed surface remains equipotential since we used in our experiments a continuous charge source and the number of charges under the surface increases with the voltage applied to the charge source and the guard ring. Thus, the hump on the charged surface (Fig. 2a) is not an analog of the multiply charged dimple formed under conditions of a weakly charged surface of bulk helium.[3]

It was mentioned in the Introduction that steady state reconstruction of a charged flat liquid surface was not observed earlier for a complete compensation of the confining field by the charges. In our experiments, the lifetime of the charged hump is quite large (over 10^3 s) in the voltage region $U_{c1}<U<U_{c2}$, and hence we can speak of a stationary reconstructed equipotential surface layer of hydrogen under conditions when the separation d between the charged surface and the control electrode is of the order of λ.

In accordance with the results of investigations of the passage of charged particles through the liquid hydrogen–vapor interface,[1] it can be assumed that positive charges practically do not pass through the surface in the investigated range of electric fields and temperatures, while the charge accumulated under the liquid–vapor interface in the steady state fully compensates the applied electric field in the bulk of the liquid. Hence the problem of finding the equilibrium shape of the surface of the liquid in an applied static electric field under these conditions is analogous to the same problem for a liquid conductor. In some recent publications,[13,16]

theoretical models were considered for describing the equilibrium reconstruction of a charged surface in the supercritical voltage region, i.e., for $U > U_{c1}$.

Shikin and Leiderer[13] considered the one-dimensional case corresponding to the formation of a periodic system of ''waves'' on the infinite surface of a thin helium film ($h \ll \lambda$) charged by electrons in a confining field $E > U_{c1}/h$. An individual wave (hump) corresponds to an infinitely long period (much larger than the diameter of the experimental cell under conditions of our experiment). The shape of the surface of the hump can be described by a bell-shaped function of the dimensionless parameter x/R, where R is the characteristic horizontal size.

In an earlier publication,[16] we developed a somewhat different theoretical model describing the reconstruction of the flat charged surface of a liquid in a finite-sized vessel for $d \ll \lambda$, taking into account the conservation of the volume of liquid in the layer and the conditions of wetting of the vessel walls by the liquid as the charges completely compensate the stretching electric field in the bulk of the liquid. The reconstructed charged surface also has the form of a periodic function. For low voltages, the shape of the surface is close to cosinusoidal. A consideration of the boundary conditions (wetting angle) leads to a situation when a number of solutions can exist for a finite-sized cell, from a single wave in the center of the cell to an infinite number of symmetrically arranged waves. As in our experiment, the height of the hump may increase with increasing voltage between the plates of the diode. The question of preference of a solitary hump observed in the experiments over other solutions requires further analysis.

The profile of the hump presented in Fig. 3 can be described aptly by a bell-shaped function of the form $z(x) = Z \exp(-x^2/R^2)$, where Z is the height and R the characteristic size of the hump. The experimental points in Fig. 3 are connected through a curve which obeys the dependence $z(x)$ with fitting parameters $Z = 0.35$ mm and $R = 2.5$ mm The fitting function $z(x)$ chosen by us is a smooth integrable function satisfying the requirements imposed on such functions in Refs. 13 and 16. However, a quantitative comparison of the predictions of both theoretical models with experimental results is hampered mainly by the fact that the results obtained in Refs. 13 and 16 pertain to an essentially one-dimensional case and a thin layer $h \ll \lambda$ or $d \ll \lambda$, while $d \sim \lambda$ in the experiment. Moreover, the calculations made in Ref. 16 show that the field dependence of the height of the hump formed in a finite-sized vessel is highly sensitive to the choice of boundary conditions at the vessel walls. Hence the resemblance between theory and experiment may be only qualitative.

Theoretical models of reconstruction of charged surface of a liquid insulator[8,13,16] predict that the amplitude of the reconstructed surface must be a function of the supercriticality parameter $\gamma = (U^2/U_{c1}^2) - 1$. In our experiments, the evolution of the hump shape upon an increase in the applied voltage can be judged from the voltage dependence $\beta(U)$ of the angle at which a laser beam is reflected from the charged surface of hydrogen. It can be seen from Fig. 5 that there are two different regimes of variation of the shape of a free liquid surface, viz., (a) before the attainment of the lower critical voltage U_{c1} and (b) at voltages higher than U_{c1}. The initial segment $U < U_{c1}$ corresponds to a slight distortion of the charged liquid surface covering a fixed volume in the condenser field. For fields stronger than those corresponding to the lower critical voltage $U_{c1} < U < U_{c2}$ in which the surface is reconstructed, the experimental dependence may be described by the relation $\beta \propto \gamma^m$ (the exponent m lies between 2 and 3). This segment of the $\beta(U)$ curve describes the change in the inclination of the lateral surface of the hump upon an increase in the voltage U.

The values of the lower critical voltage U_{c1} corresponding to the emergence of a hump on the liquid surface were found to be close to the confining voltage at which an infinite [11], flat equipotentiality charged surface of a liquid layer of thickness much smaller than the capillary constant λ loses stability.

The solid curve in Fig. 6 shows the theoretical dependence of the critical voltage $U_{c1} = \sqrt{4\pi g \rho d^3}$ on the temperature of the liquid.[11] As the temperature increases, the quantity U_{c1} varies on account of a decrease in the density ρ and a change in the distance d between the liquid surface and the control electrode due to a redistribution of hydrogen between liquid and vapor phases in the closed volume of the container for a fixed mass of hydrogen (pressure in the container increases with temperature). It can be seen that in the temperature interval 15–26 K, the experimental values of U_{c1} are in good agreement with the theoretical curve $U_{c1}(T)$. Thus, the magnitude and temperature dependence of the lower critical voltage U_{c1} corresponding to the emergence of a hump on the liquid surface may be described by the simple model of a flat infinite thin charged surface. Like U_{c1}, the upper critical voltage U_{c2} decreases with increasing temperature, and this dependence is nearly linear (as an illustration, the experimental points U_{c2} are connected by a straight line).

For voltages higher than the upper critical value U_{c2}, the reconstructed charge surface is unstable. The jet stream emerging from the peak of the hump during discharge has a characteristic diameter of a few tenths of a millimeter, i.e., much smaller than the capillary length. An analogous effect involving the emergence of ion streams (geysers) at the surface of superfluid helium in strong fields was observed in Refs. 17, 18. Special investigations are required for studying growth of instability on the charged reconstructed surface under a voltage close to U_{c2} and the reasons behind the linear temperature dependence of U_{c2}.

A stationary hump on the charged surface can be singled out on the $U-T$ phase diagram, and hence it can be stated that we observe a phase transition from the flat charged surface to a new steady state.

Judging from the dependences $\beta(U)$ and $\beta'(U)$, the formation of a hump on an equipotentially charged surface under conditions of a complete compensation of the applied electric field by charges and conservation of the liquid volume in the layer is a transition close to the second-order phase transition.[16] The curve showing the dependence $\beta'(U)$ has a kink at the point $U = U_{c1}$. Within the limits of precision of our experiments, the height of the hump increases smoothly from zero with increasing stretching voltage for

$U > U_{c1}$. Note that the height of the hump is small in comparison with the distance d and the capillary length in the voltage range $U_{c1} < U < U_{c2}$.

It was mentioned in Ref. 16 that the height of the hump formed on the surface for $U = U_{c1}$ may have a finite value in view of the finite value of the angle of wetting of guard ring walls by the liquid. However, this initial height of the hump is small in comparison with the distance d, i.e., with the capillary length λ in our experiments because of a small wetting angle. Since liquid hydrogen was condensed in our experiments under the cut of the guard ring, the angle between the charged surface and the surface of the guard ring was indeed close to zero. Unfortunately, the specific conditions of our experiments were not considered in Ref. 16 in view of the complexity of the solution of the problem.

We shall now discuss the results obtained in our experiments with liquid hydrogen condensed on the upper plate of the diode.

We used the variational method to solve the problem about the shape of a charged drop formed on the upper plate of a diode under the action of the gravitational force and a stretching electric field in the bulk of the liquid.[19] This problem is equivalent to that of the equilibrium shape of the reconstructed surface of a charged liquid layer on the lower plate of the diode. The difference lies in the sign of the gravitational term in the expression for free energy and under the conditions of conservation of the volume of the liquid. In this problem, we find a stable minimum free energy of a drop for a constant total volume of the liquid. The expression for free energy is derived by using the longwave approximation and expansion in powers of $A/d \ll 1$, where A is the amplitude of the drop. For the trial function, we choose a certain dimensionless bell-shaped function $Af(|r|/R)$ of the variable $x = |r|/R$ (R is the effective linear size of the drop), which describes the shape of the free surface of a drop and is normalized by the condition $f(0) = 1$, $f(x) \to 0$ for $x \gg 1$. In view of a good wetting of the metallic plate by liquid hydrogen, the wetting angle at the boundary of the drop is assumed to be equal to zero.

The dependence of the amplitude of the drop on the applied voltage and the volume V of the liquid in the drop can be written in the form

$$A = \frac{c_1 V(\rho g + U^2/4\pi d^3)}{\alpha - c_2 V U^2/4\pi d^4}. \tag{1}$$

Here $c_{1,2}$ are parameters which than are determined only by the form of the trial function. For a function of the form

$$f(x) = \frac{J_0(x) - J_0(\beta_1)}{J_0(0) - J_0(\beta_1)} \quad \text{for} \quad 0 \leqslant x \leqslant \beta_1$$

$$f(x) = 0 \quad \text{for} \quad \beta_1 < x \tag{2}$$

[here $J_0(x)$ is the Bessel function, β_1 is the first zero of the first-order Bessel function, $J_1(\beta_1) = 0$], the parameters $c_{1,2}$ appearing in formula (1) have the following values: $c_1 = 0.0755$, $c_2 = 0.106$. The choice of the form (2) of the trial function $f(x)$ is justified in Ref. 19.

Unlike the case of a flat liquid layer on the lower plate of the diode, the force of gravity and the electric forces in the geometry considered by us act in the same direction (downwards), i.e., the gravity forces cannot be compensated by the electric forces. The equilibrium shape of the surface of a drop is stabilized by capillary forces. It follows from formula (1) that if gravity and electric forces stretch the surface of a charged drop, reconstruction would occur under the condition that the square of the voltage is negative and equal to $U_{c1}^2 = -4\pi\rho g d^3$ (for a positive g). In other words, the shape of the liquid surface corresponds to the reconstructed state even for $U = 0$. As the applied voltage is increased, the amplitude of the drop increases monotonically right up to voltages at which discharge occurs. This is in accord with the obtained experimental results.

The experimental profile of a charged drop is compared with the chosen trial function (2) in Fig. 7. It can be seen that the chosen trial function with fitting parameters $A = 0.7$ mm and an effective linear size $R = 1.7$ mm provide a satisfactory description of the experimental results.

The theoretical dependence (1) is compared with the experimental results in Figs. 8 and 9. In fitting of formula (1) to the experimental points, the volume V of the liquid is the only variable parameter. The theoretical dependence (1) is constructed in Fig. 8 for a drop whose volume is equal to the value estimated by integrating the profile, while the best agreement is attained in Fig. 9 by reducing the volume of the drop by 10% from the estimated value. Such a disparity in the values of V is within the limits of the experimental absolute error in the estimation of the volume of the drop. Hence it can be concluded that the theoretical dependence (1) correctly describes the experimental results.

It follows from formula (1) that the amplitude A of a drop increases indefinitely as the applied voltage U approaches the critical value $U_3 = \sqrt{40\pi\alpha d^4/V}$. For a liquid hydrogen drop of volume $V_0 = 30\ \text{mm}^3$ and for $d = 3$ mm, this critical value is estimated at $U_3 = 2500$ V. This quantity is about thrice as large as the experimentally observed value. Such a discrepancy can be explained quite easily since an indefinite increase of the amplitude A formally indicates that a drop of finite volume must be detached as a whole from the upper plate of the diode under critical voltage. Apparently, such a situation was realized in experiments with drops of large volume. An increase in the voltage in small drops led to discharge of the charged surface before the critical value U_3 was attained, i.e., the mechanism of loss of stability of a charged surface, which is different from that described in the theoretical model,[19] was realized earlier. Hence the dependence (1) correctly describes our experimental results only for voltages lower than the discharge voltage and, naturally, lower than U_3.

5. CONCLUSION

The following conclusions can be drawn from the data obtained in experiments with the charged surface of a hydrogen layer condensed on the lower plate of a horizontal diode.

The steady-state reconstruction of a flat equipotentially charged surface of the layer of an insulating liquid with a complete compensation of the applied electric field by charges is possible under the condition of conservation of

total volume of the liquid. In a finite-sized cell, the transition of the charged flat surface of a liquid of constant volume to the reconstructed state for $U=U_{c1}$ is a phase transition close to a second-order transition.

The reconstructed steady state of the charged surface of hydrogen is violated under the upper critical voltage U_{c2}. The $U-T$ phase diagram contains a region between the curves $U_{c1}(T)$ and $U_{c2}(T)$ in which the reconstructed surface is stable.

For voltages much higher than the upper critical voltage, the liquid hydrogen surface becomes flat and charges pass through the surface.

The theoretical models developed in Refs. 13 and 16 are only in qualitative agreement with the experimental results. Hence further investigations of the reconstruction of an equipotentially charged surface are necessary under conditions of total compensation of applied field by charges and conservation of the total volume of the liquid in the layer.

The amplitude of the profile of the equipotentially charged surface of a drop suspended from the upper plate of a diode varies smoothly with applied voltage. The critical voltage for the reconstruction of the charged surface of the drop is formally an imaginary quantity, i.e., it can be assumed that the surface is in reconstructed state even for zero potential difference between the diode plates.

The theoretical model of evolution of the shape of a charged drop constructed in Ref. 19 is in satisfactory agreement with the experimental results. Since the derivation of equations for the shape of surface of the hump on the lower plate and a drop on the upper plate of the diode coincide, a satisfactory agreement between the model developed for a drop and the experiment confirm the soundness of the approach used in Refs. 13 and 16 for describing the reconstruction phenomenon.

Above a certain critical voltage, the charged surface loses stability and is discharged. It is shown in the present publication that a geyser of diameter much smaller than the capillary length spurts from the surface irrespective of the geometry of the experiment, sign of charges, and properties of the insulating liquid (helium or hydrogen)(see also Refs. 17 and 18). Theoretical investigations of this phenomenon are of considerable interest.

The authors are obliged to Yu. A. Ossipyan for supporting this research, V. B. Shikin for fruitful discussions, and V. N. Khlopinski for his help in preparing and carrying out the experiments. This research was partly supported by the program NASA-RSA (Project TM-17) and FNTP FKI (Project ''Surface'').

*E-mail: levch@issp.ac.ru

[1] A. A. Levchenko and L. P. Mezhov-Deglin, Fiz. Nizk. Temp. **22**, 46 (1996) [Low Temp. Phys. **22**, 33 (1996)].
[2] L. D. Landau and E. M. Lifshitz, *Electrodynamics of Continuous Media* [in Russian], Nauka, Moscow (1982). Translation 3rd ed. Pergamon Press, Oxford 1960.
[3] P. Leiderer, W. Ebner, and V. B. Shikin, Surf. Sci. **113**, 405 (1982).
[4] P. Leiderer, Phys. Rev. **20**, 4511 (1979).
[5] M. Wanner and P. Leiderer, Phys. Rev. Lett. **42**, 315 (1979).
[6] P. Leiderer and M. Wanner, Phys. Rev. Lett. **A73**, 185 (1979).
[7] V. I. Mel'nikov and S. V. Meshkov, Zh. Éksp. Teor. Fiz. **81**, 951 (1981) [Sov. Phys. JETP **54**, 505 (1981)].
[8] V. B. Shikin and Yu. P. Monarkha, *Two-dimensional Charged Systems in Helium* [in Russian] Nauka, Moscow (1989).
[9] L. P. Gor'kov and D. M. Chernikova, Pis'ma Zh. Éksp. Teor. Fiz. **18**, 68 (1973) [sic].
[10] A. P. Volodin, M. S. Khaikin, and V. S. Edel'man, Pis'ma Zh. Éksp. Teor. Fiz. **37**, 8 (1983) [JETP Lett. **37**, 7 (1983)].
[11] D. M. Chernikova, Fiz. Nizk. Temp. **2**, 1374 (1976) [Sov. J. Low Temp. Phys. **2**, 669 (1976)].
[12] V. B. Shikin and E. V. Lebedeva, Fiz. Nizk. Temp. **24**, 299 (1998) [Low Temp. Phys. **24**, 225 (1998)].
[13] V. B. Shikin and P. Leiderer, Fiz. Nizk. Temp. **23**, 624 (1997) [Low Temp. Phys. **23**, 468 (1997)].
[14] A. A. Levchenko, E. Teske, G. V. Kolmakov *et al.*, Pis'ma Zh. Éksp. Teor. Fiz. **65**, 547 (1997) [JETP Lett. **65**, 572 (1997)].
[15] F. P. Boyle and A. J. Dahm, J. Low Temp. Phys. **23**, 477 (1976).
[16] G. V. Kolmakov and E. V. Lebedeva, Zh. Éksp. Teor. Fiz. **115**, 43 (1999) [JETP **88**, 24 (1999)].
[17] V. P. Volodin and M. S. Khaikin, Pis'ma Zh. Éksp. Teor. Fiz. **30**, 608 (1979) [JETP Lett. **30**, 572 (1979)].
[18] J. J. Niemela, J. Low Temp. Phys. **109**, 709 (1997).
[19] G. V. Kolmakov and A. A. Levchenko, *to be published.*

Translated by R. S. Wadhwa

Size effect in impuriton gas of ^{3}He–^{4}He superfluid mixture

I. N. Adamenko, L. N. Bortnik, and A. I. Chervanyov

*Kharkov State University, 310077 Kharkov, Ukraine**
(Submitted November 10, 1998)
Fiz. Nizk. Temp. **25**, 343–355 (April 1999)

The flow of quasiparticle gas under the action of gradients of thermodynamic quantities in a volume filled with a powder (crocus) is considered. The exact solution of the kinetic equation is obtained in terms of the matrix elements of the collision integral for quasiparticles and partial cross sections of quasiparticles scattering by crocus. The condition describing a steady nonequilibrium state of the quasiparticle gas in a volume filled with a porous material is determined. The obtained results are valid for arbitrary relations between the frequencies of collisions of quasiparticles with one another and with powder particles. The Knudsen effect in a degenerate quantum gas is studied, and the transition from the Knudsen to hydrodynamic flow of quasiparticle gas is analyzed. The steady nonequilibrium state of the impuriton gas in the ^{3}He–^{4}He superfluid mixture is investigated in a confined geometry.
 [S1063-777X(99)00304-7]

INTRODUCTION

An analysis of gas transport in a porous medium under the action of gradients of thermodynamic quantities is one of the classical problems in kinetic theory.[1,2] Various conditions of gas flow through thin pipes and porous materials were investigated long ago in pioneering works by Graham,[3] Loschmidt,[4,5] and Maxwell[6] appearing in the middle of the last century. It was found that the decrease in the mean free path of particles colliding mainly with the walls of the vessel containing the gas changes the conventional pattern of diffusion of the same gas in an unbounded medium. Later, Graham[7] established the main regularities of a free molecular gas flow known as effusion. The theoretical substantiation of Graham's law of diffusion was continued by Maxwell who was the first to propose the model of ''dust-laden'' gas in 1860.[6] The essence of this semi-empirical model is that a porous medium is regarded as a component of a gas mixture consisting of heavy immobile particles. Maxwell himself did not obtain final results on the basis of his model and only described it in his work devoted to the theory of transport of molecular characteristics in gases. The ''dust-laden'' gas model was forgotten for a long time and independently proposed again by Deryagin and Bakanov[8,9] in the 1950's. This model was used by the authors for studying the conditions of gas flow close to a free molecular flow. The study of a range of problems associated with the transport of particles through various types of membranes led to a further evolution of semi-empirical models exploiting the same ideas.[10–13]

In spite of a considerable progress made in this field, some questions posed in experiments have not been subjected to an appropriate theoretical analysis. For example, only two limiting regimes of gas flow in a confined geometry, viz., the free-molecular (Knudsen) and hydrodynamic flows, are analyzed almost independently in all theoretical publications known to us.[14,15] Such an idealization does not reflect correctly the experimental situation observed when the frequencies of collisions of gas particles with one another and with the walls of the vessel containing the gas are comparable.

In this paper, we propose an approach that fills this gap. The problem of steady-state flow of a quasiparticle gas through a porous medium under the action of gradients of thermodynamic quantities is solved by us exactly by using a strictly kinetic approach. The method developed here makes it possible to avoid traditional simulation of the collision integral, which ensures the generality of the results.

All the results obtained by us are applicable to any (quantum or classical) gas of particles and were used by us for analyzing the steady nonequilibrium state of a specific physical system, viz., ^{3}He–^{4}He superfluid mixture.

SOLUTION OF KINETIC EQUATION

In order to describe the steady nonequilibrium state of an impuriton gas in ^{3}He–^{4}He superfluid mixture in the absence of thermal excitations, we use the linearized kinetic equation

$$\mathbf{v}\frac{\partial f_0}{\partial \mathbf{r}} = (\hat{I}+\hat{L})g, \tag{1}$$

where $\mathbf{v}$ is the velocity of an impuriton, f_0 a locally equilibrium distribution function, $f_0' g \equiv f - f_0$ a small correction to it, which is proportional to gradients of thermodynamic quantities responsible for the lack of equilibrium, and $\hat{I}$ and $\hat{L}$ the impurity–impurity collision operator; the prime denotes differentiation with respect to the argument.

The procedure for solving Eq. (1) involves the separation of the zeroth eigenspace of the collision operator and its subsequent inversion.[16,17] For this purpose, we consider the Hilbert space of the momentum function to be added with the scalar product

$$\langle h(\mathbf{p})|g(\mathbf{p})\rangle = \int f_0' h g^* d\Gamma, \tag{2}$$

introduced into it, where $d\Gamma$ is the volume element of the momentum phase momentum space and **p** the impuriton momentum. We also introduce the operator $\hat{P}_c$ projecting vectors of the Hilbert space onto the kernel of the collision operator. The basis of the latter operator is formed by linearly independent vectors, i.e., elements of the eigen subspace of the operator $\hat{I}+\hat{L}$ corresponding to zero eigenvalue.

For the one-to-one inversion of collision operator, we must project all the vectors appearing in Eq. (1) onto the subspace orthogonal to the kernel. For this purpose, we use the projection operator $\hat{P}_n$ defined as $\hat{P}_n=\hat{E}-\hat{P}_c$, where $\hat{E}$ is the identity operator. As a result, we obtain the solution of the kinetic equation (1) in operator form:

$$g=[\hat{P}(\hat{I}+\hat{L})\hat{P}_n]^{-1}\hat{P}_n\left(\mathbf{v}\frac{\partial f_0}{\partial \mathbf{r}}\right). \tag{3}$$

A stationary situation takes place in the system under investigation in the absence of a flow of the impuriton gas in the direction of gradients. In our notation, this condition can be written in the form

$$\langle v_z|g\rangle=0, \tag{4}$$

the subscript z denoting here and below the projection of vectors on the direction of gradients.

Using formula (3) and assuming that the gradients of thermodynamic quantities are directed along the z-axis, we can write condition (4) in the form

$$2\frac{F_{1/2}}{F_{-1/2}}\frac{\nabla n}{n}\langle v_z|[\hat{P}_n(\hat{I}+\hat{L})\hat{P}_n]^{-1}\hat{P}_n|v_z\rangle + \frac{\nabla T}{T}\left\{\left\langle v_z\left|[\hat{P}_n(\hat{I}+\hat{L})\hat{P}_n]^{-1}\hat{P}_n\right|\frac{\varepsilon_3}{T}v_z\right\rangle - 3\frac{F_{1/2}}{F_{-1/2}}\langle v_z|[\hat{P}_n(\hat{I}+\hat{L})\hat{P}_n]^{-1}\hat{P}_n|v_z\rangle\right\}=0, \tag{5}$$

where n is the number of impuritons per unit volume, T the temperature of the mixture, $H_3=\varepsilon_0+\varepsilon_3$ the Hamiltonian of impuritons, $\varepsilon_3=p^2/(2m^*)$,

$$F_\nu\left(\frac{\mu_3}{T}\right)=\frac{1}{\pi^2\hbar^3}\int_0^\infty\frac{x^\nu dx}{1+\exp(x-\mu_3/T)} \tag{6}$$

is the Fermi function, and μ_3 the chemical potential of an impuriton in the mixture.

Equation (5) is the relation between gradients of concentration and temperature, which ensures the steady state of the impuriton gas. In order to analyze this relation, we must calculate the corresponding moments of the operator $[\hat{P}_n(\hat{I}+\hat{L})\hat{P}_n]^{-1}$, inverse to the collision operator. These moments are determined in turn by the type of interaction. The analysis of relation (5) is simplified considerably if we use the Lorentz approximation for the operator $\hat{L}$ describing the scattering of ''light'' impuritons by ''heavy'' particles of the powder. It is well known[1] that the particles of a ''light'' gas diffusing in a ''heavy'' gas change only the direction of their motion as a result of collisions so that their energy remains unchanged. Consequently, the corresponding impurity–powder collision operator acts only on the polar and azimuthal components of the arbitrary function of momentum.

For the inversion of the total collision operator $\hat{I}+\hat{L}$, it is expedient to introduce the orthonormal system of vector functions of the Hilbert space, i.e.,

$$|\tilde{\psi}_{nlm}\rangle=|\varphi_n^{(l,m)}(\tilde{p})Y_{lm}(\theta,\vartheta)\rangle, \tag{7}$$

where $Y_{lm}(\theta,\vartheta)$ are spherical functions[18] and $\varphi_n^{(l,m)}(\tilde{p})$ the corresponding radial functions which can be conveniently represented in the form of polynomials containing powers of the dimensionless momentum $\tilde{p}=p/\sqrt{2m^*T}$ according to the definition

$$\varphi_n^{(l,m)}(\tilde{p})=\sum_{j=0}^{\infty}c_{nj}^{(l,m)}\tilde{p}^j\tilde{p}^{\delta_l^1\delta_m^0\delta_n^0}. \tag{8}$$

The coefficients $c_{nj}^{(l,m)}$ are defined uniquely from the orthonormalization relation

$$\langle\tilde{\psi}_{nlm}|\tilde{\psi}_{ijk}\rangle=\delta_n^i\delta_l^j\delta_m^k. \tag{9}$$

It should be noted that the function $|\tilde{\psi}_{010}\rangle$, defined in accordance with formulas (7)–(9), has the form

$$|\tilde{\psi}_{010}\rangle=\frac{p_z}{\sqrt{\langle p_z|p_z\rangle}} \tag{10}$$

and is the normalized value of the z-component of momentum, which is conserved in impurity–impurity collisions. In order to take into account the laws of conservation of the number of impuritons and energy in the collisions of impuritons with one another and with powder particles, it is convenient to choose the following orthonormal basis in the Hilbert space introduced above:

$$|\psi_{nlm}\rangle=|\tilde{\psi}_{nlm}\rangle[1-\delta_m^0\delta_l^0(\delta_n^1+\delta_n^2)]+\delta_n^1\delta_m^0\delta_l^0[\alpha|\tilde{\psi}_{100}\rangle+\beta|\tilde{\psi}_{200}\rangle]+\delta_n^2\delta_m^0\delta_l^0[\beta|\tilde{\psi}_{200}\rangle-\alpha|\tilde{\psi}_{100}\rangle], \tag{11}$$

where

$$\alpha=\frac{\langle\varphi_1^{(0,0)}|\tilde{p}^2\rangle}{(4\pi\langle\tilde{p}^2|\tilde{p}^2\rangle-\langle\varphi_1^{(0,0)}|\tilde{p}^2\rangle^2)^{1/2}};$$

$$\beta=\left(\frac{4\pi\langle\tilde{p}^2|\tilde{p}^2\rangle-\langle\varphi_0^{(0,0)}|\tilde{p}^2\rangle^2-\langle\varphi_1^{(0,0)}|\tilde{p}^2\rangle^2}{4\pi\langle\tilde{p}^2|\tilde{p}^2\rangle-\langle\varphi_1^{(0,0)}|\tilde{p}^2\rangle^2}\right)^{1/2},$$

and

$$|\varphi_0^{(0,0)}\rangle=\sqrt{4\pi}\,\frac{|1\rangle}{\sqrt{\langle1|1\rangle}};$$

$$|\varphi_1^{(0,0)}\rangle=\sqrt{4\pi}\frac{|\tilde{p}\rangle\langle1|1\rangle-|1\rangle\langle1|\tilde{p}}{\sqrt{\langle1|1\rangle^2\langle\tilde{p}|\tilde{p}\rangle-\langle1|\tilde{p}\rangle^2\langle1|1\rangle}}$$

are radial functions constructed in accordance with the definition (8) and the normalization condition (9). The laws of conservation of the number of particles, energy, and the z-component of the impuriton momentum in collisions mentioned above can be expressed by the equalities

$$(\hat{I}+\hat{L})|\psi_{000}\rangle=(\hat{I}+\hat{L})|\psi_{100}\rangle=\hat{I}|\psi_{010}\rangle=0. \tag{12}$$

Besides, the linear subspace of the functions $\{|\psi_{n00}\rangle\}_{n=0}^{\infty}$ corresponding to the zeroth harmonics $Y_{00}(\theta,\vartheta)$ forms the basis of the kernel of the Lorentz collision operator $\hat{L}$ so that

$$\hat{L}|\psi_{n00}\rangle=0; \quad n=0,1,2,3,\ldots . \tag{13}$$

Using the orthonormal basis (11) introduced above, we can present the result of action of the collision operator on the nonequilibrium correction $|g\rangle$ in the form

$$(f_0')^{-1}(\hat{I}+\hat{L})|g\rangle=-\upsilon N\sum_{nlm}\sigma_t^{(l,m)}(\theta,\vartheta)|\varphi_n^{(l,m)}(\tilde{p})\rangle\langle\psi_{nlm}|g\rangle + \sum_{nlm}\sum_{ijk}|\psi_{nlm}\rangle\langle\psi_{nlm}|\hat{I}|\psi_{ijk}\rangle\langle\psi_{ijk}|g\rangle, \tag{14}$$

where N is the number of powder particles per unit volume,

$$\sigma_t^{(l,m)}=\int_{-\pi}^{\pi}d\vartheta'\int_0^{\pi}[Y_{lm}(\cos\theta,\vartheta)-Y_{lm}(\cos\alpha\cos\theta + \sin\alpha\sin\theta\cos(\vartheta-\vartheta'),\vartheta')]W(p,\alpha)\sin\alpha\, d\alpha \tag{15}$$

is partial transport scattering cross section of the Lorentz collision operator $\hat{L}$, and $W(p,\alpha)\sin\alpha\, d\alpha$ the differential scattering cross section.

Since only one preferred direction for gradients exists in the system under investigation, the nonequilibrium correction $|g\rangle$ cannot be a function of the polar angle. In this case, formulas (14)–(15) can be simplified, and the kinetic equation (1) is transformed to

$$\nabla_3|v_z\rangle=-\tilde{p}\sum_{nl}\nu_{\mathrm{Kn}}^{l}|\psi_{nl0}\rangle\langle\psi_{nl0}|g\rangle + \sum_{nl}\sum_{jk}|\psi_{nl0}\rangle\langle\psi_{nl0}|\hat{I}|\psi_{jk0}\rangle\langle\psi_{jk0}|g\rangle, \tag{16}$$

where

$$\nu_{\mathrm{Kn}}^{l}=N\left(\frac{2T}{m^*}\right)^{1/2}2\pi\int_0^{\pi}[1-P_l(\cos\alpha)]W(p,\alpha)\sin\alpha\, d\alpha, \tag{17}$$

$\nabla_3=(\partial/\partial z)(H_3-\mu_3/T)$ and $P_l(\cos\alpha)$ is a Legendre polynomial of the lth order.

In the case when powder particles can be regarded as rigid spheres of radius a, and partial frequencies (17) of the impurity–powder collisions are given in the form

$$\nu_{\mathrm{Kn}}^{l}=N\frac{\pi a^2}{2}\left(\frac{2T}{m^*}\right)^{1/2}\int_0^{\pi}[1-P_l(\cos\alpha)]\sin\alpha\, d\alpha. \tag{18}$$

The general solution of Eq. (16) can be written as the sum of the general solution of the corresponding homogeneous equation and a particular solution of the nonhomogeneous equation (16).

The general solution of the homogeneous equation corresponding to Eq. (16) forms a subspace which is a linear envelope of the vectors forming the kernel of the collision operator $\hat{I}+\hat{L}$:

$$|g_0\rangle=C_1|\psi_{000}\rangle+C_2|\psi_{000}\rangle, \tag{19}$$

where C_1 and C_2 are arbitrary constants.

In order to find a solution of the nonhomogeneous equation (16), it is convenient to write the latter equation in the form

$$-i\left(\frac{4\pi}{3}\right)^{1/2}\upsilon\nabla_3|Y_{10}\rangle = \sum_{l=0}^{\infty}|Y_{l0}\rangle\sum_{j=0}^{\infty}\tilde{p}^j\sum_{m=0}^{\infty}\sum_{k=0}^{\infty}\{\langle\phi_{jl}|\hat{I}|\psi_{mk0}\rangle[1-\delta_k^0(\delta_m^0 + \delta_m^1)-\delta_k^1\delta_m^0]-\theta(m-j+1)(1-\delta_j^0)(1-\delta_l^0)\delta_l^k\nu_{\mathrm{Kn}}^{k}[(1 - \delta_m^0\delta_k^1\delta_j^1)c_{mj-1}^{(k,0)}+\delta_m^0\delta_k^1\delta_j^2c_{mj-2}^{(k,0)}]\}\langle\psi_{mk0}|g\rangle, \tag{20}$$

where the following notation has been introduced:

$$\theta(x)=\begin{cases}1, & \text{if } x\geqslant 0\\ 0, & \text{if } x<0;\end{cases}$$

$$|\phi_{jl}\rangle=\sum_{n=j}^{\infty}c_{nj}^{(1,0)}|\psi_{nl0}\rangle[1-\delta_l^0(\delta_n^0+\delta_n^1+\delta_n^2)-\delta_l^1\delta_n^0] + \delta_l^0\delta_n^2[\delta_j^0(\beta c_{10}^{(0,0)}-\alpha c_{20}^{(0,0)})+\delta_j^1(\beta c_{11}^{(0,0)} - \alpha c_{21}^{(0,0)})-\delta_j^2\alpha c_{22}^{(0,0)}]|\psi_{200}\rangle. \tag{21}$$

It should be noted that while transforming Eq. (16) to the form (20), we took into account the properties of the kernel of the operator $\hat{I}$ which are expressed by equalities similar to (12):

$$\hat{I}|\psi_{000}\rangle=\hat{I}|\psi_{100}\rangle=\hat{I}|\psi_{010}\rangle=0. \tag{22}$$

Since the system of spherical functions $\{|Y_{l0}\rangle\}_{l=0}^{\infty}$ is orthonormal, and the set of monomial vectors $\{|\tilde{p}^n\rangle\}_{n=0}^{\infty}$ is linearly independent, equality (20) is satisfied only when all the coefficients of the products of the type $\tilde{p}^j|Y_{l0}\rangle$ on its right- and left-hand sides are identical. Such a condition can be written in the form of a nonhomogeneous system of linear equations in the moments $\{\langle\psi_{nl0}|g\rangle\}_{l,n=0}^{\infty}$

$$\sum_{m=0}^{\infty}\sum_{k=0}^{\infty}\{\langle\phi_{jl}|\hat{I}|\psi_{mk0}\rangle[1-\delta_k^0(\delta_m^0+\delta_m^1)-\delta_k^1\delta_m^0]-\theta(m - j+1)(1-\delta_j^0)(1-\delta_l^0)\delta_l^k\nu_{\mathrm{Kn}}^{k}[(1-\delta_m^0\delta_k^1\delta_j^1)c_{mj-1}^{(k,0)} + \delta_m^0\delta_k^1\delta_j^2c_{mj-2}^{(k,0)}]\}\langle\psi_{mk0}|g\rangle = i\delta_l^1\left(\frac{4\pi}{3}\frac{2T}{m^*}\right)^{1/2}\left[\delta_j^1\nabla\left(\frac{\mu_3}{T}\right)+\delta_j^3\frac{\partial T}{T}\right]. \tag{23}$$

It should be noted that this system holds for any values of the moments $\langle\psi_{000}|g\rangle,\langle\psi_{100}|g\rangle$, which is a natural consequence of relations (12) expressing the laws of conservation of the number of particles and energy in collisions of impuritons with one another and with powder particles. The quantities $\langle\psi_{000}|g\rangle$ and $\langle\psi_{100}|g\rangle$ are the coefficients of the expansion of the general solution of the kinetic equation in the basis of the kernel of the collision operator $\{|\psi_{000}\rangle,|\psi_{100}\rangle\}$.

Thus, system (23) has a general solution that can be given in the form of a direct sum of the subspace in the

form of a linear envelope of the basis of the kernel (19) and the vector solution of system (23) from which the moments $\langle\psi_{000}|g\rangle$ and $\langle\psi_{100}|g\rangle$ are eliminated. Such a solution is unique by virtue of the Kronecker–Capelli theorem. Indeed, in view of the same conservation laws, the set of functions $\{|\phi_{j0}\rangle\}_{j=0}^{\infty}$ (21) is linearly dependent, which leads to dependence of equations of the system (23) corresponding to $l=0$. It can easily be verified with the help of elementary transformations of the rows of the extended matrix of the system that any two equations from the above set can be obtained from the remaining equations. Thus, not only two unknowns ($\langle\psi_{000}|g\rangle$ and $\langle\psi_{100}|g\rangle$), but also two equations are eliminated from the system: the ranks of the coefficient matrix and of the extended matrix (23) coincide, which is the compatibility condition for the system.

After eliminating the above-mentioned equations, it is most convenient to solve the system (23) with a nondegenerate coefficient matrix by using Cramer's method. The principal determinant of the system can be written in the form

$$\det A+\lim_{N\to\infty}\lim_{L\to\infty}\det A_{NL}, \tag{24}$$

where $A_{NL}\equiv(a_{nf})_{NL}$ is a square matrix of order $L\times(N-2)$. The common matrix element is defined as

$$\begin{aligned}a_{nf}=&\langle\phi_{jl}|\hat{I}|\psi_{mk0}\rangle[1-\delta_k^0(\delta_m^0+\delta_m^1)-\delta_k^1\delta_m^0]\\&-\theta(m-j+1)(1-\delta_j^0)(1-\delta_l^0)\delta_l^k\nu_{\mathrm{Kn}}^k[(1\\&-\delta_m^0\delta_k^1\delta_j^1)c_{mj-1}^{(k,0)}+\delta_m^0\delta_k^1\delta_j^2c_{mj-2}^{(k,0)}],\end{aligned} \tag{25}$$

where the indices n, f and m, l, j, and k are connected through the relations

$$\begin{aligned}&n=j-1+(N+1)l;\quad l=\left[\frac{n+2}{N+1}\right],\quad j=n+1-(N+1)\\&\quad\times\left[\frac{n+2}{N+1}\right];\quad 0\leqslant l\leqslant L;\quad 2\delta_l^0\leqslant j\leqslant N;\\&f=m-1+(N+1)k;\quad k=\left[\frac{f+2}{N+1}\right],\\&m=f+1-(N+1)\left[\frac{f+2}{N+1}\right];\quad 0\leqslant k\leqslant L;\quad 2\delta_k^0\leqslant m\leqslant N,\end{aligned}$$

and the brackets denote the integral part of the number.

Using the determinant (24), we can write the general solution of system (23) in the form

$$\begin{aligned}|g^H\rangle=&C_1|\psi_{000}\rangle+C_2|\psi_{100}\rangle\\&+\frac{\Sigma_{n=0}^{\infty}\Sigma_{l=0}^{\infty}|\psi_{nl0}\rangle\Delta^{(n,l)}[1-\delta_l^0(\delta_n^0+\delta_n^1)]}{\det A},\end{aligned} \tag{26}$$

where C_1 and C_2 are arbitrary constants, and

$$\Delta^{(n,l)}=\lim_{N\to\infty}\lim_{L\to\infty}\det A_{NL}^{(n,l)} \tag{27}$$

are the determinants of the matrices obtained from the matrix A_{NL} by replacing its $n-1+(N+1)l$th column by the column of free terms $(d_{nl})_{NL}$ with the common element

$$(d_{nl})_{NL}=i\left(\frac{4\pi}{3}\frac{2T}{m^*}\right)^{1/2}\left[\delta_n^{N+1}\nabla\left(\frac{\mu_3}{T}\right)+\delta_n^{N+3}\frac{\nabla T}{T}\right]. \tag{28}$$

The result (26) can be conveniently presented in a more compact form:

$$|g^H\rangle=|\psi_{000}\rangle\langle\psi_{000}|g^H\rangle+|\psi_{100}\rangle\langle\psi_{100}|g^H\rangle-\left|\frac{\det B}{\det A}\right\rangle, \tag{29}$$

where $\det B$ is the determinant of an infinite-dimensional matrix whose elements in the first row starting from the second one coincide with the functions $|\psi_{nl0}\rangle$ appearing in the third term of the sum (26) and ordered so that the index n increases with a fixed value of the index l, the latter increasing from zero to infinity. The elements of the first column are defined as

$$b_{nl}=i\left(\frac{4\pi}{3}\frac{2T}{m^*}\right)^{1/2}\left[\delta_n^{N+2}\nabla\left(\frac{\mu_3}{T}\right)+\delta_n^{N+4}\frac{\nabla T}{T}\right], \tag{30}$$

while the remaining element left after the elimination of the first row and first column of the matrix B form a matrix identical to matrix A (i.e., the matrix A_{NL} for $N\to\infty$ and $L\to\infty$).

In the limiting cases when the entire gas kinetics is determined in fact by only one type of collisions, formula (29) must be refined. For example, if we can neglect the contribution of impurity–powder collisions (hydrodynamic limit), $\nu_{\mathrm{Kn}}^l=0$, and the solution of kinetic equation (16) is defined to within a linear combination of invariants of the collision operator $\hat{I}$ including $|\psi_{010}\rangle$. For this reason, the coefficient of $|\psi_{010}\rangle$ in expansion (26) remains indeterminate, which corresponds to degeneracy of the Nth column of the matrix A_{NL} (25). Formally, only the cofactor to the element $|\psi_{010}\rangle$ of the first row changes in solution (26), which should now be written in the general form: $\langle\psi_{010}|g\rangle$.

In the opposite limiting case, when impurity–impurity collisions are absent (Lorentz approximation), the Nth row in the matrix A_{NL} degenerates, i.e., the condition of the equality of the terms in Eq. (23) corresponding to the harmonic $|Y_{10}\rangle$ and free of $\tilde{p}$ becomes an identity. The solution of the system (23) by Cramer's method leads in this approximation to the trivial result:

$$|g\rangle=-i\left(\frac{4\pi}{3}\frac{2T}{m^*}\right)^{1/2}\frac{1}{\nu_{\mathrm{Kn}}^1}\nabla_3|Y_{10}\rangle. \tag{31}$$

It should also be noted that result (29) combined with the general formula (5) derived above allows us to obtain explicit expressions for average values of the operator $[\hat{P}_n(\hat{I}+\hat{L})\hat{P}_n]^{-1}$ inverse to the collision operator. In particular, we can obtain the following expressions for the moments appearing in formula (5):

$$\langle v_z|(\hat{P}_n(\hat{I}+\hat{L})\hat{P}_n)^{-1}\hat{P}_n|v_z\rangle=-i\left(\frac{4\pi}{3}\frac{2T}{m^*}\right)^{1/2}\frac{\Delta_1^{(0,1)}}{\det A}, \tag{32}$$

$$\left\langle v_z\left|\{\hat{P}_n(\hat{I}+\hat{L})\hat{P}_n\}^{-1}\hat{P}_n\right|\frac{\varepsilon_3}{T}v_z\right\rangle=-i\left(\frac{4\pi}{3}\frac{2T}{m^*}\right)^{1/2}\frac{\Delta_2^{(0,1)}}{\det A}, \tag{33}$$

where

$$\Delta_1^{(0,1)} = \lim_{N\to\infty} \lim_{L\to\infty} (A_{2N}^{(0,1)})_{NL}, \tag{34}$$

$$\Delta_2^{(0,1)} = \lim_{N\to\infty} \lim_{L\to\infty} (A_{4N}^{(0,1)})_{NL} \tag{35}$$

are cofactors of nonzero elements of the column containing free terms of the determinant $\Delta^{(0,1)}$.

Adding the general solution of the homogeneous equation (19) to the solution of the nonhomogeneous equation (29), we obtain the general solution of the initial kinetic equation (1) in terms of the matrix elements of the impurity–impurity collision operator and Lorentzian partial collision frequencies $\nu_{\rm Kn}^l$ (18):

$$|g\rangle = C_1|\psi_{000}\rangle + C_2|\psi_{100}\rangle - \left|\frac{\det B}{\det A}\right\rangle, \tag{36}$$

where C_1 and C_2 are arbitrary constants.

The obtained solution of kinetic problem is exact and in combination with condition (4) allows us to analyze the relation between the gradients (5) ensuring the steady state of a quasiparticle gas with an arbitrary type of interaction.

A comparison of formulas (10), (11), (26), (29), and (36) leads to the following expression for the average velocity of impuritons in the direction of ∇T:

$$V \equiv \frac{\langle v_z|g\rangle}{n} = \frac{\sqrt{\langle v_z|v_z\rangle}}{n}\frac{\Delta^{(0,1)}}{\det A}. \tag{37}$$

It can be seen that the average velocity (37) coincides (to within a factor that does not vanish anywhere) with the cofactor of the element $|\psi_{010}\rangle$ of the determinant $\det B$ [cf. (26)]. Consequently, the steady-state condition (4) can be expressed by the equality

$$\Delta^{(0,1)} = 0. \tag{38}$$

The obtained relation can be analyzed to any degree of accuracy by calculating the corresponding matrix elements of the collision operator.

MODEL REPRESENTATION OF IMPURITY–IMPURITY COLLISION OPERATOR AND FURTHER ANALYSIS OF A STEADY NONEQUILIBRIUM STATE OF IMPURITON GAS

The exact solution of the kinetic equation (36) allows us to construct various approximations taking into account certain properties of the collision operator, which are typical of the given physical system. For example, in an analysis of the steady-state condition (4), we can confine ourselves to the simplest model representation of the impurity–impurity collision operator, assuming that its spectrum consists of only two eigenvalues: $\lambda_1 = 0$ with the kernel of the true operator $\hat{I}$ belonging to it and $\lambda_2 = -\nu$ with the subspace of eigenvectors orthogonal to the kernel belonging to it. Such an approach makes it possible to simplify considerably the expression for matrix elements of the impurity-impurity collision operator, whose action on any vector that does not belong to the kernel is now reduced to the multiplication by the collision frequency $-\nu$:

$$\langle \psi_{ml0}|\hat{I}|\psi_{nl0}\rangle = -\nu\delta_n^m\delta_l^k[1-\delta_n^0(\delta_l^0+\delta_l^1)-\delta_l^0\delta_n^1]. \tag{39}$$

The matrix of the coefficient of system (23) is also simplified significantly after the substitution of formula (39) into the definition of the matrix element (25):

$$\begin{aligned} a_{nf} = -\delta_k^l\{\nu\{\theta(m-j)c_{mj}^{(l,0)}(1-\delta_k^1\delta_m^0-\delta_k^0\delta_m^2\} \\ + \delta_k^0\delta_m^2[\delta_j^0(\beta c_{10}^{(0,0)}-\alpha c_{20}^{(0,0)})+\delta_j^1(\beta c_{11}^{(0,0)}-\alpha c_{21}^{(0,0)}) \\ - \alpha\delta_j^2 c_{22}^{(0,0)}]) + \nu_{\rm Kn}^k\theta(m-j+1)(1-\delta_l^0)(1-\delta_j^0) \\ \times[(1-\delta_m^0\delta_k^1\delta_j^1)c_{mj-1}^{(k,0)} + \delta_m^0\delta_k^1\delta_j^2 c_{mj-2}^{(k,0)}]\}, \end{aligned} \tag{40}$$

where the same system of notation as in formula (25) is used. It can be seen from formula (40) that matrix A_{NL} is now of the block-diagonal form. Its nonzero elements form square block submatrices of dimension $N-1$ for $l=0$ and $N+1$ for $l\neq 0$, which are arranged along the principal diagonal of A_{NL}. This corresponds to the splitting of system (23) into independent subsystems each of which corresponds to its own value of the index l. All the subsystems except the only one corresponding to the value of $l=1$ are homogeneous systems of linear equations with a nondegenerate matrix of coefficients, and hence have only the trivial solution

$$\langle \psi_{mk0}|g\rangle = 0 \quad \text{for } k\neq 1. \tag{41}$$

A nontrivial solution exists only for a nonhomogeneous system of equations with a nondegenerate matrix of coefficients, corresponding to $l=1$. Using elementary transformations, we can simplify the latter system and write it in the form

$$\sum_{f=1}^{\infty} a_{nf}^{(0)}\langle \psi_{f10}|g\rangle = b_{n1}^{(0)}, \tag{42}$$

where

$$a_{nf}^{(0)} = \delta_f^1(-1)^{n+1}c_{00}\gamma^{2-n} + \theta(n-f)c_{f-1\ n-1}, \tag{43}$$

$$\begin{aligned} d_{n1}^{(0)} = \frac{(-1)^{n+1}i}{\nu}\left(\frac{4\pi}{3}\frac{2T}{m^*}\right)^{1/2}\gamma^{2-n}\Bigg[\theta(n-2)\nabla\left(\frac{\mu_3}{T}\right) \\ + \gamma^2\theta(n-4)\frac{\nabla T}{T}\Bigg], \end{aligned} \tag{44}$$

and $\gamma = \nu/\nu_{\rm Kn}$; the indices $l=1$ and $m=0$ of the coefficients $c_{ij}^{(l,m)}$ and frequency $\nu_{\rm Kn}^l$ are omitted for convenience.

The general solution of the system (42) can be written in the form similar to the third term in formula (36):

$$|g'\rangle = \sum_{n=0}^{\infty} |\psi_{n10}\rangle\langle\psi_{n10}|g'\rangle = -\left|\frac{\det B^{(0)}}{\det A^{(0)}}\right\rangle, \tag{45}$$

where $\det A^{(0)}$ is the determinant of matrix (43), and $\det B^{(0)}$ is the determinant of the matrix $B^{(0)}$ whose elements in the first row starting from the second are the functions $|\psi_{nl0}\rangle$ arranged in increasing order of index n. The elements of the first column are defined by the equality

$$b_{n1}^{(0)} = (1-\delta_n^1)d_{(n-1)1}^{(0)}, \tag{46}$$

while the remaining elements left after the removal of the first row and the first column from the matrix $B^{(0)}$ form a

matrix identical to $A^{(0)}$. Applying elementary transformations to the rows of determinant $\det B^{(0)}$, we can transform it to an identical determinant whose first row has only two nonzero elements:

$$b_{1n}^{(0)} = -\delta_n^1 \frac{\nabla_3 |v_z\rangle}{\nu + \nu_{\mathrm{Kn}}\tilde{p}} + \delta_n^2 \frac{|\psi_{010}\rangle}{1+\gamma^{-1}\tilde{p}}, \tag{47}$$

the elements of other rows remaining unchanged.

Paying attention to the fact that the cofactor of the first element of the row (47) is the determinant $\det A^{(0)}$, while the cofactor of the second element is the quantity $\langle \psi_{010}|g\rangle$ [cf. (45)], and expanding $\det B^{(0)}$ in the first row, we obtain from (45)

$$|g'\rangle = -\frac{\nabla_3 |v_z\rangle}{\nu + \nu_{\mathrm{Kn}}\tilde{p}} + \frac{|\psi_{010}\rangle\langle\psi_{010}|g'\rangle}{1+\gamma^{-1}\tilde{p}}. \tag{48}$$

It should be noted that the result (48) obtained consecutively from the general solution (36) corresponds to the BGK approximation[14] with the artificially introduced collision integral:

$$\hat{I}_{BGK} = -(\nu + \nu_{\mathrm{Kn}}\tilde{p}) + \nu \frac{|p_z\rangle\langle p_z|}{\langle p_z|p_z\rangle}. \tag{49}$$

This approximation can hence be regarded as a consequence of the above-described assumption concerning the degeneracy of the spectrum of impurity–impurity collision integral to two eigenvalues 0 and $-\nu$.

In accordance with the structure of the general solution of the kinetic equation (36), solution (48) should be supplemented with vectors from the linear envelope of the basis of the kernel of the collision operator $\hat{I}+\hat{L}$ (19):

$$|g\rangle = |\psi_{000}\rangle\langle\psi_{000}|g\rangle + |\psi_{100}\rangle\langle\psi_{100}|g\rangle + \frac{|\psi_{010}\rangle\langle\psi_{010}|g\rangle}{1+\gamma^{-1}\tilde{p}} - \frac{\nabla_3 |v_z\rangle}{\nu + \nu_{\mathrm{Kn}}\tilde{p}}. \tag{50}$$

Forming a scalar product of this equality and the vector $\langle\psi_{010}|$ and expressing $\langle\psi_{010}|g\rangle$ from the obtained equation, we get

$$\langle\psi_{010}|g\rangle - \frac{1}{\nu_{\mathrm{Kn}}} \frac{\left\langle \psi_{010}\left|\frac{\nabla_3}{\gamma+\tilde{p}}\right|v_z\right\rangle}{\left\langle \psi_{010}\left|\frac{\tilde{p}}{\gamma+\tilde{p}}\right|\psi_{010}\right\rangle}. \tag{51}$$

This expression is also the cofactor of the second element of the first row of the determinant $\det B^{(0)}$ and can be obtained independently by calculating the corresponding determinant. It allows us to derive an explicit expression for the nonequilibrium correction $|g\rangle$ in the given approximation:

$$|g\rangle = C_1|\psi_{000}\rangle + C_2|\psi_{100}\rangle - \frac{|v_z\rangle}{\nu+\nu_{\mathrm{Kn}}\tilde{p}} \times \left(\nabla_3 + \frac{\left\langle p_z\left|\frac{\nabla_3}{1+\gamma^{-1}\tilde{p}}\right|p_z\right\rangle}{\left\langle p_z\left|\frac{\gamma^{-1}\tilde{p}}{1+\gamma^{-1}\tilde{p}}\right|p_z\right\rangle}\right), \tag{52}$$

where C_1 and C_2 are arbitrary quantities independent of momentum.

Expression (37) for the average velocity of the impuriton gas can also be simplified considerably:

$$V = -\frac{\langle v_z|v_z\rangle}{n\nu_{\mathrm{Kn}}} \frac{\left\langle \psi_{010}\left|\frac{\nabla_3}{\gamma+\tilde{p}}\right|\psi_{010}\right\rangle}{\left\langle \psi_{010}\left|\frac{\tilde{p}}{\gamma+\tilde{p}}\right|\psi_{010}\right\rangle}. \tag{53}$$

The solution (52) allows us to analyze various kinetic properties of the impuriton gas in ^{3}He–^{4}He superfluid mixture in the given physical situation, for example, to analyze the steady-state condition (4) and (38). The latter can be reduced with the help of the procedure described above to the relation

$$\int \frac{\partial f_0}{\partial z} \frac{v_z p_z}{\nu+\nu_{\mathrm{Kn}}\tilde{p}}\, d\Gamma = 0. \tag{54}$$

In the hydrodynamic limit, when the contribution of impurity–powder collisions can be neglected, relation (54) is transformed into the conventional gas-kinetic condition of mechanical equilibrium in the system: the pressure of the impuriton gas must be constant in the entire volume of the mixture. In the opposite (Knudsen) limit, when the contribution of mutual collisions of impuritons is insignificant, and the entire kinetics is determined by impurity–powder collisions, relation (54) in the classical temperature range acquires the form of the well-known Knudsen condition:

$$n\sqrt{T} = \text{const}. \tag{55}$$

In the classical temperature range $T \gg T_F$, expression (53) for the average velocity of impuritons becomes

$$V = -\frac{T}{\nu_{\mathrm{Kn}} m^*}\left[h(\gamma)\frac{\nabla n}{n} + w(\gamma)\frac{\nabla T}{T}\right], \tag{56}$$

where

$$h(\gamma) = \frac{\int_0^\infty \frac{y^{3/2}e^{-y}}{\gamma+\sqrt{y}}\,dy}{\int_0^\infty \frac{y^2 e^{-y}}{\gamma+\sqrt{y}}\,dy}, \tag{57}$$

$$w(\gamma) = \frac{\int_0^\infty \frac{y^{5/2}e^{-y}}{\gamma+\sqrt{y}}\,dy}{\int_0^\infty \frac{y^2 e^{-y}}{\gamma+\sqrt{y}}\,dy} - \frac{3}{2}h(\gamma). \tag{58}$$

Relation (54), which is the requirement of vanishing of the average velocity (56) of impuritons, can be conveniently expressed in the form of the condition of the coordinate independence of a certain dimensionless function of concentration and temperature. For this purpose, we must integrate the differential factor in formula (56). The results of such an integration is determined by the specific form of the dependence of the quantity γ on concentration and temperature. For example, assuming that $\gamma \sim n^k T^{l-1/2}$, we obtain

$$V=-\frac{T}{\nu_{\mathrm{Kn}}m^*}\left[h(\gamma)-\frac{2k}{2l-1}w(\gamma)\right]\nabla(\ln\Psi), \tag{59}$$

where

$$\Psi=x\exp\left[\int^{\gamma}\frac{\Phi(t)}{t}dt\right], \tag{60}$$

$\Phi(\gamma)=2w(\gamma)/[(2l-l)h(\gamma)-2kw(\gamma)]$ and $x=n/n_{40}$ is the ratio of the number of impuritons per unit volume to the number of particles per unit volume of pure helium at $T=0$.

Relation (51) describing the steady state of impuriton gas accordingly acquires the form

$$\nabla\Psi=0. \tag{61}$$

If impurity–powder collisions dominate over mutual collisions of impuritons, the Knudsen limit is realized in the system under investigation, so that the function Ψ (60) differs from $x\sqrt{T}$ only to the extent determined by the smallness of the ratio $\gamma\equiv\nu/\nu_{\mathrm{Kn}}$.

Since the values of concentration and temperature are connected through the condition close to the Knudsen condition, the impurity–impurity collision frequency $\nu\sim x^kT^m$ is different at different points of the mixture. This leads to an additional coordinate dependence of the average velocity of impuritons and is manifested, in turn, in the steady-state condition (61). Thus, it can be stated that the corresponding correction to the purely Knudsen expression for the function $\Psi(\Psi_{\mathrm{Kn}}=(x\sqrt{T})^{[2l/(2l-k)]}$ is determined by the form of the dependence of the impurity–impurity collision frequency on concentration and temperature. The only exception is the case when $\nu\sim xT$, when the value of γ is virtually the same at all points of the mixture, and the average velocity of impuritons is virtually independent of coordinates.

In order to analyze quantitatively the deviation of the steady-state condition (61) from the well-known Knudsen relation, it is sufficient to use the expansion of the function Ψ in the small parameter γ. As a result, equation (61) is transformed to

$$\nabla\left(x\sqrt{T}\left(1+\frac{\gamma\sqrt{\pi}}{2(2l-k-1)}+\ldots\right)\right)=0. \tag{62}$$

It should be noted that formula (62) is valid only under the condition $\gamma/(2l-k-1)\ll 1$ which is violated in the above-mentioned case $l=(k+1)/2$, when the dependence $\gamma(n\sqrt{T})$ takes place. Then the expansion of the function Ψ (60) and its substitution into relation (62) leads to the condition

$$\nabla\left(x\sqrt{T}\left(1+\gamma\left(\frac{4}{\sqrt{\pi}}\ln\gamma-\frac{n\sqrt{\pi}}{2}\ln x\right)\right)\right)=0. \tag{63}$$

Formulas (62) and (63) describe a steady state of the impuriton gas in the limit $\gamma\ll 1$ and can be regarded as the conventional Knudsen condition taking into account the small correction describing the contribution of impurity–impurity collisions. The sign of the correction is positive for $2l-1>k$ and negative for $2l-1\leqslant k$. This difference can be explained as follows. In view of the fact that the value of $x\sqrt{T}$ under the Knudsen conditions is virtually constant at all points of the mixture, the parameter $\gamma(x^kT^{l-1/2})\equiv\gamma((x\sqrt{T})T^{(2l-k-1)/2k}$ is actually a function of temperature, which increases for $2l-1>k$, decreases for $2l-1<k$, and constant at $2l-1=k$. Owing to the sign reversal mentioned above, the factors in the parentheses in formulas (62) and (63) are always increasing functions of the coordinate z. In order to compensate their increase, the factor $x\sqrt{T}$ must conversely decrease slowly, thus ensuring the constancy of the entire product on the whole. Thus, a natural situation arises in the mixture when the temperature gradient is compensated by a small (in view of the smallness of the quantity γ) oppositely directed gradient of the Knudsen parameter $[\nabla(x\sqrt{T})]/(x\sqrt{T})\sim-\gamma(\nabla T/T)$. In the special case $\gamma\sim x^kT^{k/2}$, the latter relation should be written in the form $\nabla\gamma/\gamma^2\sim-\nabla T/T$, which explains the emergence of the logarithmic term $\sim\ln T$ in the exact expansion (63). Thus, the factor in the parentheses in formula (62) containing γ varies according to the power law, while the similar factor in formula (63) increases in proportion to $\ln T$. Such a singularity leads to coordinate dependences of the Knudsen parameter $x\sqrt{T}$ which differ slightly in power for $2l-1=k$ [see (63)] and $2l-1\neq k$ (see (62)). This difference is the more pronounced, the larger the deviation of the value of $2l-k-1$ from zero. The above circumstance can be used for experimental determination of the true dependence of the impurity–impurity collision frequency on the impuriton density and temperature. It is well known[19] that the experimentally observed dependences $\nu(n,T)$ can be correctly described by the empirical law $\nu\sim nT^l$, where the quantity l can assume the values 1 or 1/2 depending on the temperature range under investigation. The former case with $l=1$ exactly corresponds to the dependence $\gamma(x\sqrt{T})$ specified above and can be determined from the characteristic logarithmic temperature dependence of the value of correction $\sim\gamma$.

Formulas (62) and (63) can form the basis for processing the results of experiments for studying the steady nonequilibrium state of ^{3}He–^{4}He superfluid mixture filling a porous medium.[20] The traditional setup normally used for measuring osmotic pressure is made in the form of two vessels filled with a superfluid mixture and connected through a supergap containing a porous material. The containers are maintained at constant but different temperatures so that unbalanced gradients of thermodynamic quantities leading to the flow of the mixture through the supergap emerge in the system. For example, the conditions under which the chemical potential of ^{4}He in the mixture is constant at all its points $[\mu_4(z)=\mathrm{const}]$ set in rapidly (during a few seconds) for the superfluid component of the mixture that does not encounter any resistance. At this stage, in the absence of thermal excitations, the values of pressure in the containers differ exactly by the value of the osmotic pressure of impuritons placed initially in one of the containers.[21] This difference in pressures is just the object of investigation in experiments.[20] However, the regime with $\mu_4=\mathrm{const}$ that sets in almost immediately is not stationary. The slow impuriton flow induced by unbalanced gradients of temperature and concentration continues in the system. The actual steady state sets in only when the concentration gradient balances the temperature

gradient so that the total diffusion flow of impuritons is equal to zero. According to estimates based on the analysis of experiments described by Ebner and Edwards,[20] such a regime may require several hours to set in. It should be noted that this time can be changed by varying the experimental conditions. Thus, an increase in the expectation time in experiments similar to those described in Ref. 20 could be used to analyze the Knudsen mechanism of stabilization of a steady flow in the system under investigation.

In the hydrodynamic limit, when impurity–impurity collisions prevail over impurity–powder collisions, mechanical equilibrium in the system is attained by levelling out the pressure in the mixture. The inclusion of the small contribution of impurity–impurity collisions to the stabilization of a steady flow in this approximation can be taken into account with the help of the expansion of the function Ψ (60) in the small parameter γ^{-1} and the substitution of the result into the steady-state condition (61). This gives

$$\nabla\left(xT\left(1+\frac{8}{3\gamma\sqrt{\pi}}\frac{1}{2(l-k)-1}+\ldots\right)\right)=0. \tag{64}$$

This formula is similar in structure to the result (62) obtained from an analysis of the Knudsen condition. Its applicability is limited by the inequality $2\gamma^{-1}/[2(l-k)-1] \ll 1$. The role of special case in this case is played by the dependence $\gamma^{-1}(xT)$ defined by the equality $l-1/2=k$. Since the osmotic pressure of impuritons in the hydrodynamic approximation is virtually constant at each point of the mixture, the quantity γ^{-1} in this case is in fact independent of coordinates also. Without repeating here the arguments concerning a comparison of formulas (62) and (63), we give here the result corresponding to the limit $\gamma^{-1}\ll 1$ for $l-1/2=k$:

$$\nabla\left(xT\left(1+\frac{4k}{3\sqrt{\pi}}\gamma^{-1}\ln x-\frac{15\pi-32}{8\sqrt{\pi}}\gamma^{-1}\ln\gamma^{-1}+\ldots\right)\right)=0. \tag{65}$$

For a more detailed analysis of the steady-state condition (61) in the intermediate region with arbitrary values of γ, we write it in the form

$$\frac{\nabla n}{n}+G(\gamma)\frac{\nabla T}{T}=0, \tag{66}$$

where $G(\gamma)\equiv w(\gamma)/h(\gamma)$ is a monotonically increasing function assuming the value 1/2 in the Knudsen limit $\gamma=0$ and 1 in the hydrodynamic limit $\gamma\to\infty$. The results of numerical analysis of the behavior of the function $G(\gamma)$ for intermediate values of γ are shown in Fig. 1. It can be seen that the function $G(\gamma)$ attains the value corresponding to the hydrodynamic approximation at an exponentially high rate. Thus, if the impurity–impurity collision frequency is higher than the impurity–powder collision frequency only by a factor of several units, a hydrodynamic situation is virtually realized in the impuriton gas.

In the degeneracy region $T\ll T_F$, the impurity–impurity collision frequency can be expressed through the relation[19]

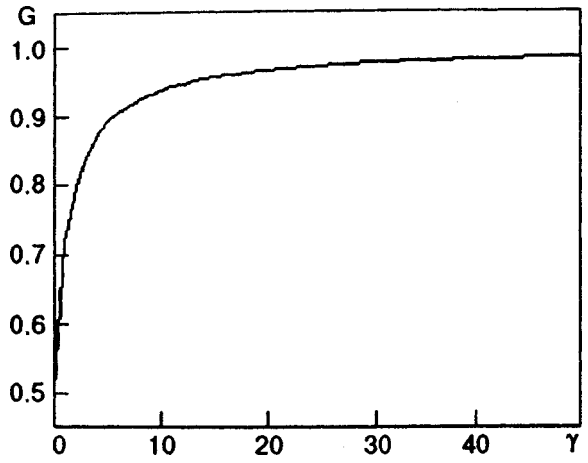

FIG. 1. Dependence of the ratio of the temperature and concentration gradients on the parameter γ in the steady state.

$$\nu=A^{-1}T^2\left(1-B\frac{T^2}{T_F^2}\right), \tag{67}$$

where A and B are the coefficients determined by the concentration of impuritons. It is convenient for further analysis to present expression (67) in the form

$$\nu=\nu^F\frac{T^2}{T_F^2}f(T_F)\left(1-B\frac{T^2}{T_F^2}\right), \tag{68}$$

where ν^F is a constant coinciding in order of magnitude with the collision frequency ν and having the same dimension and $f(T_F)\equiv A^{-1}T_F^2/\nu_F$ is the dimensionless function of the Fermi temperature, reflecting the dependence of ν on the concentration of impuritons.

Substituting expression (68) into relation (54) and confining the analysis to terms of the order of $\sim T^2/T_F^2$, we can write the condition ensuring the steady state of the impuriton gas in the form

$$\nabla\left[\int_0^{T_F}t\exp[-\gamma_F u(t)]dt+\frac{\pi^2}{12}T^2\exp[-\gamma_F u(T_F)]\right]=0, \tag{69}$$

where $\gamma_F=\nu^F/\nu^F_{\mathrm{Kn}}$, $\nu^F_{\mathrm{Kn}}=N\sigma^{(1,0)}\sqrt{2T_F/m^*}$, $u(t)\equiv 12/\pi^2\int_0^t f(y)/y\,dy$.

In the Knudsen limit $\gamma_F\ll 1$, relation (69) can be conveniently expressed in the form of the condition of constancy of the function of temperature and pressure of the impuriton gas at all points of the mixture:

$$P_F\left[1-\frac{15}{\pi^2}\gamma_F\int_0^1\frac{f(yT_F)}{y}(1-y^2)dy-\frac{5\pi^2}{24}\frac{T^2}{T_F^2}\times\left(1+\frac{12}{\pi^2}\gamma_F\int_0^1\frac{f(yT_F)}{y}dy\right)\right]=\text{const}, \tag{70}$$

where $P_F=(2/5)nT_F(1+(5\pi^2/12)(T^2/T_F^2))$ is the pressure of impuriton gas at $T\ll T_F$. It can be seen from formula (70) that the condition of mechanical equilibrium of the gas, which is valid in an infinite medium ($P_F=\text{const}$) is inapplicable when the main contribution to its stabilization comes from impurity–powder collisions. As in the case of the clas-

sical Knudsen effect, the pressure gradient emerging in this case has the same direction as the temperature gradient.

Concluding the section, we note that the Knudsen effect in a degenerate quantum gas is a unique physical phenomenon that has not been investigated experimentally. The impuriton gas in ^{3}He–^{4}He superfluid mixture is in fact the only known physical system in which this effect can be realized in pure form. The theoretical results discussed here can be used for analyzing the results of experiment on the steady nonequilibrium state of impuriton gas at low temperatures proposed earlier.

CONCLUSION

We have solved the problem on the flow of a quasiparticle gas under the action of gradients of thermodynamic quantities in a volume filled with a powder. The exact solution (36) obtained for the kinetic equation (1) is expressed in terms of the matrix elements of the quasiparticle–quasiparticle collision operator and the partial cross sections of scattering of quasiparticles at powder particles. The obtained solution makes it possible to analyze the transport of quasiparticle gas through a porous medium without resorting to model representations concerning the form of interaction between quasiparticles. The exact solution (36) is used for obtaining the expression (37) for the average rate of filtration of the quasiparticle gas through the porous medium. We obtained the condition (4), (5), and (38) describing the steady thermodynamically nonequilibrium state of a quasiparticle gas in a volume filled with a porous material. All the obtained results are valid for a classical as well as a degenerate gas of quasiparticles.

It has been proved that the exact expression (14) describing the result of action of the collision operator on an arbitrary function of momentum can be used for constructing various approximations. Among other things, a model in which the action of the particle–particle collision operator on any function that does not belong to its kernel is reduced to the multiplication by a phenomenological parameter (collision frequency) is investigated. Such an approach allowed us to derive consecutively expression (49) for the model collision integral introduced artificially in the BGK theory, The model representation of the collision integral has made it possible to simplify all the results obtained in the general form. For example, the approximation in question was used for deriving an explicit expression for (53), (56) for the filtration rate of a quasiparticle gas, and relation (54) ensuring its steady state was derived. The steady-state condition (38) was reduced to the form of a relation between the gradients of the gas temperature and density and analyzed in detail in the range of high ($T \gg T_F$) (66) and low ($T \ll T_F$) (69) temperatures. The obtained results are valid for arbitrary relations between the frequencies ν and ν_{Kn} of collisions of quasiparticles with one another and with powder particles. The steady-state condition (54) was studied in detail in the hydrodynamic $\nu \gg \nu_{\mathrm{Kn}}$ (64) and (65) and in the Knudsen $\nu \ll \nu_{\mathrm{Kn}}$ (62), (63) limiting cases. For the intermediate region $\nu \sim \nu_{\mathrm{Kn}}$, the steady-state condition (66) was analyzed numerically. A continuous transition from the Knudsen to the hydrodynamic quasiparticle gas flow was studied, and the Knudsen effect (70) in a degenerate quantum gas was investigated.

The obtained results are applicable for analyzing the steady nonequilibrium state of the impuriton gas in ^{3}He–^{4}He superfluid mixture in a confined geometry. Two stages of stabilization of such a state were discovered and studied. Experiments were proposed for determining the temperature and concentration dependence of the impurity–impurity collision frequency.

This research was partly supported by EPSRS Grant No. GR/M/22543 and ISEP Grant No. QSU082002.

*E-mail: alex@viola.kharkov.ua

[1] L. D. Landau and L. P. Pitaevskii, *Physical Kinetics* [in Russian], Nauka, Moscow (1979).
[2] A. V. Lykov, *Transport Phenomena in Capillary-Porous Materials* [in Russian], Nauka, Moscow (1954).
[3] T. Graham, Quart. J. Sci. **2**, 74 (1829).
[4] J. Loschmidt, Sitzber. Akad. Wiss. Wien **61**, 367 (1870).
[5] J. Loschmidt, Sitzber. Akad. Wiss. Wien **62**, 468 (1870).
[6] J. C. Maxwell, Philos. Mag. **20**, 21 (1860).
[7] T. Graham, Philos. Trans. R. Soc. London **136**, 573 (1846).
[8] B. V. Deryagin and S. P. Bakanov, Dokl. Akad. Nauk SSSR **115**, 267 (1957) [Sov. Phys. Dokl. **2**, 326 (1957)].
[9] B. V. Deryagin and S. P. Bakanov, Zh. Tekh. Fiz. **27**, 2056 (1957) [Sov. Phys. Tech. Phys. **2**, 1904 (1957)].
[10] R. H. Aranow, Proc. Natl. Acad. Sci. USA **50**, 1066 (1963).
[11] J. P. Breton and D. Massingnon, J. Chim. Phys. Phys.-Chim. Biol. **60**, 294 (1963).
[12] M. M. R. Williams, J. Phys. D **6**, 759 (1973).
[13] M. C. Mackey, Biophys. J. **11**, 75 (1971).
[14] C. Cercignani, *Theory and Application of the Boltzmann Equation*, Plenum, New York (1975).
[15] J. Ferziger and H. Kaper, *Mathematical Theory of Transport Processes in Gases*, North-Holland, Amsterdam (1972).
[16] I. N. Adamenko, A. V. Zhukov, and K. E. Nemchenko, Fiz. Nizk. Temp. **23**, 574 (1997) [Low Temp. Phys. **23**, 428 (1997)].
[17] I. N. Adamenko and K. E. Nemchenko, Fiz. Nizk. Temp. **21**, 498 (1995) [Low Temp. Phys. **21**, 386 (1995)].
[18] L. D. Landau and E. M. Lifshitz, *Quantum Mechanics*, Nauka, Moscow (1989) Translation of 3rd ed. Pergamon, Oxford 1977.
[19] I. N. Adamenko and È. Ya. Rudavskii, Fiz. Nizk. Temp. **13**, 3 (1987) [Sov. J. Low Temp. Phys. **13**, 1 (1987)].
[20] C. Ebner and D. O. Edwards, Phys. Rep., Phys. Lett. **2C**, 79 (1971).
[21] I. N. Adamenko, K. È. Nemchenko, V. I. Tsyganok, and A. I. Chervanev, Fiz. Nizk. Temp. **20**, 636 (1994) [Low Temp. Phys. **20**, 498 (1994)].

Translated by R. S. Wadhwa

Nonmonotonic temperature dependence of the mass transfer rate during isotopic phase separation of ^{3}He–^{4}He solid mixtures

A. N. Gan'shin, V. N. Grigor'ev, V. A. Maidanov, N. F. Omelaenko, A. A. Penzev, E. Ya. Rudavskii, and A. S. Rybalko

*B. Verkin Institute for Low Temperature Physics and Engineering, National Academy of Sciences of the Ukraine, 310164 Kharkov, Ukraine**

(Submitted November 9, 1998)
Fiz. Nizk. Temp. **25**, 356–361 (April 1999)

It is discovered that the characteristic phase separation time constant of solid ^{3}He–^{4}He mixtures at low temperatures exhibits a nonmonotonic temperature dependence with a minimum. It means that the rate of mass transport slows down at very low temperatures, and the corresponding values of the effective diffusion coefficient also depend nonmonotonically on temperature and concentration and differ significantly from the spin diffusion coefficient measured earlier in NMR experiments on quantum diffusion. The discovered nonmonotonicity may be associated with the influence of the nonuniform field of elastic stresses in the crystal because of the difference in the molar volumes of the phases. © *1999 American Institute of Physics.* [S1063-777X(99)00404-1]

1. INTRODUCTION

The determination of the growth mechanism for the new phase is one of the most important and least studied questions associated with the kinetics of the first-order phase transition. In the case the isotopic phase separation of solid ^{3}He–^{4}He mixtures, this problem emerges when we analyze the growth of ^{3}He inclusions in a ^{4}He crystal. It is usually assumed that the transport of ^{3}He atoms from the surrounding mixture undergoing separation to the nuclei of the new phase is governed by diffusion.

The first attempt to study this problem experimentally was made by Iwasa and Suzuki[1] who applied the method of measuring pressure for studying phase separation of a mixture with the initial concentration 0.84% ^{3}He under a pressure of 3.16 MPa. They observed that the characteristic separation time constant τ is independent of temperature and concentration, which contradicts the concept of impurity-induced excitations. According to this concept, the value of τ must decrease with temperature (mixture concentration) due to quantum diffusion.

The temperature dependence of the time constant τ predicted by the quantum theory of impuritons was observed later[2] in NMR experiments on the kinetics of separation of a mixture with a ^{3}He concentration of 3.18% under a pressure of 3.7 MPa. It turned out, however, that the observed dependence $\tau(T)$ matched only qualitatively with the theory.[3] The quantitative agreement can be reached in this case if the fitting parameter corresponds to the value of diffusion coefficient much smaller than the quantum spin diffusion coefficient measured in NMR experiments.[4]

The subsequent analysis of this problem carried out quite recently by the method of pressure measurements[5] proved that at lower temperatures the value of τ increases upon cooling. The existence of such a nonmonotonicity in the temperature dependence of phase separation time does not follow from the impuriton model of ^{3}He atoms in the mixture either.

Being the continuation of experiments,[5] this work is devoted to finding the reasons behind the difference in experimental results obtained in Refs. 1, 2, and 5 on the one hand and to analyzing the possibility of their interpretation in the model of the diffusion mechanism of transport of ^{3}He atoms during phase separation.

2. FEATURES OF EXPERIMENTAL TECHNIQUE

In our experiments, we used the experimental cell described earlier[5] and the method of preparing the crystal with the initial concentration 2.05% ^{3}He. The experiments were made in the temperature range 50–300 mK for the molar volume 20.23 cm^3/mol corresponding to a pressure of 35.99 bar at the phase-transition temperature.

Isotopic phase separation was initiated by cooling a homogeneous mixture in small steps (10–15 mK) below the phase separation curve followed by a prolonged temperature stabilization. The phase transition was detected by precision measurement of pressure in the crystal. At each step, the equilibrium pressure in the two-phase crystal was attained according to an exponential law with the characteristic time constant τ. The concentration of both phases at the end of each step corresponded to the equilibrium phase-separation curve.

3. TEMPERATURE DEPENDENCE OF PHASE-SEPARATION TIME CONSTANT

The values of characteristic phase-separation time constant τ obtained by us for different molar volumes are presented in Fig. 1 as a function of temperature together with the results obtained earlier.[1,2,5] It can be seen from Fig. 1 that our results for the molar volume 20.23 cm^3/mol ($P = 35.99$ bar) are in good agreement with the results obtained in Ref. 5 for samples with a close density of

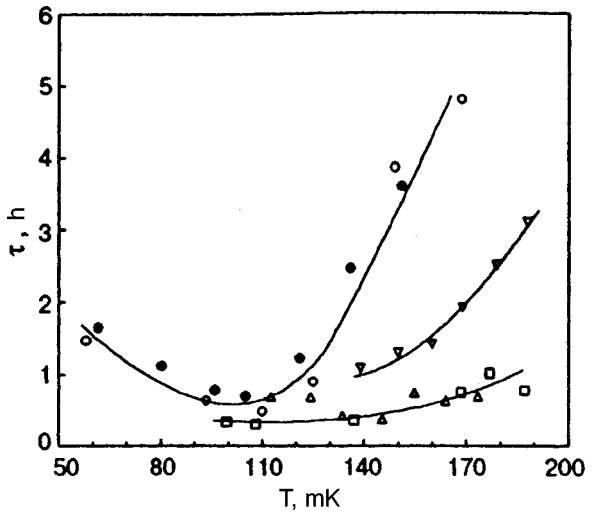

FIG. 1. Temperature dependence of the characteristic phase-separation time for mixtures. Symbols on curves correspond to the results obtained in the following works: (○)—Ref. 5 ($P=35.70$ bar, $x_0=2.05\%$), (●) our results ($P=35.99$ bar, $x_0=2.05\%$); △—Ref. 1 ($P=31.6$ bar, $x_0=0.84\%$); □—Ref. 5 ($P=31.7$ bar, $x_0=2.05\%$); ▽—Ref. 2 ($P=37.3$ bar, $x_0=3.18\%$).

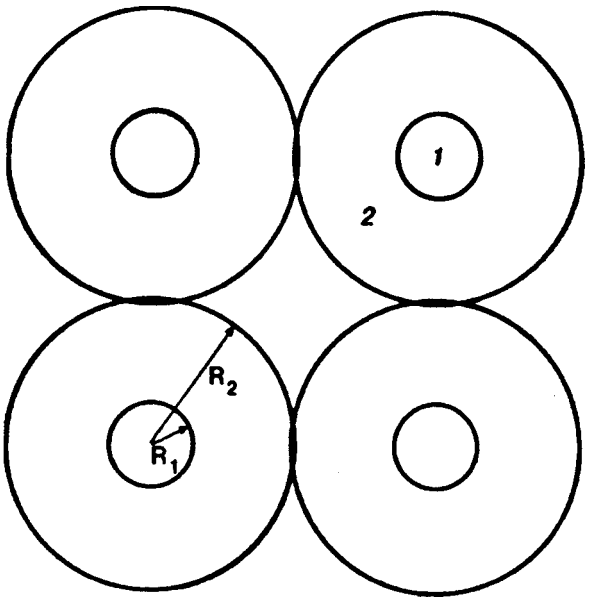

FIG. 2. Schematic diagram of the model illustrating the calculation of the effective diffusion coefficient: inclusion of the concentrated phase (*1*) and region of surrounding mixture from which diffusion to the inclusion takes place (*2*).

20.28 cm^3/mol ($P=35.7$ bar). A clearly manifested minimum on the temperature dependence of τ is observed near ~110 mK.

Figure 1 shows that crystals with a higher molar volume of 20.54 cm^3/mol ($P=31.7$ bar) exhibit a weak temperature dependence of the phase-separation time. The obtained results are in good agreement with the data presented in Ref. 1 for samples with a close density ($P=31.6$ bar) for the initial concentration 0.84% ^{3}He. In this case, no low-temperature measurements were made since solid inclusions of the concentrated phase for the given density below ~82 mK must melt and transform into liquid drops according to the phase diagram.

Figure 1 also shows the results obtained in Ref. 2 for the initial concentration 3.18% ^{3}He and the molar volume 20.24 cm^3/mol ($P=37$ bar). In this case, a nonmonotonicity in the $\tau(T)$ dependence was not detected since these experiments could not be continued below 140 mK in view of specific features of NMR measurements used.[2] A comparison with the results obtained in Ref. 2 shows, that apart from pressure, the initial concentration of the mixture also has a considerable effect on the kinetics of phase separation. The value of τ probably decreases with increasing initial concentration for the same density of the crystal due to an increase in the number of nuclei of the new phase and a decrease in the average distance between them.

Thus, the analysis carried out by us proved that the results of different experiments (obtained in Refs. 1, 2, 5 and by us) are not in a serious contradiction. The value of τ depends considerably on the density of the crystal as well as the initial concentration of the mixture. Further investigations of the kinetics of phase separation for different pressures and concentrations are required to determine the mechanisms of the influence of these factors.

4. EFFECTIVE COEFFICIENT OF DIFFUSION ASSOCIATED WITH PHASE SEPARATION

The experimental data on the characteristic time constant τ phase separation presented in Fig. 1 allow us to determine the effective coefficient D_{eff} of mass diffusion ensuring the transport of ^{3}He atoms to the inclusions of the new phase.

Figure 2 shows a simple model usually considered for solving problems associated with diffusion separation of solid mixtures (see, for example, Ref. 6). The inclusions of the new phase formed can be presented in the form of identical spheres of radius R_1 distributed uniformly in the volume of the matrix mixture. The relation between D_{eff} and τ can be obtained from the solution of the corresponding diffusion problem written in spherical coordinates:

$$\frac{\partial x}{\partial t}=D\left(\frac{\partial^2 x}{\partial r^2}+\frac{2}{r}\frac{\partial x}{\partial r}\right), \tag{1}$$

where x is the concentration of the mixture and r the particle coordinate. The boundary conditions for the concentration $x(r,t)$ of the mixture corresponding to the growth of the new phase under investigation, can be written in the form

$$x(r,t)\big|_{r=R_1}=x_k \quad \text{and} \quad \left.\frac{\partial x(r,t)}{\partial r}\right|_{r=R_2}=0, \tag{2}$$

while the initial condition can be written as

$$x(r,0)=x_i, \tag{3}$$

where x_i is the initial concentration of the mixture, x_k the concentration determined from the phase separation diagram for the temperature specified in the given experiment, and R_2 the radius of the region in which ^{3}He atoms diffuse to the given inclusion.

TABLE I. Average radius of inclusions of concentrated phase obtained by different experimental methods.

Measuring technique	Reference	P, atm	$T_{\min}$, mK	R_1, μm
Thermal conductivity	11	32	100	0.75
NMR and ΔP	12	26.9	50	2
NMR	13	32	100	2
NMR	14	36	16	2.25

Disregarding the change in the inclusion radius in the course of phase separation, we can write the solution of Eq. (1) in the form of a series[1)]

$$x_i - x(r,t) = \sum_{n=0}^{\infty} A_n \frac{\sin \lambda_n (r - R_1)}{r} \exp(-D_{\text{eff}} \lambda_n^2 t), \quad (4)$$

where A_n are constant coefficients, and the parameters λ_n can be determined from the solution of the transcendental equation

$$\tan \lambda_n (R_2 - R_1) = \lambda_n R_2 . \quad (5)$$

It was noted above that Eq. (4) is a solution of the problem for $R_1 = \text{const}$. The solution determined by taking into account the variation of R_1 during the growth (and dissolution) of inclusions is given in Ref. 6. The solution is complicated considerably in this case, but the emerging additional corrections do not alter the time dependence and are insignificant in the given case.

The obtained series (4) converges quite rapidly, and hence it is sufficient to analyze only its first term. Since the change in the value of pressure ΔP measured in experiments is proportional to Δx,[8] the time dependence of ΔP can also be described by Eq. (4). Since $\Delta P \sim e^{-t/\tau}$,[5] the required diffusion coefficient can be determined from the relation

$$D_{\text{eff}} = (\lambda_0^2 \tau)^{-1}. \quad (6)$$

The important factor in determining λ_0, and hence D_{eff}, is the calculation of the radius of inclusion R_1.

The radius of inclusions of the new phase formed during isotopic phase separation of ^{3}He–^{4}He mixtures was determined earlier from other experiments[11–14] whose results are given in Table I.

The values of R_1 presented in the table correspond to quite low temperatures, i.e., give the maximum radius of an inclusion. For subsequent calculations, we used the value $R_{1(\max)} = 2.25\ \mu$m.

The value of R_1 changes with temperature (concentration) in the course of phase separation. It follows from the law of conservation of the amount of ^{3}He in the mixture undergoing phase separation that R_1 varies according to the law

$$R_1 = R_{1(\max)} (1 - x/x_i)^{1/3}, \quad (7)$$

and the relation between $R_{1(\max)}$ and R_2 has the form

$$R_2^3 = R_{1(\max)}^3 \frac{V_0}{x_i V_c}, \quad (8)$$

where V_0 and V_c are the molar volumes of the initial mixture and the concentrated phase forming the inclusion respectively. While calculating D_{eff}, we took into account the concentration dependence of R_1 described by formula (7). Formula (8) shows that the value of R_2 for the given concentration amounts to 7.5 μm.

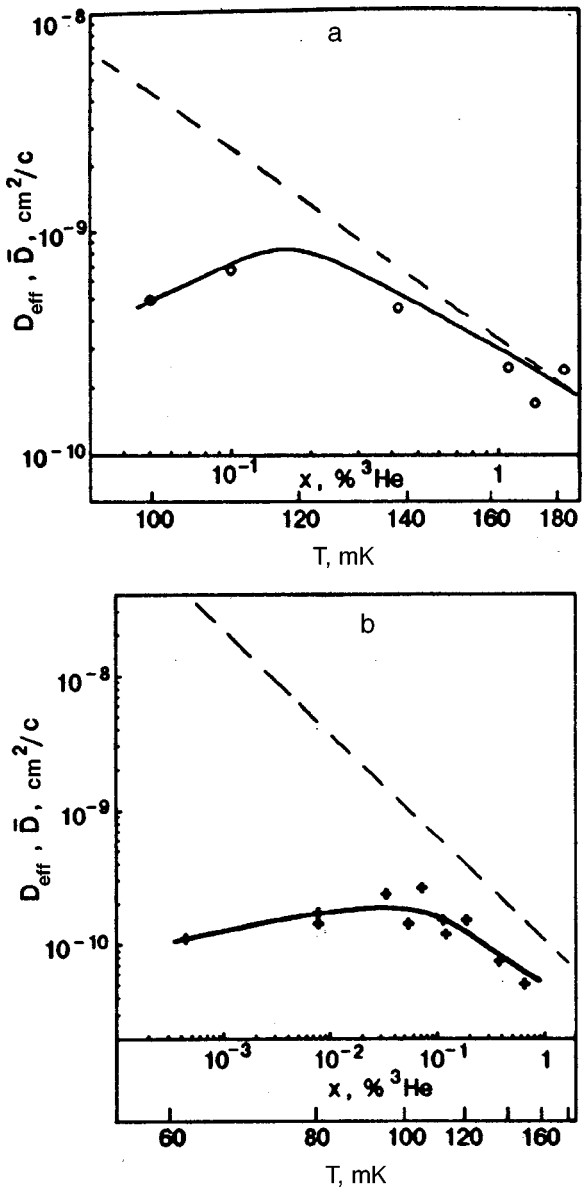

FIG. 3. Dependence of the effective diffusion coefficient D_{eff} corresponding to the measured values of time constant τ on the concentration and temperature: $P = 31.70$ bar (a) and $P = 35.99$ bar (b). The dashed line corresponds to the average value of spin diffusion coefficient $\bar{D}$ (calculated by formulas (9) and (10). The equilibrium concentration shown in the figure was determined according to the theory of regular mixtures.[16]

The values of D_{eff} determined for two molar volumes are presented in Fig. 3. It is expedient to compare these data with the self-diffusion coefficient D_s for impuritons determined in NMR experiments by the method of spin echo.[4] Some complications arise due to the fact that the value of D_s depends considerably on concentration in the quantum diffusion region at low temperatures and small ^{3}He concentrations (see, for example, Ref. 9). However, the situation is simplified in view of the fact that, according to Ref. 10 the growth rate in the case when D_s depends on concentration corresponds to

the rate calculated for a certain constant diffusion coefficient determined by the averaging:

$$\overline{D}=\frac{1}{x_k-x_i}\int_{x_i}^{x_k}D_s(x)dx. \tag{9}$$

Thus, the values of $D_{\rm eff}$ were compared with the values of $\overline{D}$ obtained by the averaging of D_s for the concentration range typical of the given stage of cooling. According to Ref. 9, D_s can be written in the form

$$D_s=D_0\ \frac{1}{x}(1-x/x_c)^{1.7}, \tag{10}$$

where D_0 and x_c are the quantities depending on density.

The values of $\overline{D}$ calculated by formula (9) taking into account (10) are shown in Fig. 3 by the dashed line as functions of concentration (temperature). Since the measurements were made along the phase-separation curve, a one-to-one correspondence between temperature and concentration takes place. It can be seen from the figure that $D_{\rm eff}$ and $\overline{D}$ at high temperatures exhibit similar temperature dependences. The quantitative difference between them can be due, for example, to inaccurate values of the radius of the new phase inclusion. The coincidence of the values of $D_{\rm eff}$ and $\overline{D}$ in this region can be attained if we assume that the diameter of the inclusion is larger by a factor of $\sim$1.6 (for a pressure of 35.99 bar) than the value used by us here.

It should also be noted that the mutual diffusion coefficient estimated in the given experiments may differ from the value of D_s measured by the NMR method when the probability of U-processes in impuriton collisions differs from unity significantly.

At low temperatures, the value of $D_{\rm eff}$ is much smaller that the values of diffusion coefficient obtained from NMR experiments on quantum diffusion. This difference increases upon cooling and leads to the emergence of a maximum on the temperature dependence of $D_{\rm eff}$.

A possible explanation of the observed nonmonotonic dependences $D_{\rm eff}(T)$ and $\tau(T)$ can be the consideration of elastic fields near the boundary of the ^{3}He inclusion emerging during its growth due to the difference in the molar volumes of the initial mixture and the bcc phase formed. A similar effect was observed more than once in an analysis of other systems.[6,10]

In the presence of a nonuniform potential field characterized by the potential gradient ∇U, the diffusion flux can be written in the form (see, for example, Ref. 15)

$$J=-\frac{Dx}{w}\left(\frac{\nabla x}{x}+\frac{\nabla U}{kT}\right), \tag{11}$$

where w is the atomic volume.

If ∇x and ∇U have opposite directions (which is the case in our situation when the phase formed has a larger molar volume), the mass transport may become noticeably smaller (and the value of τ may become larger) at low temperatures if the second term in (11) becomes comparable to the first term.

The presence of a noticeable gradient of elastic forces can also produce a specific effect on quantum diffusion process, slowing it down due to mismatching of levels at neighboring lattice sites. However, the explanation of the increase in τ upon cooling by using this mechanism requires the fulfillment of an additional condition, viz., an increase in ∇U with the inclusion radius. The possibility of this mechanism can be determined only if we comprehensively take into account potential fields in this specific case.

The authors are grateful to A. F. Andreev, Yu. M. Kagan, and M. A. Strzhemechnyi for fruitful discussion of the results of this research.

This research was partly supported by the International Research Program on Science and Education (Grants Nos. QSU 082169 and QSU 082048).

*E-mail: rudavskii@ilt.kharkov.ua

[1)]The solution of a similar problem can be found, for example, in Ref. 7.

[1] I. Iwasa and H. Suzuki, in *Proc. LT-17*, North-Holland, Amsterdam (1984).
[2] V. A. Shvarts, N. P. Mikhin, E. Ya. Rudavskii *et al.*, Fiz. Nizk. Temp. **21**, 717 (1995) [Low Temp. Phys. **21**, 556 (1995)].
[3] T. N. Antsygina, K. A. Chishko, N. P. Mikhin *et al.*, J. Low Temp. Phys. **111**, 19 (1998).
[4] V. A. Mikheev, N. P. Mikhin, and V. A. Maidanov, Fiz. Nizk. Temp. **9**, 901 (1983) [Sov. J. Low Temp. Phys. **9**, 465 (1983)].
[5] A. N. Ganshin, V. A. Maidanov, N. F. Omelaenko *et al.*, Fiz. Nizk. Temp. **24**, 815 (1998) [Low Temp. Phys. **24**, 611 (1998)].
[6] B. Ya. Lyubov, *Diffusion Processes in Heterogeneous Solid Media* [in Russian], Nauka, Moscow (1981).
[7] B. M. Budak, A. A. Samarskii, and A. N. Tikhonov, *A collection of Problems in Mathematical Physics* Pergamon, Oxford 1980.
[8] W. J. Mullin, Phys. Rev. Lett. **20**, 254 (1968).
[9] V. N. Grigor'ev, Fiz. Nizk. Temp. **23**, 5 (1997) [Low Temp. Phys. **23**, 1 (1997)].
[10] J. Christian, *The Theory of Transformations in Metals and Alloys*, Pergamon Press, Oxford (UK) (1975).
[11] A. E. Burgess and M. J. Crooks, Phys. Lett. **A39**, 183 (1972).
[12] A. S. Greenberg, W. C. Thomlinson, and R. C. Richardson, J. Low Temp. Phys. **8**, 3 (1972).
[13] V. A. Mikheev, V. A. Maidanov, N. P. Mikhin *et al.*, Fiz. Nizk. Temp. **14**, 563 (1988) [Sov. J. Low Temp. Phys. **14**, 309 (1988)].
[14] S. C. J. Kingsley, V. Maidanov, J. Saunders, and B. Cowan, J. Low Temp. Phys. **113**, 1017 (1998).
[15] V. V. Slezov, Fiz. Tverd. Tela (St. Petersburg) **36**, 557 (1994) [Phys. Solid State **36**, 308 (1994)].
[16] D. O. Edvards, A. S. McWilliams, and J. G. Daunt, Phys. Rev. Lett. **9**, 195 (1962).

Translated by R. S. Wadhwa

ELECTRONIC PROPERTIES OF METALS AND ALLOYS

On the contribution of dislocations to the resistivity of niobium

V. I. Sokolenko

*National Scientific Center ''Kharkov Institute of Physics and Engineering,'' 310108 Kharkov, Ukraine**
(Submitted June 30, 1998; revised October 27, 1998)
Fiz. Nizk. Temp. **25**, 362–366 (April 1999)

The change of the resistivity increment $\Delta\rho/N_d$ normalized to the average density of dislocations in the core of niobium single crystals is studied in different structural states (after rolling deformation at 20 K and consecutive removal of surface layers). For a homogeneous structure with a high density of uniformly distributed dislocations ($N_d = 13\times10^{10}\,\mathrm{cm}^{-2}$), the value of resistivity produced by a single dislocation $r_d \simeq (9\pm3)\cdot10^{-19}\,\Omega\cdot\mathrm{cm}^3$ is determined, taking into account the contribution from vacancies to $\Delta\rho$. A quantitative analysis of the value of r_d for niobium is carried out on the basis of models of resonant electron scattering by dislocations.
 [S1063-777X(99)00504-6]

INTRODUCTION

Being a type of crystal lattice defects, dislocations are responsible for scattering of charge carriers and influence the parameters of electric charge transfer. The contribution of dislocations to the resistivity of metals was analyzed in many experimental and theoretical publications. An analysis of the available experimental data[1–3] shows that fcc crystals such as Cu, Au, Ag, and Al for which the dislocation resistivity is $r_d \simeq (1-2)\times10^{-19}\,\Omega\times\mathrm{cm}^3$ and the spread in the values for each metal amounts to ~20% are studied most thoroughly. Transition bcc metals have been studied less extensively in this respect. They exhibit higher values of r_d, and the spread in the data is much larger than for the above-mentioned fcc metals. For example, the values of r_d for Mo and W differ by a factor of ~3.8[4,5] and ~2.5.[6,7] Systematic studies of r_d of group V elements have not been carried out. An estimate obtained by Aksenov *et al.*[8] for vanadium with a low average density of dislocations is $r_d \sim 10\times10^{-19}\,\Omega\times\mathrm{cm}^3$. The available results for Nb should be accepted with caution. The values of $r_d \sim 70\times10^{-19}\,\Omega\times\mathrm{cm}^3$ given in Refs. 9, 10 were obtained indirectly and are much higher that the corresponding parameters for other transition metals.

A satisfactory agreement between the theoretical and experimental values of r_d for some metals and a good agreement for some other (especially noble) metals was attained by using the theoretical models[1–3] taking into account peculiarities of charge carrier scattering in local regions near the dislocation core. The values of r_d for group V elements have not been calculated in these publications.

This research aims at determining the value of r_d for Nb with a high density of uniformly distributed dislocations and comparing it with the values calculated on the basis of the models of resonant scattering of electrons at quasi-stationary states associated with dislocations.[1,3] The high density of dislocations is a necessary condition for correct calculation of r_d in the presence of a finite impurity concentration in view of the interrelation between the electron–impurity and electron–dislocation scattering at low temperatures for a metal with an anisotropy of the electron relaxation time at a nonspherical Fermi surface (FS).[11,12]

SAMPLES AND EXPERIMENTAL TECHNIQUE

We investigated Nb with a purity of 99.956 wt.% obtained by electron-beam melting. The effect of rolling deformation at 20 K {the direction of rolling close to [110] and the rolling plane close to (001)} followed by heating to room temperature as well as consecutive symmetrical removal of surface layers by polishing on the variation of a number of physical parameters including the resistivity ρ_n measured at $T = T_c + 0.5\,\mathrm{K}$, where T_c is the superconducting transition temperature was investigated earlier[13] for single crystals of this material (with $T_{c0} = 9.15\,\mathrm{K}$ and $\rho_{n0} = 0.937\,\mu\Omega\times\mathrm{cm}$ for samples in the initial state). The change in the average density N_d of dislocations at the core of the sample was also studied. In the present work, we used the results obtained in Ref. 13 for calculating the values of $\Delta\rho/N_d (\Delta\rho = \rho_n - \rho_{n0})$ for niobium in different structural states and singled out the characteristic of the homogeneous dislocation structure with a high density of dislocations. The value of r_d was determined taking into account the contribution of vacancion-type defects to $\Delta\rho$ under the assumption that the contributions of linear and point defects are additive.

DISCUSSION OF RESULTS

The errors in experimental determination of the value of r_d are mainly due to inaccuracy in determining the dislocation density and the contribution of points defects generated by dislocations to $\Delta\rho$. Figure 1 illustrates the effect of structural state of Nb deformed by rolling at 20 K on the value of $\Delta\rho/N_d$. According to the results obtained in Ref. 13, the increase in the value of $\Delta\rho/N_d$ for a single crystal with the grain orientation (001)[110] in the interval $6\times10^{10}\,\mathrm{cm}^{-2}$

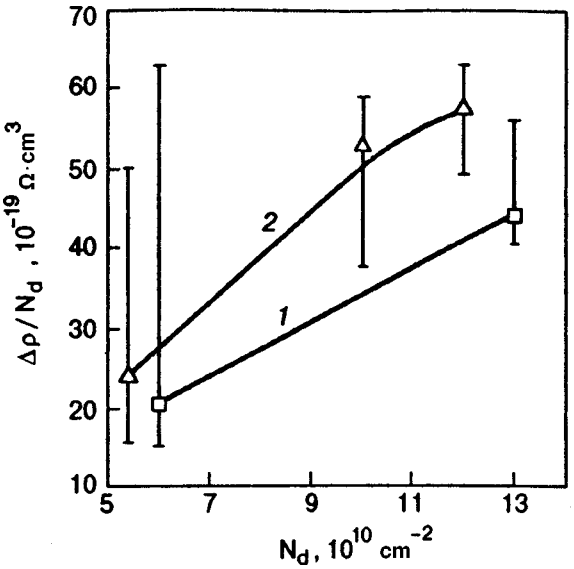

FIG. 1. Dependence of $\Delta\rho/N_d$ on N_d ($\Delta\rho$ is the resistivity increment and N_d average density of dislocations at the core) for a Nb single crystal with the grain orientation (001)[110] (curve *1*) and for a polycrystalline sample (curve *2*) deformed by rolling at 20 K. The values of $\Delta\rho$ and N_d for polycrystalline Nb are borrowed from Ref. 14. The vertical segments show the spread of N_d from minimum to maximum values.

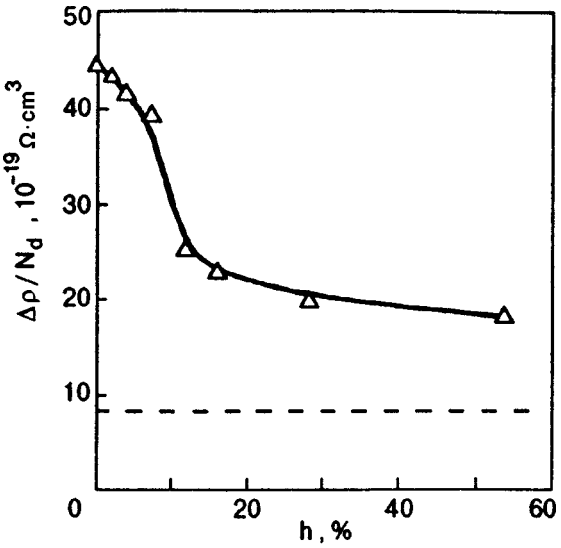

FIG. 2. Dependence of $\Delta\rho/N_d$ on the relative increase in the thickness h of a layer removed by chemical polishing for a Nb single crystal preliminarily deformed by rolling by 42%. The dashed line corresponds to a decrease in $\Delta\rho$ by ~50% as a result of vacancy annealing.

$\leqslant N_d \leqslant 13\times10^{10}\,\mathrm{cm}^{-2}$ is associated with the formation of a heterogeneous structural state in the sample cross section. This state combines uniformly distributed dislocations at the core and a higher-defective fragmented structure in the surface layers. It follows from Fig. 1 that in contrast to the single crystal, a polycrystalline sample deformed under similar conditions exhibits a stronger increase in $\Delta\rho/N_d$ upon an increase in N_d, which can be due to a higher rate of accumulation of defects in the surface layers or due to a larger contribution of elastic stress fields to $\Delta\rho$.

In our calculations of r_d, we used the characteristics of the structural state formed in the single crystal rolled by $\delta=42\%$ ($N_d=13\times10^{10}\,\mathrm{cm}^{-2}$). The maximum spread in the values of N_d for this structural state amounts to 33%, which is approximately half the spread for the structural state with $N_d=6\times10^{10}\,\mathrm{cm}^{-2}$ ($\delta=12\%$). In the case of symmetric removal of surface layers of the single crystal deformed by $\delta=42\%$, a consecutive transition from a heterogeneous to homogeneous structural state in the form of uniformly distributed dislocations is observed, and the minimum value of deformational increment to resistivity normalized to the average density of dislocations is attained for the sample core: $\Delta\rho_{\min}/N_d\approx18\times10^{-19}\,\Omega\times\mathrm{cm}^3$ (Fig. 2). It should be noted that this structural state is characterized by the minimum factor of compressive stresses.[13] The value of $\Delta\rho_{\min}/N_d$ indicated above is smaller approximately by a factor of 2.5 than the value corresponding to the structural state formed after rolling by 42%. For the sample rolled by 10% ($N_d=6\times10^{10}\mathrm{cm}^{-2}$), the difference amounts to ~12%. It follows from Fig. 2 that the use of the value of $\Delta\rho$ characterizing the sample deformed by rolling to the ''average'' extent without the removal of surface layers for calculating r_d leads to considerably exaggerated values. This explains the strong (by a factor of ~3.8) difference between the values of r_d for Mo deformed by rolling by 44% (without the removal of surface layers)[5] and deformed by extension.[4]

Apart from the dislocation contribution, the quantity $\Delta\rho_{\min}/N_d\approx18\times10^{-19}\,\Omega\times\mathrm{cm}^3$ also contains the contribution from defects of the vacancion type remaining in the sample after heating to room temperature. These defects start moving over the Nb lattice at $T>420\,\mathrm{K}$.[15] It was established[16] that a polycrystalline Nb sample deformed as a result of rolling by 37% at 20 K exhibits a two-stage variation of $\Delta\rho$ and T_c during annealing in the temperature range $423\,\mathrm{K}\leqslant T\leqslant553\,\mathrm{K}$, the stage of increasing T_c due to the removal of vacancion-type defects to sinks corresponding to a decrease in $\Delta\rho$ by ~65%. Additional experiments proved that rolling by 80% leads to the extension of the stage of increasing T_c to ~530 K upon a decrease in $\Delta\rho$ by ~70%. Annealing at 533 K of a Nb single crystal (identical to that studied by us) deformed by rolling by 78% at 20 K ensures a decrease in $\Delta\rho$ by 56%.[17] We can assume that the relation between the vacancion contributions to $\Delta\rho$ for samples of polycrystalline and monocrystalline Nb samples rolled by 37 and 80% does not differ significantly from that for samples rolled by 42 and 78%, respectively. This leads to the averages value of the dislocation contribution to resistivity $r_d\simeq0.5\Delta\rho_{\min}/N_d\simeq9\times10^{-19}\,\Omega\times\mathrm{cm}^3$. This value corresponds to the dashed line in Fig. 2. Taking into account the above-mentioned accuracy of determining N_d and the vacancion contribution to $\Delta\rho$, we finally obtain $r_d\simeq(9\pm3)\times10^{-19}\,\Omega\times\mathrm{cm}^3$. The value of r_d obtained for Nb is in good agreement with the available data for bcc transition metals such as Mo ($r_d=5.8\times10^{-19}\,\Omega\times\mathrm{cm}^3$),[4] W ($r_d=7.5\times10^{-19}\,\Omega\times\mathrm{cm}^3$),[7] Fe ($r_d=(10\pm4)\times10^{-19}\,\Omega\times\mathrm{cm}^3$),[18] and V ($r_d=10\times10^{-19}\,\Omega\times\mathrm{cm}^3$).[8]

CALCULATION OF r_d FOR Nb BY USING THEORETICAL MODELS

Brown's model[1] is based on the assumption of resonant type of scattering of Fermi electrons at the dislocation core

in the absence of interband scattering. The expression for r_d corresponds to randomly oriented dislocations and has the form

$$r_d = 8\hbar/3e^2 n_e, \quad (1)$$

where $\hbar$ is Planck's constant, e the electron charge, and n_e the carrier concentration. The applicability of Eq. (1) to metals with a complex FS was considered by Brown[1] who demonstrated a reasonable agreement with experimental results for values of n_e estimated from the volume of closed FS sheets. According to the results obtained for Nb in Refs. 19, 20, the carrier concentration amounts to $4.5\times10^{22}\,\mathrm{cm}^{-3}$ and $5.6\cdot10^{22}\,\mathrm{cm}^{-3}$, respectively. Substituting these values of n_e into formula (1), we obtain $r_d \simeq (1.8-2.4)\cdot10^{-19}\,\Omega\cdot\mathrm{cm}^3$. Thus, the value corresponding to the upper boundary of calculated values of r_d for Nb is smaller by a factor $\sim$2.5 than the value corresponding to the lower boundary of the values determined experimentally.

In the Karolik–Luchvich model,[3] the value of r_d was calculated in the relaxation time approximation on the basis of the relation

$$r_d = \hbar k_F Q/e^2 n_{\mathrm{eff}}, \quad (2)$$

where k_F is the wave vector, Q the transport scattering cross section, and n_{eff} the effective charge carrier concentration. The value of Q was calculated in the free- electron approximation[3] by using the method of partial waves. The dislocation core was regarded as a linear defect associated with the excess free volume. The reason behind resonant scattering is the possibility of short-term capture of an electron in the region of excess positive charge, accompanied by the formation of a quasi-stationary state near the Fermi energy. The values of k_F were also estimated in the free-electron approximation by using the data on the number of charge carriers per atom from Ref. 1. The values of n_{eff} for transition metals were calculated with the help of the well-known Mott model of a two-band transition metal with the estimate $n_{\mathrm{eff}} = n_e N_s(0)/N(0)$ used for elements of the beginning and middle of transition series (for Ti, Zr, Mo, and W). Here $N_s(0)$ and $N(0)$ are the density of the s-electron states at the Fermi level and the total density of states, respectively.

The parameters appearing in formula (2) can be estimated on the basis of available data from the literature. The conduction band in transition metals is formed by almost free s- and p-electrons. It follows from the data presented in Ref. 21 on contributions of partial densities of states to the total density of states of Nb that $(N_s(0)+N_p(0))/N(0)\simeq0.17$. This gives $n_{\mathrm{eff}}\approx0.17n_e\approx(0.76-0.95)\times10^{22}\,\mathrm{cm}^{-3}$. In the free electron approximation, $k_F=(3\pi^2 n_e)^{1/3}$, which gives $k_F\simeq(1.1-1.2)\times10^8\,\mathrm{cm}^{-1}$ for $n_e=(4.5-5.6)\times10^{22}\,\mathrm{cm}^{-3}$. Using the results obtained by Karolik and Luchvich,[3] we can easily prove that the value of Q for the series Na, K, Cu, Au, Al, Ni, Pt, Mo, and W of nontransition and transition fcc and bcc metals amounts to $\sim(1.1-1.3)b$ (b is the Burgers vector). We can assume that $Q\sim b$ for Nb also ($b=2.86\times10^{-8}\,\mathrm{cm}$).[22] Using the values of Q, k_F, and n_{eff} given above, we obtain, in accordance with formula (2), $r_d\sim(14-18)\times10^{-19}\,\Omega\times\mathrm{cm}^3$. Thus, the average value of r_d in this range of calculated values corresponds to the average value of r_d determined experimentally to within $\sim$50%.

CONCLUSION

The variation of the increment in resistivity of Nb single crystals with different structural states (after rolling deformation at 20 K and consecutive removal of surface layers by polishing), normalized to the average density of dislocations at the core is investigated. This allowed us to single out the characteristic of the homogeneous structure with a high density of uniformly distributed dislocations ($N_d=1.3\times10^{11}\,\mathrm{cm}^{-2}$). The resistivity of a solitary dislocation is determined for the given structural state taking into account the contribution from vacancies to the increase in resistivity. The obtained value of $r_d\simeq(9\pm3)\times10^{-19}\,\Omega\times\mathrm{cm}^3$ is in good agreement with the available results for a number of bcc transition metals (Mo, W, Fe, and V) for which $r_d\simeq(6-10)\times10^{-19}\,\Omega\times\mathrm{cm}^3$.

The results of calculations of r_d for Nb on the basis of the Karolik–Luchvich model[3] of resonant electron scattering by dislocations (which gives a clear physical pattern of electron scattering near the dislocation core) indicate a $\sim$50% agreement with the experimental value. The discrepancy between the theoretical and experimental results for the Brown theory exceeds 200%.

The author is grateful to Ya. D. Starodubov and V. D. Natsik for their support and valuable remarks.

*E-mail: nsc@kipt.kharkov.ua

[1] R. A. Brown, J. Phys. F **7**, 1283 (1977).
[2] B. R. Watts, J. Phys. F **18**, 1197 (1988).
[3] A. S. Karolik and A. A. Luchvich, J. Phys.: Condens. Matter **6**, 873 (1994).
[4] L. D. Whitemire and F. R. Brotzen, AIME Trans. **239**, 824 (1967).
[5] Z. Gierak, J. W. Moron, and A. Lehr, Phys. Status Solidi A **77**, 775 (1983).
[6] H. B. Shukovsky, R. M. Rose, and J. Wulf, Acta Metall. **14**, 821 (1966).
[7] B. Warlimont-Meier, P. Beardmore, and D. Hill, Acta Metall. **15**, 1393 (1967).
[8] V. K. Aksenov, N. A. Chernyak, O. I. Volchok *et al.*, Fiz. Nizk. Temp. **24**, 266 (1998) [Low Temp. Phys. **24**, 201 (1998)].
[9] R. B. Zubeck, T. W. Barbee, Jr., T. H. Giballe, and F. Chilton, J. Appl. Phys. **50**, 6423 (1979).
[10] T. W. Barbee, Jr., Phys. Status Solidi **31**, 535 (1969).
[11] M. Kaveh and N. Wiser, J. Phys. F **13**, 953 (1983).
[12] M. Kaveh and N. Wiser, J. Phys. F **16**, 795 (1986).
[13] V. K. Aksenov, I. F. Borisova, V. I. Sokolenko, and Ya. D. Starodubov, Fiz. Nizk. Temp. **19**, 1077 (1993) [Low Temp. Phys. **19**, 763 (1993)].
[14] V. I. Sokolenko, Ph.D. thesis, Kharkov (1991).
[15] F. Phillipp, B. Saile, and K. Urban, in *Proc. Yamada Conf. V*, Tokyo (1982).
[16] I. F. Borisova, V. I. Sokolenko, and Ya. D. Starodubov, Fiz. Nizk. Temp. **18**, 844 (1992) [Sov. J. Low Temp. Phys. **18**, 595 (1992)].
[17] V. I. Sokolenko, Ya. D. Starodubov, B. A. Merisov, and I. F. Borisova, Fiz. Nizk. Temp. **16**, 246 (1990) [Sov. J. Low Temp. Phys. **16**, 136 (1990)].
[18] K. Tanaka and T. Watanabe, Jpn. J. Appl. Phys. **11**, 1429 (1972).
[19] A. I. Golovashkin and A. L. Shelekhov, in *Proceedings of the Physical Inst. of Acad. Sci.* [in Russian], vol. **151**, Nauka, Moscow (1984).
[20] G. M. Crabtree, D. H. Dye, D. H. Karim *et al.*, Phys. Rev. Lett. **42**, 390 (1979).
[21] S. V. Vonsovskii, Yu. A. Izyumov, and E. Z. Kurmaev, *Superconductivity of Transition Metals, Their Alloys, and Compounds* [in Russian], Nauka, Moscow (1977).
[22] J. Friedel, *Dislocations*, Oxford (1972).

Translated by R. S. Wadhwa

LOW-DIMENSIONAL AND DISORDERED SYSTEMS

Kinetics of cluster growth in expanding rare-gas jet

M. A. Ratner

*B. I. Verkin Institute for Low Temperature Physics and Engineering, National Academy of Science of Ukraine, 47 Lenin Ave., 310164 Kharkov, Ukraine**

(Submitted November 5, 1998)
Fiz. Nizk. Temp. **25**, 367–375 (April 1999)

The growth of clusters in an overcooled atomic jet is calculated with the simultaneous allowance for two processes: the condensation of supersaturated gas and the cluster-cluster aggregation. These processes are consistently described within a quasi-equilibrium approach for large enough clusters, while their nucleation stage is allowed for phenomenologically by the use of a fitting parameter. The theory quantitatively describes the experimental dependence of the mean cluster size on the initial gas temperature within a broad range of sizes. The mean size of clusters, their distribution over sizes and the contribution of clusters to the total mass of the jet are calculated versus the distance from the gas ejection point (nozzle entry). It is shown that these characteristics are mainly determined by the initial gas entropy which is equivalent to the empirical law of corresponding jets. The size distribution function has a halfwidth exceeding the mean cluster size and is close (on a relative scale) to a universal curve. The broad size distribution of clusters should be taken into account when analyzing spectroscopic data on the size dependence of electronic processes in a cluster.
[S1063-777X(99)00604-0]

INTRODUCTION

Experimental study of atomic clusters provides an alluring possibility of tracing the evolution of the energy spectrum, relaxation processes and atomic structure when varying the size of an atomic aggregate from several atoms to a macroscopic number. Of particular interest are rare-gas clusters due to their distinctive feature—the simplest atomic and electronic structure that is due to a weak van der Waals binding. During recent years, the spectroscopy of rare-gas clusters has been intensively developed due to great progress in the supersonic gas-jet technique.[1–10] It has been possible to trace essential size variations in luminescence, absorption and energy spectra[2–8] as well as in the growth mechanism.[9]

The aim of spectroscopic and electronographic studies of clusters is to obtain the dependences of electronic and atomic structure on cluster size. In fact, however, experiment does not directly give a physical quantity of interest as a function of cluster size. This quantity is averaged over cluster sizes with the weight of the size distribution of clusters in the expanding jet. Due to the large width in the size distribution function, the size dependence of the quantity or phenomenon under investigation is noticeably smeared.

To infer more precise information from experimental data, it is necessary to know the size distribution function of clusters growing in the expanding jet.

The size distribution of clusters is formed in the course of their growth which is realized simultaneously in two ways: by condensation of the overcooled gas on the cluster surface and by cluster-cluster aggregation. Both mechanisms make comparable contributions to the formation of the distribution function and should be considered simultaneously.

There is a large number of theoretical works concerned with cluster growth in an expanding jet (e.g., Refs. 10–20), but the size distribution function had not been calculated in any of them. In earlier literature the condensation and aggregation mechanisms of cluster growth were considered separately.

Some thermodynamical and nonequilibrium aspects of the condensation mechanism (in particular, atom-cluster collisions and desorption of atoms from a cluster) were investigated in Refs. 10–13. In Ref. 14 the kinetics of cluster growth was calculated by taking the condensation mechanism into account. The calculations were performed on the basis of the drop model of a cluster and classical nucleation with allowance for the dependence of the surface tension coefficient on the drop radius. As was shown in Ref. 14, the drop model, fitted with the real process of cluster growth by the use of free parameters, describes some important experimental regularities of cluster growth. However, such an approach does not give the size distribution of the clusters.

The mechanism of cluster-cluster aggregation has been studied in many works e.g., in Refs. 15–20. The papers[15–17] were concerned mainly with combinatorial aspects of the aggregation process. In Refs. 18–20 the process of cluster-cluster collision was studied on a microscopic level and the cross section of fusion was considered for charged metal clusters with allowance for their structure.

The purpose of the present work consists in the calculation of the cluster growth kinetics, involving both the

mentioned growth processes, which is necessary to obtain the size distribution function of clusters in an expanding jet.

As follows from the cited works,[10–20] each of the above processes of cluster growth has a highly complicated nature even if considered separately. In order to calculate the joint process of cluster growth within a reasonable constructive approach, some simplifying assumptions are used below. In particular, although the cluster growth is an essentially nonequilibrium process, it is long enough that thermodynamic equilibrium is practically achieved within a separate cluster as well as in the gas of atoms and clusters considered as structureless particles with translational degrees of freedom. (But intrinsic degrees of freedom of clusters are not in equilibrium with gas, and it is just the lack of this equilibrium which causes the condensation of gas on clusters).

The nucleation stage of cluster growth is taken into account in a phenomenological way, so that the consistent consideration is restricted to a region of large enough clusters. In this region shell effects, although generally important,[18,19] can not be taken into account. A nonmonotonic size dependence of bond energy, originated by shell effects, is inessential for the growth of a large cluster due to the large number of shells subsequently filled.

2. CONDENSATION OF OVERCOOLED GAS ON THE CLUSTER SURFACE

Let us consider the nonequilibrium process of gas condensation on the surface of a cluster with the intrinsic temperature $T_{\rm cl}$. An atom-cluster collision results in their merging in the cluster temperature region

$$T_{\rm cl} < T_c(N,S_g) \tag{1}$$

where the merging is attended by an increase in the total entropy of the nonequilibrium system. The critical temperature of a cluster, T_c, is defined by the condition that the total entropy of the system does not change as a gas atom joins to the cluster. T_c is a function of the cluster size N (the number of atoms) and the gas entropy S_g. It is assumed for simplicity that every collision of an atom with a cluster of size N results in their merging with unit probability if the inequality (1) is fulfilled and with zero probability in the opposite case.

Based on this premise, a quasi-stationary approach is introduced: during the process of cluster growth the temperature of every cluster is equal to its critical temperature $T_c(N,S_g)$ which varies with cluster size and gas state. If cluster temperature becomes lower than $T_c(N,S_g)$, i.e., the joining of an atom to the cluster is attended by an increase of the total entropy, then gas condensation on the cluster surface increases cluster temperature until it achieves T_c. This process is very fast since every atom-cluster collision, attended by merging, enhances intrinsic cluster energy by the atom-cluster binding energy U and cluster temperature by $U/3N$. Thus, the number of atom-cluster collisions, required to adjust cluster temperature to T_c, is of the order of $NT/U \ll N \ll \nu$ where ν is the total number of cluster-atom collisions during the growth process. If the cluster temperature becomes higher than $T_c(N,S_g)$, then the desorption of atoms from the cluster surface becomes thermodynamically favorable and results in a fast decrease of the cluster temperature down to T_c.

The critical temperature of a cluster, $T_c(N,S_g)$, is defined from the condition that the augmentation of the cluster entropy, $S_{\rm cl}$, when joining one atom equals by magnitude the decrease of the gas entropy, S_g, when removing one atom:

$$S_g(T_g,V,N_g) - S_g(T_g,V,N_g-1) = S_{\rm cl}(\tilde{T}_c,N+1) - S_{\rm cl}(T_c,N) \tag{2}$$

where T_g, N_g and V are the temperature, the number of atoms and the volume of the gas. $\tilde{T}_c$ is the temperature of the cluster immediately after joining one atom if the initial temperature of the cluster was equal to T_c. $\tilde{T}_c$ is defined by the equation

$$E_{\rm cl}(\tilde{T}_c,N+1) - E_{\rm cl}(T_c,N) = w[Z(N+1) - Z(N)] \tag{3}$$

where $E_{\rm cl}$ is the intrinsic energy of a cluster, w is the energy of one interatomic bond and $Z(N)$ is the total number of bindings between adjacent atoms in the N-atomic cluster. The w value is assumed to be independent of the cluster temperature and size. This assumption means that the interatomic distances in a cluster are equal for all pairs of adjacent atoms and independent of cluster temperature (the latter is justified by a weak thermal expansion at low temperature). In addition, only the interaction between adjacent atoms is allowed for; this is justified by a fast decrease of the van der Waals interaction energy with distance.

In order to find the critical temperature, T_c, from the Eqs. (2) and (3), it is necessary to substitute into them the expressions for thermodynamic functions of the gas and the cluster. The entropy of ideal single-atomic gas can be written in the well-known form

$$S_g = N_g s_g, \quad s_g = \ln(eV/N_g) + c_V \ln(T_g e) \quad (e = \exp(1)) \tag{4}$$

where s_g is the gas entropy per atom; N_g is the number of atoms in the gas; V is gas volume and c_V is the heat capacity of the gas per atom at a constant volume. Here and below the temperature is expressed in energy units, so that $c_V = 3/2$ for a single-atomic gas.

Since the structure of an arbitrary-size cluster is unknown, it is reasonable to write down its thermodynamic functions within the Debye model. However, it is necessary to take account of the discreteness of the energy spectrum which can manifest itself at low temperatures for not very large clusters. For that purpose the cluster of the size $N = L^3$ is represented in the form of a cube with the lattice constant a and the edge containing L atoms (for definiteness L is even). The phonon wavevector $\mathbf{K}$ takes up the values

$$\mathbf{K} = (i-1/2,\ j-1/2,\ k-1/2)(\pi/La)$$

with $i,j,k = -L/2, ..., L/2$. Within the Debye model the vibration frequencies of the cluster are equal to $s_l|\mathbf{K}|$ for the longitudinal branch and to $s_t|\mathbf{K}|$ for the transverse branches. For a crystal with the van der Waals binding $s_l/s_t = \sqrt{3}$.[21] Thus, the vibration spectrum of the cluster takes the form

$$\omega^{\alpha}_{i,j,k}=\frac{\hbar\omega_D q_\alpha}{T_{\rm cl}}\,\frac{\sqrt{(i-1/2)^2+(j-1/2)^2+(k-1/2)^2}}{L}. \quad (5)$$

Here ω_D is the Debye frequency, index α numbers vibrational branches. The coefficients $q_1=2.515$, $q_2=q_3=1.452$ fit the expression (5) with the Debye model for $N\to\infty$. Using the vibrational spectrum, one can write down the thermodynamical functions of the cluster:

$$E_{\rm cl}=NT_{\rm cl}\sum_{\substack{i,j,k=-L/2\\ \alpha=1,2,3}}^{L/2}\left[\frac{\hbar\omega^{\alpha}_{i,j,k}/T_{\rm cl}}{1-\exp(-\hbar\omega^{\alpha}_{i,j,k}/T_{\rm cl})}\right], \quad (6)$$

$$S_{\rm cl}=N\sum_{\substack{i,j,k=-L\\ \alpha=1,2,3}}^{L}\hbar\left\{\frac{\hbar\omega^{\alpha}_{i,j,k}/T_{\rm cl}}{1-\exp(-\hbar\omega^{\alpha}_{i,j,k}/T_{\rm cl})}-\ln[1-\exp(-\hbar\omega^{\alpha}_{i,j,k}/T_{\rm cl})]\right\}. \quad (7)$$

The expressions (6) and (7) relate to a cluster with $N\gg 1$. In this case the contribution of the translational and rotational degrees of freedom to thermodynamic functions is negligibly small and is also weakly dependent on N. In Eqs. (6) and (7) these degrees of freedom are omitted. Using interpolation nodes $N=L^3$, one can obtain $E_{\rm cl}$ and $S_{\rm cl}$ for an arbitrary N via the interpolation of the quantities $E_{\rm cl}/N$ and $S_{\rm cl}/N$ weakly dependent on N.

The relations (2)–(7) define the critical temperature of a cluster, T_c, as a function of its size and the gas state. Figure 1 shows the dependence of T_c on cluster size at various fixed values of gas entropy per atom s_g. For a given N, T_c lowers with an increase of s_g, i.e., with raising gas temperature or lowering pressure. For a given s_g, T_c increases with cluster size (which corresponds to the effect of surface tension on cluster growth within the drop model[14]) and achieves saturation for $N\gtrsim 1000$.

In Fig. 2 the gas-temperature dependence of T_c is shown for $N=500$ and different concentrations of atoms in the gas. T_c decreases with an increase of gas temperature due to the corresponding increase of gas entropy. This means that the cluster temperature (maintained close to T_c) *heightens* as the gas *cools*; such a relation between the temperatures of the gas and clusters illustrates a nonequilibrium character of the growth process in an expanding jet (due to a fast cooling of the gas, gas pressure much exceeds its equilibrium value).

A cluster grows if the difference T_c-T_g (equal to the cluster-gas jump of temperature) is *positive* (contrary to the usual notion about the deposition of a gas on a cold surface). A positive gas-cluster jump of temperature in the course of cluster growth is necessary to provide an outflow of the heat, released due to gas condensation on the cluster surface, into gas. The difference T_c-T_g is shown in Fig. 2 by a dashed line; the gas-temperature region of cluster growth is limited by the intersection point of the dashed line with the abscissa axis.

The cluster growth rate is proportional to the thermal flux $q(N)$ from the cluster surface to the gas, i.e., to the difference between cluster temperature (assumed to be equal to T_c) and the gas temperature:

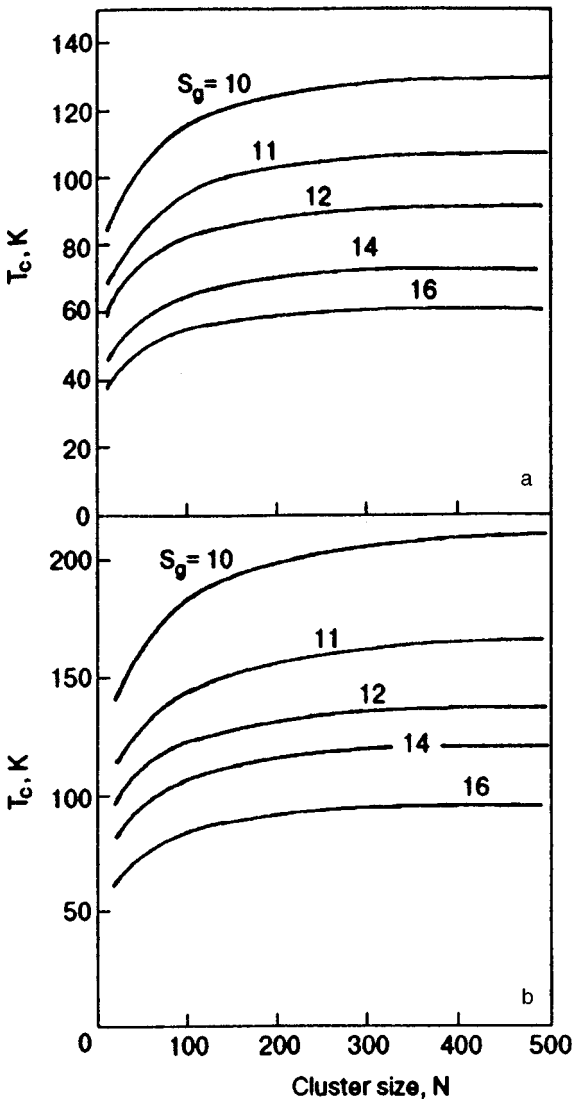

FIG. 1. Size dependence of the critical temperature, T_c, of a cluster for different fixed values of gas entropy per atom s_g (indicated in the figure): argon (a), krypton (b).

$$\frac{dN}{dt}=\frac{q(N)}{dE_{\rm cl}[T_c(N,S_g),N]/dN}, \quad (8)$$

$$q(N)=\tfrac{3}{2}(T_c-T_g)\sigma(N,1)\langle v\rangle N_g/V. \quad (9)$$

Here $\langle v\rangle$ is the mean thermal velocity of gas atoms; $\sigma(N,1)$ stands for collision section of an atom with the cluster of the size N. In the denominator of Eq. (8) the total derivative is meant. The expression for the collision section will be derived in Sec. 3 [see Eq. (17)].

3. CLUSTER-CLUSTER AGGREGATION

Although the cluster growth is an essentially nonequilibrium process, it is long enough that thermodynamic equilibrium is practically achieved not only within the gas and within every separate cluster but also within the subsystem of the translation degrees of freedom related to all the particles in the jet (this subsystem includes also the rotation motion of every cluster as a whole). The equilibrium in this

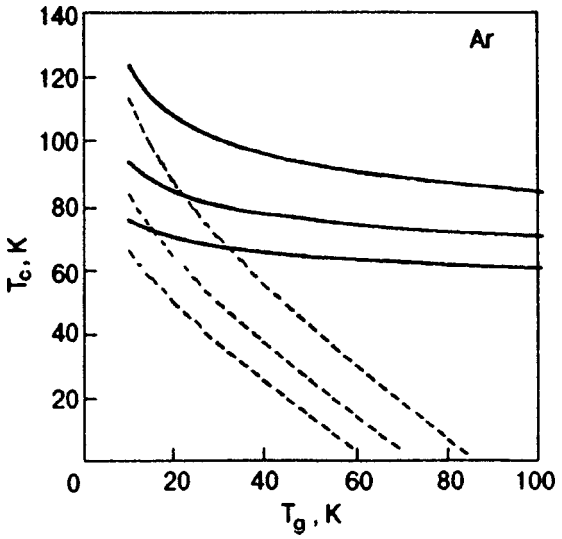

FIG. 2. Dependence of the critical temperature, T_c, of the argon cluster with $N=500$ on gas temperature, T_g, for the gas concentrations (from top to bottom): 10^{17}, 10^{16} and 10^{15} cm^{-3} solid lines). Dashed lines—the same for the difference T_c-T_g.

subsystem is maintained in the course of the growth of clusters since the total number, ν, of collisions between the cluster and gas atoms much exceeds the number of atoms joined to the cluster i.e. $\nu \gg N$. Thus, the gas-cluster exchange of energy (the exchange per one collision, T_g/N, multiplied by ν is large compared to the kinetic energy of a cluster as a whole ($\sim T_g$). Taking this into account, we can describe distribution of clusters over translation motion velocities by the Boltzmann statistics with the temperature equal to T_g.

The probability of the collision of two clusters, numbered by the subscripts i and j, per unit time is

$$\langle P_{ij}\rangle=\langle \mathbf{v}_i-\mathbf{v}_j\rangle\langle\sigma_{ij}\rangle/V=(8T_g/\pi\mu_{ij})^{1/2}\langle\sigma_{ij}\rangle/V. \quad (10)$$

Here $\mathbf{v}_i$ is the velocity vector of the ith cluster; σ_{ij} is the collision section of the ith and jth clusters; $\langle ...\rangle$ denotes the Boltzmann averaging; μ_{ij} is the reduced mass of the clusters,

$$\mu_{ij}=m_{\rm at}N_iN_j/(N_i+N_j) \quad (11)$$

($m_{\rm at}$ is the atomic mass). In Eq. (10) σ_{ij} is assumed to be weakly dependent on cluster velocities which permits one to take it out of the averaging.

In order to derive σ_{ij}, let us substitute a cluster by the point particle with the same mass (the validity range of this approximation will be indicated below). Neutral clusters are attracted to each other by van der Waals forces, which create the potential

$$U(r_{ij})=-C_{ij}r_{ij}^{-6}, \quad C_{ij}=C_{\rm at}N_iN_j \quad (12)$$

with the atomic van der Waals constant $C_{\rm at}$. It follows from the classical motion equation of two interacting particles that there exist two types of motion: the particles can either fall onto each other or move away from each other after drawing together to the minimal distance. These types of motions are separated by the critical aiming distance

$$d_{ij}=(27C_{ij}/2\mu)^{1/6}|\mathbf{v}_i-\mathbf{v}_j|^{-1/3}. \quad (13)$$

The quantity (13), weakly dependent on velocities, can be averaged approximately over the Boltzmann distribution

$$\langle d_{ij}\rangle\cong(27C_{ij}/2\mu)^{1/6}\langle \mathbf{v}_i^2+\mathbf{v}_j^2\rangle^{-1/6}=(9C_{\rm at}N_iN_j/2T_g)^{1/6}. \quad (14)$$

The averaged collision section of point particles, representing the clusters, can be estimated as

$$\langle\sigma_{\rm attr}(N_i,N_j)\rangle\cong\pi\langle d_{ij}\rangle^2\cong\pi(9C_{\rm at}N_iN_j/2T_g)^{1/3} \quad (15)$$

(the subscript ''attr'' indicates that the collision of particles is caused but their van der Waals attraction).

The attraction section of cluster-cluster collisions (15) should be compared with the geometrical collision section

$$\sigma_{\rm geom}(N_i,N_j)\cong\pi l^2(N_i^{1/3}+N_j^{1/3})^2/4 \quad (16)$$

where l is the interatomic distance in solid. The true collision section is

$$\sigma(N_i,N_j)=\max\{\sigma_{\rm attr}(N_i,N_j)\sigma_{\rm geom}(N_i,N_j)\}. \quad (17)$$

The ratio of the attractive and geometrical sections is

$$\sigma_{\rm attr}(N_i,N_j)/\sigma_{\rm geom}(N_i,N_j)\cong(9U_{\rm mol}/2T_g)^{1/3}4(N_iN_j)^{1/3}\times(N_i^{1/3}+N_j^{1/3})^{-2} \quad (18)$$

where $U_{\rm mol}=C_{\rm at}l^{-6}$ stands for the bond energy of the two-atomic van der Waals molecule. For argon, krypton or xenon $U_{\rm mol}>T_g$, and for clusters of comparable sizes the ratio (18) exceeds unity. The collision section (15) will be used as applied to cluster-cluster aggregation by taking this into account.

However, for atom-cluster collisions the ratio (18) becomes less than unity starting from $N\sim1000$. Therefore, the collision section $\sigma(N,1)$ in the form (17) is substituted into the expression (9) for thermal flux.

Since the collision of two clusters is caused by their attraction, and the attraction energy at the collision moment much exceeds the initial kinetic energy of the colliding clusters in magnitude, it can be assumed that every collision of clusters results in their fusion. Indeed, if the final kinetic energy (slightly exceeding in magnitude the attraction energy at the collision moment) is partially transformed to heat, the rest of the kinetic energy becomes less than the magnitude of the attraction energy and is insufficient for the clusters to move away from each other.

The aggregation of the clusters with the sizes N_1 and N_2 and temperatures equal to their critical temperatures T_{c1} and T_{c2} results in the formation of a cluster with the size $N_3=N_1+N_2$ and temperature T_3. The difference between T_3 and $T_c(N_3,S_g)$ is found to be negligibly small so that the temperature of the formed cluster can be put equal to $T_c(N_3,S_g)$.

4. KINETICS OF CLUSTER GROWTH INVOLVING CONDENSATION AND AGGREGATION MECHANISMS

The processes of cluster growth via gas condensation and cluster-cluster aggregation, considered in the previous sections, are determined by the gas state in the expanding jet as a function of time t. We trace the gas state within a small volume V which moves together with the jet and contains a

constant number of atoms, N_{tot} (part of them, denoted by ξN_{tot}, has joined to clusters). The motion of the volume V begins from the nozzle entry, which is a small hole through which the gas flows out from the reservoir to the vacuum through the nozzle. The gas state is described by the usual equation:

$$PV = N_g T_g, \quad N_g = N_{\text{tot}}(1-\xi), \quad N_{\text{tot}} = \text{const} \tag{19}$$

(P is gas pressure; the number of clusters is negligibly small compared to the number of free atoms $N_{\text{tot}}[(1-\xi)]$). The adiabatic expansion of the jet is described by the known equations (see, e.g.,[14]):

$$uS/V = \text{const}, \tag{20}$$

$$(N_{\text{tot}} m_{\text{at}}/V) u \frac{du}{dx} + \frac{dP}{dx} = 0, \tag{21}$$

$$N_g m_{\text{at}} c_P (T_g - T_0) + N_{\text{tot}} m_{\text{at}} u^2/2 = \int_0^t \sum_t q(N_i)\, dt. \tag{22}$$

Here x is the distance of the chosen elementary volume from the nozzle entry at the moment t; $u = dx/dt$ is the jet velocity at the point x; S is the cross section of the chosen volume at the point x (the transverse nonuniformity of the jet is neglected); $c_P = 5/2$ is the heat capacity of gas per atom at a constant pressure; T_0 is the temperature at the nozzle entry. The right-hand part of Eq. (22) is the total heat released due cluster formation (the sum is taken over all the clusters), the thermal flux $q(N_i)$ is given by Eq. (9). It is implied in Eqs. (21) and (22) that the clusters are moving with the same velocity as the gas.

The equations (19)–(22) describe the gas state for a given distribution of clusters over sizes. For a given gas state, the time evolution of the size distribution of clusters is calculated with the simultaneous allowance for the condensation and aggregation mechanisms (Secs. 2 and 3). Thus, the self-consistent variations of the gas and cluster subsystems is calculated.

Such approach is realized in the region of large sizes, where the thermodynamic consideration of Sec. 2 is valid, and must be complemented by the initial conditions which are formed on the stage of the formation of cluster nuclei in the jet. The microscopic consideration of the nucleation process is a highly complicated problem which is beyond the framework of the present work. Therefore, the formation of cluster nuclei is described in a phenomenological way on the basis of the following considerations.

The heat release due to the formation of nuclei does not make any noticeable contribution to the thermal balance of the jet. On the other hand (as was shown in Ref. 14 and by the present calculations), the duration of the nucleation stage is short compared with the total time of cluster growth in the jet. Therefore, the influence of nucleation stage on the further growth of clusters is determined by two parameters: the number of the nuclei formed, n_{nucl}, and the moment of the nucleation onset, t_{on}. The mean size of clusters decreases with increasing n_{nucl} and t_{on} (the earlier clusters arise and begin to grow the larger they become at a given time moment or at a given point x).

Within the phenomenological description, the nucleation onset t_{on} is determined by the critical temperature of nucleation, T_{nucl}, and is defined by the equation

$$T_g(t_{\text{on}}) = T_{\text{nucl}} \tag{23}$$

(here T_g is the gas temperature in the elementary volume of the expanding atomic jet devoid of clusters). Without nucleation, gas temperature in the expanding jet would decrease below T_{nucl}; due to the heat release, accompanying the rise and subsequent growth of clusters, the gas temperature T_g is maintained at the level T_{nucl} until the moment t_{end} when T_g begins to heighten in the course of cluster growth. In the time interval $t_{\text{on}} < t < t_{\text{end}}$, the number of arising clusters is determined by the competition between nucleation and cluster growth. This competition is regulated by the initial cluster size, N_{init}, and cluster growth rate; n_{nucl} decreases with an increase in every one of these parameters. Since they are unknown, it is reasonable to choose each of them in such a way that the related errors partially compensate each other. Hence, N_{init} is put equal to the minimal size, 4, of a cluster with the 3-dimensional configuration of atoms. To compensate the corresponding error, the cluster growth rate, defined by Eqs. (8) and (9), is somewhat overestimated: the critical temperature T_c is taken for a cluster with $N = 64$ (this is the minimal cluster size for which the thermodynamic consideration of Sec. 2 is certainly applicable).

The critical temperature of nucleation, T_{nucl}, depends on the gas pressure P. It is assumed that this dependence does not essentially differ in its character from the known relation between temperature and pressure for the gas-solid or gas-liquid equilibrium. So, the dependence of T_{nucl} on gas pressure P is written down in the form

$$T_{\text{nucl}} = w\Delta Z/\ln(P^*/P). \tag{24}$$

Here $\Delta Z = 3$ is the variation of the number of bonds when joining or removing one atom from the incipient cluster with $N = 4$; w is the energy per one bond. P^* is a fitting parameter of the phenomenological description of nucleation and by no means cannot be identified with a true equilibrium parameter. Note that the nucleation process, in view of its complicated character, can hardly be described by the law of corresponding states; hence, this law is generally not met by Eq. (24) either.

The results below are related to the fitting parameter values $P^* = 500$ atm for argon and 10^5 atm for krypton which provide the best agreement of the theory with the experimental data on the mean cluster size.

5. CALCULATION RESULTS AND COMPARISON WITH EXPERIMENT

The calculation of the cluster growth kinetics in an expanding gas jet was carried out according to the above scheme, including condensation and aggregation processes, for argon and krypton. The following characteristics of a cluster jet have been calculated.

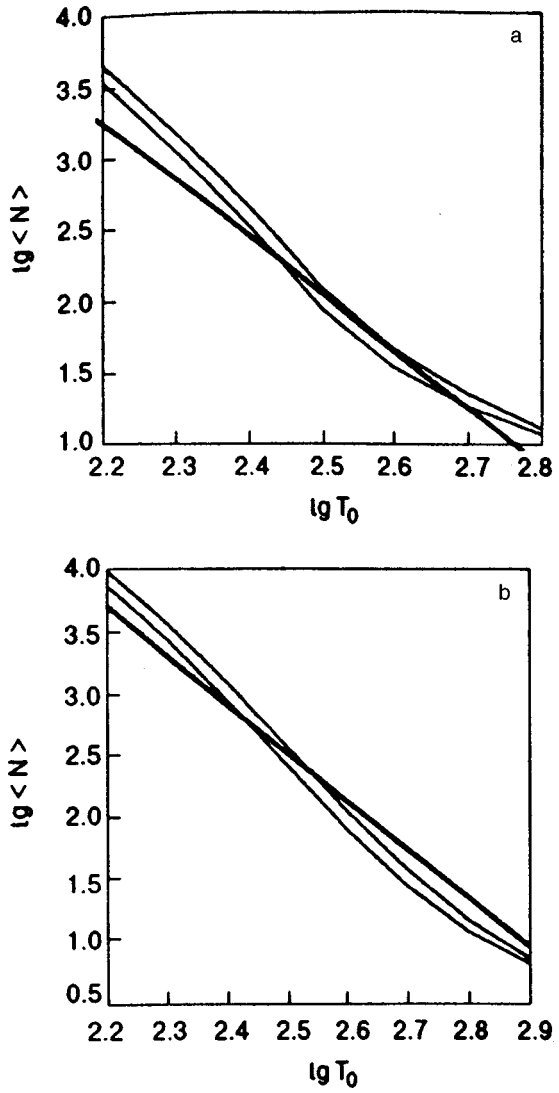

FIG. 3. Dependence of the mean cluster size on the initial gas temperature, T_0, at the 4.1 cm distance from the nozzle entry for argon (a) and krypton (b) (the initial pressure P_0 is constant and equal to 1 atm). Thick lines—experimental data[14,22]; thin lines—calculation results for the fitting parameter values (from top to bottom): $P^*=100$ atm and 500 atm (the best fit) for argon; $P^*=10^5$ atm (the best fit) and 10^6 atm for krypton.

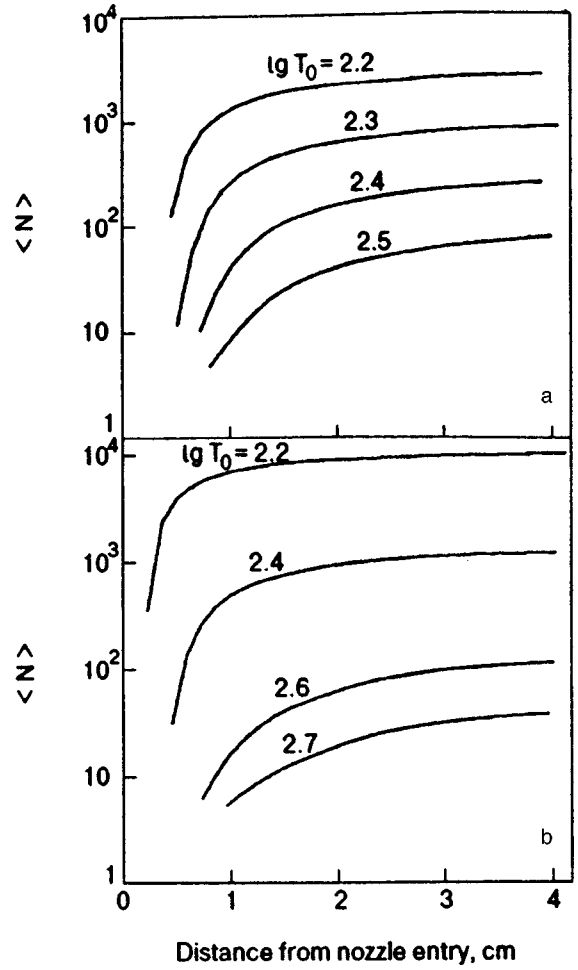

FIG. 4. Mean cluster size, $\langle N\rangle$, versus distance from the nozzle entry for the same initial pressure $P_0=1$ atm and different initial temperatures (in Kelvins): argon (a) and krypton (b).

Every characteristic of clusters, that can be measured experimentally is determined by the distribution of the total mass of clusters over their sizes. This distribution function is defined as

$$F(N)=d\left(\sum_{N_i<N} N_i\right)/dN. \tag{25}$$

The mean size of clusters in the jet is defined by means of the distribution function (25):

$$\langle N\rangle=\frac{\int F(N)NdN}{\int F(N)dN}=\frac{\Sigma N_i^2}{\Sigma N_i}. \tag{26}$$

The results below are related to a conical nozzle with entry diameter equal to 0.34 mm and apex angle 8.6°.

Figure 3 shows the mean size of clusters as a function of the gas temperature at the nozzle entry, T_0, for the constant pressure at the nozzle entry $P_0=1$ atm. The thick line denotes the experimental data measured at the distance $x=4.1$ cm from the nozzle entry[14,22] and the thin lines represent the corresponding calculation results related to different values of the fitting parameter P^*. As seen from the figure, in the case of the best fit ($P^*=500$ atm for argon and 10^5 atm for krypton) the theoretical curve agrees with the experimental one with the accuracy up to the multiplier 1.3 to 1.8, while the mean cluster size varies by two orders of magnitude. Note that the agreement between the theory and experiment takes place on the absolute scale (x is expressed in centimeters, T_0 in Kelvins and $\langle N\rangle$ in the number of atoms). This supports validity of the theory based on the above-enumerated assumptions.

The calculation results, presented in Figs. 4 to 6, are related to the case of the best fit ($P^*=500$ atm for argon and 10^5 atm for krypton) and to the pressure $P_0=1$ atm at the nozzle entry. In Fig. 4 mean cluster size is presented versus distance, x, from the nozzle entry for different fixed temperatures at the nozzle entry. It is interesting to compare these data with Fig. 5 which shows the relative fraction of clusters in the total mass of the substance as a function of the same variable x. As can be seen from Fig. 5, at the distance $x=1$ to 4 cm the mass of clusters achieves saturation (gas condensation is blocked due to a growth of gas entropy and

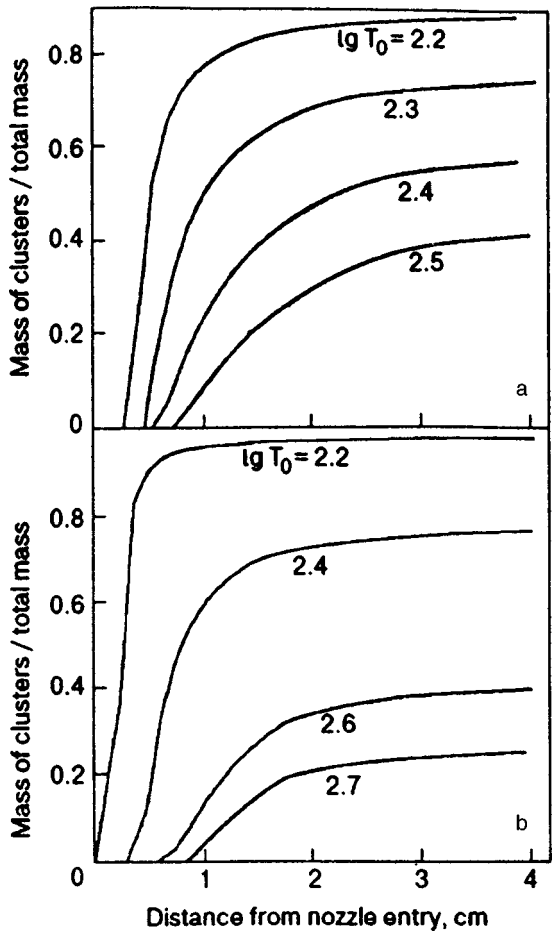

FIG. 5. The fraction of clusters in the total mass of the substance versus distance from the nozzle entry for the same initial pressure $P_0=1$ atm and different initial temperatures (in Kelvins): argon (a) and krypton (b).

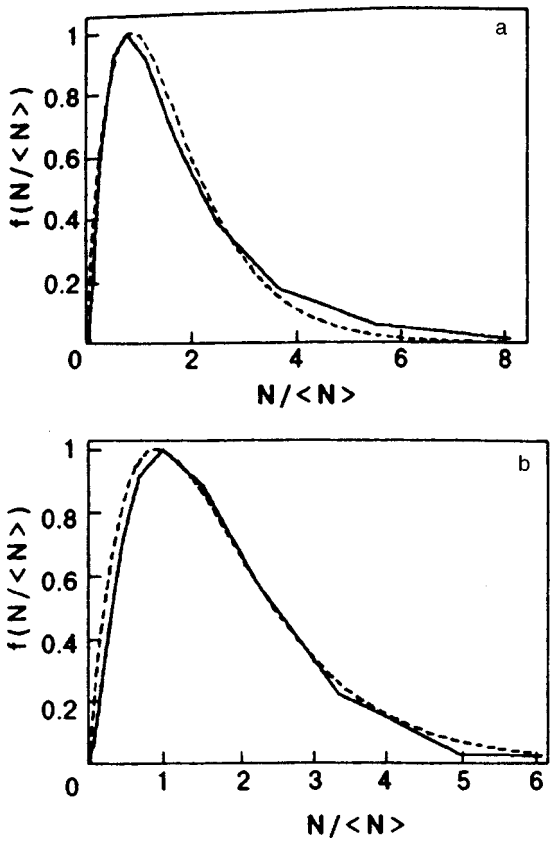

FIG. 6. The function of the cluster mass distribution $f(N/\langle N\rangle)$ over cluster sizes for argon (a) and krypton (b) normalized to the unit value of the maximum ordinate. Solid line—calculation results, dashed line—approximation (27) with $k=1.2$ for argon and 1.1 for krypton. The figure relates to $P_0=1$ atm, lg $T_0(K)=2.4$ and the 4.1 cm distance from the nozzle entry.

the corresponding lowering of T_c demonstrated by Fig. 1). But in the region of mass saturation, as is obvious from Fig. 4, the mean cluster size continues to grow due to cluster-cluster aggregation (the slopes of the curves in Figs. 4 and 5 should be compared with the allowance for different-type scales on the ordinate axes). This indicates an essential contribution of the cluster-cluster aggregation process to the formation of the size distribution of clusters.

Another evidence for a dominant role of the aggregation mechanism in the formation of the size distribution function (25) is provided by the form of the distribution function. As a result of calculations, it was found that the function, $f(n)$, of the cluster mass distribution over relative cluster size $n=N/\langle N\rangle$ is well enough approximated in the simple form

$$f(n)\equiv F(n\langle N\rangle)=\text{const}\, n\exp(-kn) \tag{27}$$

with a constant multiplier k which takes up values in a narrow interval

$$1.1\leqslant k\leqslant 1.2 \tag{28}$$

in all the cases examined. The approximation (27) holds in the total range of mean sizes $\langle N\rangle>50$ where the developed method of calculation is applicable. For krypton k is always close to 1.1; in the case of argon k is near to 1.1 for $\langle N\rangle\leqslant 100$ and to 1.2 for $\langle N\rangle\geqslant 300$. As an example, Fig. 6 represents the distribution function, calculated for the initial conditions $P_0=1$ atm, lg $T_0=2.4$ (solid line) and its approximation (27) with $k=1.2$ for argon and 1.1 for krypton (dashed line).

The distribution function (27) is formed mainly in the process of cluster-cluster aggregation. Indeed, the calculations show that in the absence of gas condensation the aggregation process results in the formation of the size distribution function (27) with $k=1$. A slight deviation of the coefficient k from unity is connected with the condensation growth of clusters: the condensation flux of atoms onto the cluster surface, being proportional to $N^{2/3}$, grows with cluster size N slower than N which results in a slight shortening of the large-size tail of the distribution function. This is allowed for by the coefficient $k>1$ in Eq. (27).

The size distribution function (27) also gives the distribution of clusters over intrinsic temperature which is maintained close to T_c in the course of cluster growth (T_c as a function of the gas state and cluster size N is given by Eqs. (2)–(9)].

It should be noted in conclusion that the developed approach explains the physical meaning of an important experimental regularity (usually called the similarity law): all the properties of the jet related to clusters depend on a combination of the nozzle-entry parameters $P_0^{-1}T_0^n$ with n

close to 5/2.[22] The point is that the cluster growth process is mainly determined by gas entropy per atom, s_g, which dictates the cluster temperature in the course of condensation growth (see Sec. 2). It is just the variable $P_0^{-1}T_0^{5/2}$ on which the initial entropy, s_g, depends according to Eq. (4).

The author is deeply grateful to Dr. E. T. Verkhovtseva for helpful discussions.

This work was carried out within the project of Ukrainian scientific Technological Center No. 593.

*E-mail: ratner@ilt.kharkov.ua

[1] Proceedings 4th Int. Symp. of Small Particles, Inorganic Clusters, Z. Phys. **D12** (1990).
[2] J. Stapelfeld, J. Wormer, and T. Moller, Phys. Rev. Lett. **62**, 98 (1989).
[3] J. Wormer, V. Guzielaski, J. Stapelfeld, and T. Moller, Chem. Phys. Lett. **159**, 321 (1989).
[4] J. Wormer, V. Guzielaski, J. Stapelfeld, G. Zimmerer, and T. Moller, Phys. Scr. **41**, 490 (1990).
[5] J. Wormer, M. Joppien, G. Zimmerer, and T. Moller, Phys. Rev. Lett. **67**, 2053 (1991).
[6] E. T. Verkhovtseva, E. A. Bondarenko, and Yu. S. Doronin, Chem. Phys. Lett. **140**, 181 (1987).
[7] E. A. Bondarenko, E. T. Verkhovtseva, Yu. S. Doronin, and M. A. Ratner, Chem. Phys. Lett. **182**, 637 (1991).
[8] E. T. Verkhovtseva, E. A. Bondarenko, and Yu. S. Doronin, Khim. Fiz. **10**, 956 (1991).
[9] S. S. Kovalenko, D. D. Solnyshkin, E. A. Bondarenko, and E. T. Verkhovtseva, Fiz. Nizk. Temp. **23**, 190 (1997) [Low Temp. Phys. **23**, 140 (1997)].
[10] K. Kobashi and R. D. Etters, Surf. Sci. **150**, 252 (1985).
[11] S. C. Wang, Phys. Rev. Lett. **75**, 2496 (1995).
[12] V. G. Karpov, Phys. Rev. Lett. **75**, 2702 (1995).
[13] D. I. Zhukhovitskiĭ, Zh. Éksp. Teor. Fiz. **109**, 839 (1996) [JETP **82**, 451 (1996)].
[14] E. A. Bondarenko, E. T. Verkhovtseva, A. K. Kupko, and T. S. Chebanova, Fiz. Nizk. Temp. **6**, 376 (1980) [Sov. J. Low Temp. Phys. **6**, 180 (1980)].
[15] R. Thouy and R. Jullien, J. Phys. A **27**, 2954 (1994).
[16] E. Ben Naim, P. L. Krapivski, and S. Redner, Phys. Rev. E **50**, 822 (1994).
[17] U. Buck and R. Krohne, Phys. Rev. Lett. **73**, 947 (1994).
[18] R. Schmidt, G. Seifert, and H. O. Lutz, Phys. Lett. A **158**, 231 (1991).
[19] O. Knospe, R. Schmidt, E. Engel, U. R. Schmitt, R. M. Dreizler, and H. O. Lutz, Phys. Lett. A **183**, 332 (1993).
[20] R. Schmidt and H. O. Lutz, Phys. Lett. A **183**, 338 (1993).
[21] A. M. Ratner and O. Ya. Shamfarova, Fiz. Nizk. Temp. **2**, 1551 (1976) [Sov. J. Low Temp. Phys. **2**, 756 (1976)].
[22] O. F. Hagena and W. Obert, J. Chem. Phys. **56**, 1793 (1972).

This article was published in English in the original Russian journal. It was edited by R. T. Beyer.

Interaction of a quantum Hall system with waveguide elastic modes

D. V. Fil

*Institute of Single Crystals, National Academy of Sciences of the Ukraine, 310001 Kharkov, Ukraine**
(Submitted November 23, 1998)
Fiz. Nizk. Temp. **25**, 376–383 (April 1999)

The interaction of nonuniform plane elastic modes of the wave-guide type with monolayer and double-layer quantum Hall systems is considered. It is shown that in contrast to the case of propagation of surface acoustic waves, no restrictions are imposed for waveguide modes on the maximum values of wave vectors for which the value of the phase velocity shift of the wave can be observed experimentally. Fractional incompressible Hall states can be studied by using the effect for measuring the dependence of the effective magnetic length on the filling factor and for observing phase transitions in double-layer systems under the variation of the separation between the layers. © *1999 American Institute of Physics.*
[S1063-777X(99)00704-5]

1. INTRODUCTION

The interaction of surface acoustic waves (SAW) with a quantum Hall system has been studied intensely in recent years both experimentally[1–5] and theoretically.[6–12] The measurement of velocity and attenuation of SAW is an indirect method of observation of dynamic conductivity of electron gas. A comparison of experimental results obtained by this method with theoretical dependences makes it possible to verify thoroughly the existing theoretical models. For example, apart from the observation of magnetic focussing effect[13,14] and the measurements of temperature dependence of dc conductivity,[15–17] it is just experiments on propagation SAW that are considered as a proof of applicability of the composite fermion model[6,18,19] for describing the fractional quantum Hall effect.

Since a SAW is localized at the sample surface, and the two-dimensional electron layer is at a certain distance d from the surface (the characteristic values of $d=10^3-5\times10^3$ Å), the application of the SAW method for measuring the momentum dependence of the conductivity of the electron subsystem is restricted by the wave vectors $q\lesssim q_0\sim d^{-1}$. It is especially important to leave this range while studying dynamic characteristics of fractional incompressible states.

It was proved in Ref. 20 that the interaction of a two-dimensional electron system in the fractional quantum Hall regime with acoustic phonons leads to a noticeable renormalization of the phonon phase velocity (Δv) for finite wave vectors. According to the results obtained in Ref. 20, the $\Delta v(q)$ dependence is of the oscillatory type with the scale of oscillations $\sim\lambda_{\rm eff}^{-1}$, where $\lambda_{\rm eff}$ is the effective magnetic length in the model of composite fermions. Consequently, the measurement of $\Delta v(q)$ can serve as a method for indirect experimental observation of the dependence of $\lambda_{\rm eff}$ on the filling factor ν. Moreover, it was demonstrated earlier[21] that the measurements of Δv for finite q can be used as a method of detection of phase transitions between fractional states with different quantum numbers in double-layer quantum Hall systems upon a variation of the separation between layers. (Here and below, we speak of generalized Laughlin states corresponding to the Halperin wave function.[22] The description of such states in double-layer systems was developed by Lopez and Fradkin[23] on the basis of the approach of composite fermions used by us here.)

Numerical estimates given in Refs. 20 and 21 correspond to a bulk acoustic wave propagating in a superlattice of $2D$ electron layers. The measurements in a monolayer (or a double-layer system) for large values of q require an experimental geometry in which an elastic wave is localized near the electron layer rather than at the sample surface as in the case of SAW. Such a situation is possible in layered elastic media in which an elastic mode (modes) can be localized in a layer of a material whose acoustic properties differ from those in the bulk (this is a particular case of wave-guide propagation of waves; see Ref. 24). Here we consider the interaction of a quantum Hall system with nonuniform plane transverse elastic modes propagating in such a medium. The wave vectors and polarization vectors of elastic modes lie in a plane parallel to the interface between the media. The velocity of transverse sound in the layer is assumed to be smaller than in the bulk, which is a necessary condition for localization of such waves. The piezoelectric mechanism of coupling of the elastic mode with the two-dimensional electron layer is implied.

Heterostructures $Al_xGa_{1-x}As-GaAs$ used for creating double-layer Hall systems are in fact a ready-made elastic medium with the required properties. For example, structures of the type A–B–A–B–A (double quantum well) and A–B–A, where A stands for $Al_xGa_{1-x}As$ and B for GaAs were used in Refs. 25 and 26. On account of characteristic values of wave vectors considered below and specific thicknesses of layers in Refs. 25 and 26, the acoustic properties of these structures approximately correspond to a model in which a bulk AlGaAs sample contains a layer of pure GaAs in which the transverse velocity of sound is lower than in AlGaAs. It will be proved below that the renormalization of the velocity of the elastic mode localized in the GaAs layer in such a system has a measurable value in spite of the small

nonuniformity in the elastic properties of the system. The effect can be enhanced by using the structures with a high acoustic heterogeneity. We propose as a possible structure a system in which the AlGaAs–GaAs heterostructure containing a two-dimensional electron layer is in the three-dimensional matrix of the material with a much higher velocity of transverse sound. The value of Δv in such a system can be an order of magnitude higher than in the previous case.

2. MATRIX ELEMENTS OF INTERACTION

We start our analysis with the general formulas describing the renormalization of phase velocity v of acoustic phonons interacting with electrons. The Hamiltonian of phonons can be written in the form

$$H_{\rm ph}=\sum_{\mathbf{q}}\ \omega_q(b_{\mathbf{q}}^{+}b_{\mathbf{q}}+1/2), \tag{1}$$

where $\omega_q=vq$ is the phonon spectrum and $b^{+}(b)$ are the creation (annihilation) operators for phonons. We choose the Hamiltonian of the electron–phonon interaction in the form

$$H_{\rm int}=\frac{1}{\sqrt{S}}\sum_{\mathbf{q},k}\ \int d^2r g_{qk}\Psi_{\mathbf{r}k}^{+}\Psi_{\mathbf{r}k}\mathbf{e}^{i\mathbf{qr}}(b_{\mathbf{q}}+b_{-\mathbf{q}}^{+}), \tag{2}$$

where $\Psi^{+}(\Psi)$ are the electron creation (annihilation) operators, k the electron layer index, S the area of the layer, g are the matrix elements of the interaction, and the vectors $\mathbf{q}$ and $\mathbf{r}$ lie in the plane of the layer.

With such a choice of $H_{\rm ph}$ and $H_{\rm int}$, the quantity Δv is defined as

$$\frac{\Delta v}{v}=\frac{1}{vq}\sum_{k,k'}\ g_{qk}^{*}g_{qk'}D_{kk'}(q,vq), \tag{3}$$

where $D(q,\omega)$ is the electron density–density response function. A transition to the model of composite fermions is made through the introduction of an additional statistical interaction between electrons, leading to the corresponding modification of the functions D appearing in (3).

Let us calculate the matrix elements g_{qk}. We shall use the approach developed by Knäbchen *et al.*[7] The piezoelectric interaction of the elastic wave with electrons is determined by the Hamiltonian

$$H=\sum_{k}\ \int d^2r\, e\varphi_{\mathbf{r}k}\Psi_{\mathbf{r}k}^{+}\Psi_{\mathbf{r}k}, \tag{4}$$

where φ is the scalar potential of the electric field generated by the elastic mode (in accordance with the theory of linear response, φ in (4) is the external potential, i.e., its magnitude is calculated without taking into account the effect of the electron subsystem).

We shall use the smallness of the piezoelectric interaction constant. (The form of the small parameter in which the expansion is carried out will be given below.) We solve first the elastic problem disregarding piezoelectric interaction. We direct the x-axis along q and the z-axis at right angles to the interface between elastic media. The origin is chosen so that the coordinates of the interfaces are $z_b=\pm a$. Let the velocity of transverse sound be c_l in the layer ($|z|<a$) and c_b in the bulk ($|z|>a$) ($c_b>c_l$). For the sake of definiteness, we assume that both elastic media have cubic symmetry and equal elastic moduli c_{44}, and the difference between c_l and c_b is determined by the difference in the densities ρ (such a relation between parameters approximately corresponds to the parameters of AlGaAs and GaAs). The crystallographic axes of the system are directed along the coordinate axes.

Let us consider a transverse wave with the displacement vector directed along the y-axis. The wave equation for the Fourier component $u_y(q,z,\omega)=u$ has the form

$$\frac{\partial^2 u}{\partial z^2}-(c_{l(b)}^2q^2-\omega^2)u=0. \tag{5}$$

The boundary conditions are the requirements of the continuity of $u(z)$ and $\partial u(z)/\partial z$ at the interfaces and vanishing of u for $z\to\pm\infty$ (we consider a localized wave). The solution of Eq. (5) with such boundary conditions gives

$$u_e(q,z)=A_q^e\begin{cases}\cos(\eta qa)\mathrm{e}^{-\lambda q(|z|-a)} & |z|\geqslant a\\ \cos(\eta qz) & |z|\leqslant a\end{cases} \tag{6}$$

(even mode) and

$$u_0(q,z)=A_{q'}^0\begin{cases}\sin(\eta qa)\mathrm{e}^{-\lambda q(z-a)} & z\geqslant a\\ \sin(\eta qz) & |z|\leqslant a\\ -\sin(\eta qa)\mathrm{e}^{\lambda q(z+a)} & z\leqslant -a\end{cases} \tag{7}$$

(odd mode). In (6) and (7), we have $\lambda=\sqrt{1-v^2/c_b^2}$, $\eta=\sqrt{v^2/c_l^2-1}$. The velocity v in the case of an even solution is determined by the equation

$$\tan(\eta qa)=\lambda/\eta, \tag{8}$$

while in the case of an odd solution it is determined by

$$\cot(\eta qa)=-\lambda/\eta. \tag{9}$$

For $q<\pi/(2a\sqrt{c_b^2/c_l^2-1})$ only one (even) mode exists. An increase in q leads to the emergence of additional solutions of Eqs. (8) and (9) (waveguide modes).

We write the transverse component of the displacement vector in terms of operators b:

$$u_{e(0)}(\mathbf{r},z)=\sum_{\mathbf{q}}\ u_{e(0)}(q,z)\mathrm{e}^{i\mathbf{qr}}(b_{\mathbf{q}}+b_{-\mathbf{q}}^{+}) \tag{10}$$

and substitute it into the expression for the energy of elastic vibrations:

$$E_u=\frac{1}{2}\int d^2rdz\left\{\rho(z)\left(\frac{\partial u}{\partial t}\right)^2+c_{44}\left[\left(\frac{\partial u}{\partial x}\right)^2+\left(\frac{\partial u}{\partial z}\right)^2\right]\right\}. \tag{11}$$

Equating (11) (after the substitution of (10)) and (1), we obtain the value of the normalization factor

$$A_q^e=A_q^0=\frac{1}{\alpha}\sqrt{v/2Sc_{44}}\,, \tag{12}$$

where $\alpha=[qa(1+\eta^2)+1/\lambda]^{1/2}$.

The scalar potential is determined by the solution of the Poisson equation

$$\Delta\varphi = -\frac{4\pi}{\varepsilon}\beta_{i,jm}\frac{\partial^2 u_m}{\partial x_i \partial x_j}, \tag{13}$$

where ε is the dielectric constant and $\beta_{i,jm}$ the piezoelectric tensor. In crystals with cubic symmetry, nonzero components of the tensor $\beta_{i,jm}$ (with $i \neq j \neq m$) have the same value (we denote it by β).

The solution of Eq. (13) taking into account (10) and (12) can be written in the form

$$\varphi_{\mathbf{rz}} = i\chi\sqrt{2\pi v/S\varepsilon}\sum_{\mathbf{q}} \gamma_q(z)e^{i\mathbf{qr}}(b_{\mathbf{q}} + b^{+}_{-\mathbf{q}}), \tag{14}$$

where $\chi = \beta\sqrt{16\pi/\varepsilon c_{44}}$ is the dimensionless parameter of piezoelectric interaction (the quantity χ is the small parameter in the above derivation), and γ_q is the structural function defined by the boundary conditions imposed on φ and by the type of the elastic mode. Comparing (2), (4), and (14), we obtain

$$g_{qk} = i\sqrt{2\pi/\varepsilon}\, ev^{1/2}\chi\gamma_q(z_k), \tag{15}$$

where z_k is the coordinate of the two-dimensional electron layer. The values of $\gamma_q(z_k)$ will be given in Sec. 4 during an analysis of specific structures.

3. RESPONSE FUNCTIONS IN THE MODEL OF COMPOSITE FERMIONS

Let us now consider the algorithm of calculation of the response functions D in the model of composite fermions. For definiteness, we choose a monolayer system. In the random-phase approximation, we have

$$D = (1 - D_0 V)^{-1} D_0, \tag{16}$$

where $V = 2\pi e^2/\varepsilon q$ is the Fourier component of the Coulomb potential, and D_0 is connected with the polarization operator $\Pi_{\mu\nu}$ of electromagnetic field through the relation

$$D_0 = -(1/e^2)\Pi_{00}. \tag{17}$$

In order to calculate Π_{00}, we use an approach that is a Lagrangian formulation of the modified random-phase approximation for composite fermions.[27] The essence of the approximation[27] lies in the inclusion of the Fermi-liquid interaction with the constant[28] F_1 defined by the effective mass m^* of composite fermions and the band mass m_b of electrons. Simon and Halperin[27] proved that the inclusion of this interaction makes it possible to construct the response function satisfying the f-sum rule.

We write the Lagrangian of the system in the form

$$L = \Psi^*\Big(i\partial_t + \mu_F - a_0 - eA_0 - \frac{1}{2m^*}(i\nabla_i + a_i + eA_i + b_i)^2\Big)\Psi + \frac{1}{4\pi\psi}a_0\varepsilon_{ij}\partial_i a_j + \frac{1}{2}\xi b_i^2, \tag{18}$$

where a_μ is the Chern-Simons gauge field potential, A_μ the electromagnetic field potential, ε_{ij} the antisymmetric unit tensor, μ_F the Fermi energy, ψ the model parameter corresponding to the number of gauge field flux quanta carried by a composite quasiparticle (ψ is even), b_i the additional field introduced for simulating the Fermi-liquid interaction, and the subscripts i and j assume the values x and y. In formula (18), we used the transverse gauge of the field a.

In order to determine value of ξ, we require that Lagrangian (18) gives the value of current satisfying the requirement of Galilean invariance:[28]

$$\left\langle \frac{\delta L}{\delta A_i} \right\rangle = \langle j_i \rangle - \frac{en_0}{m^*}\langle b_i \rangle = \frac{m^*}{m_b}\langle j_i \rangle, \tag{19}$$

where $j_i = -(e/m^*)\Psi^*(i\nabla_i + a_i + eA_i)\Psi$; and n_0 the average electron concentration. The mean value of the field b is determined from the condition that the Lagrangian be stationary:

$$\left\langle \frac{\delta L}{\delta b_i} \right\rangle = 0 = \frac{1}{e}\langle j_i \rangle - \frac{n_0}{m^*}\langle b_i \rangle + \xi\langle b_i \rangle. \tag{20}$$

The condition for the compatibility of (19) and (20) gives $\xi = n_0/(m^* - m_b)$.

The condition that L be stationary relative to fluctuation a_0 gives the value of effective magnetic field $B_{\text{eff}} = B(1 - \nu\psi)$ (B is the external magnetic field), which is equal to $B^f_{\text{eff}} = \pm n_0\varphi_0/N$ (φ_0 is the magnetic flux quantum) for the filling factor $\nu_f = N/(N\psi \pm 1)$ (N is an integer). The field B^f_{eff} corresponds to the integer N of filled Landau levels in the effective magnetic field, which shows that the filling factors ν_f correspond to incompressible states. The field B^f_{eff} determines the effective cyclotron frequency $\omega_{ce} = 2\pi n_0/m^*N$ and the effective magnetic length $\lambda_{\text{eff}} = (N/2\pi n_0)^{1/2}$.

In order to determine the value of Π_{00}, we find the component of the effective action of the electromagnetic field, which is quadratic in A. In order to calculate this component, we carry out functional integration with respect to fields Ψ followed by functional integration over the fields a and b (in the vicinity of the saddle point) in the expression for the partition function of the system defined by Lagrangian (18). Omitting intermediate calculations, we write the final results for $T = 0$:

$$\Pi_{00} = -\frac{e^2q^2}{2\pi\omega_{ce}}\frac{S_0}{\Delta_1}, \tag{21}$$

where

$$S_0 = \Sigma_0 - p(\Sigma_0(\Sigma_2 + N) - \Sigma_1^2), \tag{22}$$

$$\Delta_1 = (1 - \psi\Sigma_1)^2 - \psi^2\Sigma_0(\Sigma_2 + N) - pF, \tag{23}$$

$$F = \Sigma_2 + N + (\omega/\omega_{ce})^2 S_0, \tag{24}$$

with $p = (m^* - m_b)/m^*N$ and

$$\Sigma_j = [\operatorname{sgn}(B_{\text{eff}})]^j e^{-x}\sum_{n=0}^{N-1}\sum_{m=N}^{\infty}\frac{n!}{m!}\frac{x^{m-n-1}(m-n)}{(\omega/\omega_{ce})^2 - (m-n)^2} \times [L_n^{m-n}(x)]^{2-j}\Big[(m-n-x)L_n^{m-n}(x) + 2x\frac{dL_n^{m-n}(x)}{dx}\Big]^j. \tag{25}$$

In expression (25), $x = (q\lambda_{\text{eff}})^2/2$ and $L_n^{m-n}(x)$ is the generalized Laguerre polynomial.

Taking into account (15)–(17) and (21), we can transform expression (3) to

$$\frac{\Delta v}{v}=\chi^2\gamma_q^2(z_1)\frac{f_qS_0}{\Delta_1-f_qS_0}, \tag{26}$$

where $f_q=e^2q/\varepsilon\omega_{ce}$.

A similar procedure can be carried out for a double-layer Hall system. Two types of Chern–Simons fields and two types of fermion fields (corresponding to two electron layers) are introduced in this case. A nontrivial generalization of the model is the inclusion of terms nondiagonal in layers in the free Lagrangian of Chern–Simons fields:

$$L_{CS}=\frac{1}{4\pi}\varepsilon_{ij}a_{0k}M_{kk'}\partial_i a_{jk'} \tag{27}$$

with

$$M=\frac{1}{\psi^2-s^2}\begin{pmatrix}\psi & -s\\ -s & \psi\end{pmatrix}, \tag{28}$$

where (integer) s corresponds to the number of flux quanta of type 1 carried by a quasiparticle of type 2, and vice versa (the system displays the statistical interaction between layers). Here we consider the system of two equivalent layers. For $\psi=s$, we consider only the combination of the fields $a_{\mu k}$ symmetric in the layer indices as the integration variable since there are no fluctuations of combinations of fields a antiphase in layers.

Incompressible states in a double-layer system correspond to filling factors

$$\nu_f=\frac{N}{N(\psi+s)\pm 1} \tag{29}$$

(per layer). The expressions for the remaining parameters ($B^f_{\rm eff}$,ω_{ce}, and $\lambda_{\rm eff}$) coincide with those given above. Equation (16) assumes the matrix form with

$$V=\frac{2\pi e^2}{\varepsilon q}\begin{pmatrix}1 & e^{-qd_0}\\ e^{-qd_0} & 1\end{pmatrix}, \tag{30}$$

where d_0 is the separation between the layers.

As a result, we obtain the following expression for the renormalization velocity of a double-layer Hall system:

$$\frac{\Delta v}{v}=\frac{1}{2}\chi^2S_0f_q\left(\frac{|\gamma_q(z_1)+\gamma_q(z_2)|^2}{\Delta_+-f_qE_+S_0}+\frac{|\gamma_q(z_1)-\gamma_q(z_2)|^2}{\Delta_--f_qE_-S_0}\right), \tag{31}$$

where

$$E_\pm=1\pm\exp(-qd_0);$$

$$\Delta_\pm=[1-(\psi\pm s)\Sigma_1]^2-(\psi\pm s)^2\Sigma_0(\Sigma_2+N)-pF. \tag{32}$$

The phase of a double-layer system is determined by quantum numbers ψ and s. According to (29), the same value of ν may correspond to different sets of ψ and s, i.e., different phases. If the correlation between the layers is weak (for large d_0), the phase with $s=0$ is realized. As the value of d_0 decreases, a transition to a phase with $s\neq 0$ may occur (see, for example, Ref. 29) During such a phase transition, the value of quantity (31) changes in general, i.e., a phase velocity jump takes place.

4. RENORMALIZATION OF THE VELOCITY OF ELASTIC MODE

Formulas (26) and (31) give the value of Δv relative to the phase velocity of the wave in the system containing no electron layer (layers). Since electron layers are not removed from the system in the experiments, the value of velocity in zero magnetic field is used as the reference point. In this case, a comparison of experimental data with the theory generally requires the knowledge of the quantity $\sigma_{xx}(q,\omega)$ (the longitudinal component of the conductivity tensor) in zero magnetic field. It is normally assumed that $\sigma_{xx}\to\infty$ for $B=0$. In the given case, such an approximation seems to rough since we are interested in the dependence $\Delta v(q)$. We propose that the value of velocity for $\nu=1$ to be used as the reference point. The case $\nu=1$ is also described by the formulas (26) and (31) if we put $\psi=s=0$, $N=1$, and $m^*=m_b$ in all the functions appearing in these formulas. Thus, the quantity that will be sought and compared with the experimental value is defined as

$$\frac{\Delta v_0}{v}=\left.\frac{\Delta v}{v}\right|_{\nu=\nu_f}-\left.\frac{\Delta v}{v}\right|_{\nu=1}. \tag{33}$$

Let us consider the structure $Al_{0.3}Ga_{0.7}As$–GaAs –$Al_{0.3}Ga_{0.7}As$ in which two electron layers are located at heterojunctions ($z_k=\pm a$, $d_0=2a$). We assume that quantities β and ε are constant in the entire system. The boundary conditions imposed on φ are reduced to the requirement of continuity of the Fourier component $\varphi(q,z)$ and the derivative $\partial\varphi(q,z)/\partial z$ at the interfaces and the equality to zero of the function φ for $z\to\infty$.

For definiteness, we consider a transition from the phase $\psi=4$, $s=0$ to the phase $\psi=2$, $s=2$ for $\nu=1/5$. The solution of Eq. (13) into which we substitute (6) (even mode) gives a function φ odd in z, while the substitution of (7) (odd mode) gives a function φ even in z. It follows from (31) that during the propagation of an even mode, the phase transition with a change in quantum numbers ψ and s is accompanied by a jump in the phase velocity of the elastic mode. On the other hand, the effect is not observed for the odd mode.

The quantities $\gamma_q(z_k)$ for the even mode are defined as

$$\gamma_q(a)=-\gamma_q(-a)=\alpha^{-1}\frac{\cos(\eta qa)}{1+\eta^2}\left(\frac{E_-(\eta^2+\lambda^2)}{2(1+\lambda)}-\lambda\right). \tag{34}$$

Figure 1 shows the dependences of $\Delta v_0/v$ on the wave vector for the states $\psi=4$, $s=0$ and $\psi=2$, $s=2$. We have used the parameters $\beta=4.5\times10^4\,\mathrm{dyne}^{1/2}/\mathrm{cm}$, $\varepsilon=12.5$, $n_0=10^{11}\,\mathrm{cm}^{-2}$, $m_b=0.07m_e$ (m_e is the electron mass), $m^*=4m_b$, $c_{44}=6\times10^{11}\,\mathrm{dyne/cm}^2$, $\rho_l=5.3\,\mathrm{g/cm}^3$, $c_b/c_l=1.05$, and $d_0=300$ Å. It can be seen from the curves that the jump in phase velocity at finite values of wave vector has a value that can be reliably measured in experiments.

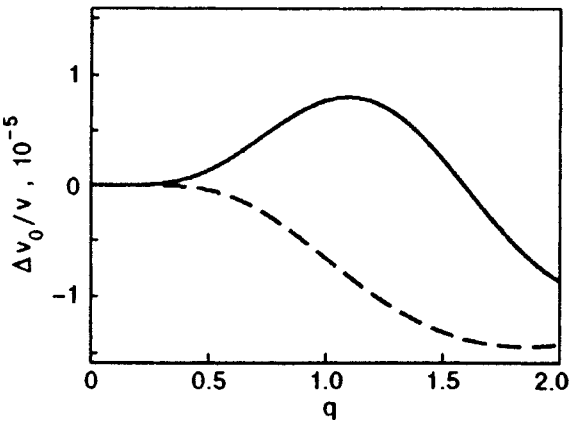

FIG. 1. Relative renormalization of the velocity of a localized elastic mode (lower even harmonic) in a double-layer Hall system for $c_b/c_l=1.05$ and $\nu=1/5$. The solid curve corresponds to $\psi=4$, $s=0$, and the dashed curve to $\psi=2$, $s=2$; q is given in the units of $\sqrt{4\pi n_0}$.

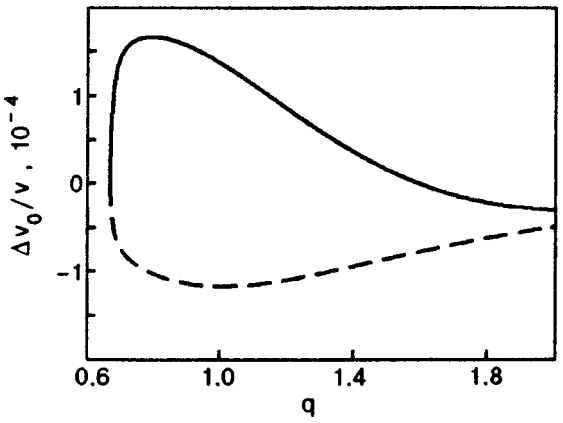

FIG. 3. Relative renormalization of the velocity of a localized elastic mode (third even harmonic) in a double-layer Hall system for $c_b/c_l=1.5$ and $\nu=1/5$. The solid curve corresponds to $\psi=4$,$s=0$, and the dashed curve to $\psi=2$, $s=2$; q is given in the units of $\sqrt{4\pi n_0}$.

Let us now consider the systems in which a considerable enhancement of the observed effect can be reached. We shall assume that the heterostructure containing two-dimensional electron layers is in the matrix of a material with considerably different acoustic properties. In this case, the heterostructure itself will be regarded as acoustically homogeneous. In order to avoid the specification of dielectric and piezoelectric properties of the matrix, we assume that the interfaces contain a thin screening layer. In this case, the boundary conditions imposed on φ can be reduced to the requirement $\varphi(z=\pm a)=0$.

Let the heterostructure contain a single electron layer for $z=0$. Then it follows from the symmetry of $\varphi(z)$ that only the velocity of the odd elastic mode is renormalized in such a system. The effect is of the threshold type relative to q (for small q, the odd localized mode is absent). The structural function calculated from (13) after the substitution of (7) assumes the value

$$\gamma_q(0)=\alpha^{-1}\frac{\eta}{1+\eta^2}\left(1-\frac{\cos(\eta qa)}{\cosh(qa)}\right). \tag{35}$$

Figure 2 shows $\Delta v_0/v$ as a function of q for $\nu_f=2/5$, 3/7, and 4/9 ($N=2$, 3, and 4, respectively) for the lower odd elastic mode. We have used the parameters $c_b/c_l=1.5$ and $2a=1500$ Å (the thickness of the heterostructure). The remaining parameters are the same as in the previous case. The $\Delta v_0(q)$ curves in different incompressible cases differ considerably and have a clearly manifested oscillatory structure (reflecting the increase in the effective magnetic length as ν_f tends to $\nu=1/2$). The renormalization is an order of magnitude higher than in the previous case. The main restriction on further enhancement of the effect is the impossibility to create such structures with very small a without violating the properties of the electron layer.

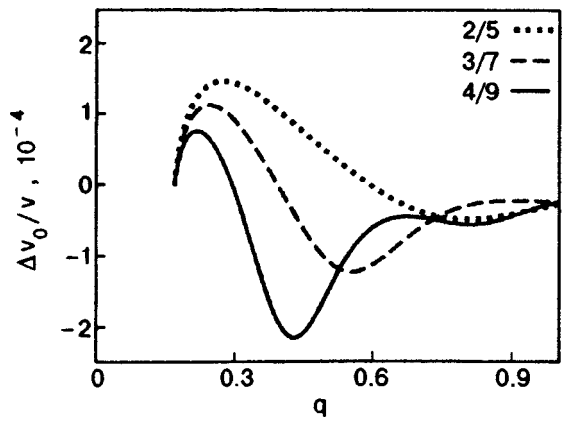

FIG. 2. Relative renormalization of the velocity of a localized elastic mode (lower odd harmonic) in a monolayer Hall system for $c_b/c_l=1.5$ and $\nu=2/5$, 3/7 and 4/9; q is given in units of $\sqrt{4\pi n_0}$.

If the heterostructure contains a system of double electron layers with coordinates $z=\pm d_0/2$, the velocity of the even elastic mode must be measured as before in order to observe the phase transition from $\psi=4$, $s=0$ to $\psi=2$, $s=2$ for $\nu=1/5$. The maximum effect in this case is attained at a higher harmonic (we assume that $d_0 \ll 2a$). The computation of structural function in the latter case gives

$$\gamma_q(d_0/2)=-\gamma_q(-d_0/2)=\alpha^{-1}\frac{\eta}{1+\eta^2}\left[\frac{\sin(\eta qa)\sinh(qd_0/2)}{\cosh(qa)} - \sin(\eta q d_0/2)\right]. \tag{36}$$

Figure 3 shows $\Delta v_0/v$ as a function of q for the third even harmonic for $\nu_f=1/5$ for the states $\psi=4$, $s=0$ and $\psi=2$, $s=2$ ($d_0=300$ Å, $2a=1500$ Å). In this case, the magnitude of the effect also increases significantly as compared to the former case.

Thus, an analysis of the propagation of nonuniform plane elastic modes of the waveguide type localized in layered media such as AlGaAs–GaAs heterostructures can be regarded as a method of studying the electron structure of monolayer and double-layer quantum Hall systems. The study of incompressible Hall states by such a method is of special interest. The expected values of renormalization of phase velocities of such modes coincide with a similar value for surface acoustic waves interacting with compressible Hall liquids.

*E-mail: fil@isc.kharkov.com

[1] A. Wixforth, J. P. Kotthaus, and G. Weimann, Phys. Rev. Lett. **56**, 2104 (1986); A. Wixforth, J. Scriba, M. Wassermeier *et al.*, Phys. Rev. B **40**, 7874 (1989).
[2] R. L. Willett, M. A. Paalanen, R. R. Ruel *et al.*, Phys. Rev. Lett. **65**, 112 (1990); M. A. Paalanen, R. L. Willett, P. B. Littlewood *et al.*, Phys. Rev. B **45**, 11342 (1992); R. L. Willett, R. R. Ruel, K. W. West, and L. N. Pfeiffer, Phys. Rev. Lett. **71**, 3846 (1993); R. L. Willett, R. R. Ruel, M. A. Paalanen *et al.*, Phys. Rev. B **47**, 7344 (1993).
[3] R. L. Willett, K. W. West, and L. N. Pfeiffer, Phys. Rev. Lett. **75**, 2988 (1995); *ibid.* **78**, 4478 (1997).
[4] J. M. Shilton, D. R. Mace, V. I. Talyanskii *et al.*, Phys. Rev. B **51**, 14770 (1995).
[5] G. R. Nash, S. J. Bending, M. Boero *et al.*, Phys. Rev. B **54**, R8337 (1996).
[6] B. I. Halperin, P. A. Lee, and N. Read, Phys. Rev. B **47**, 7312 (1993).
[7] A. Knäbchen, Y. B. Levinson, and O. Entin-Wohlman, Phys. Rev. B **54**, 10696 (1996).
[8] S. H. Simon, Phys. Rev. B **54**, 13878 (1996).
[9] A. L. Efros and Yu. M. Halperin, Phys. Rev. Lett. **64**, 1959 (1990).
[10] A. D. Mirlin and P. Wölfle, Phys. Rev. Lett. **78**, 3717 (1997).
[11] F. von Oppen, A. Stern, and B. I. Halperin, Phys. Rev. Lett. **80**, 4494 (1998).
[12] A. D. Mirlin, P. Wölfle, Y. B. Levinson, and O. Entin-Wohlman, Phys. Rev. Lett. **81**, 1070 (1998); Y. B. Levinson, O. Entin-Wohlman, A. D. Mirlin, and P. Wölfle, Phys. Rev. B **58**, 7113 (1998).
[13] V. J. Goldman, B. Su, and J. K. Jain, Phys. Rev. Lett. **72**, 2065 (1994).
[14] J. H. Smet, D. Weiss, R. H. Blick *et al.*, Phys. Rev. Lett. **77**, 2272 (1996).
[15] R. R. Du, H. L. Stormer, D. C. Tsui *et al.*, Phys. Rev. Lett. **70**, 2944 (1993); R. R. Du, H. L. Stormer, D. C. Tsui *et al.*, Phys. Rev. Lett. **73**, 3274 (1994).
[16] D. R. Leadly, R. J. Nicholas, C. T. Foxon, and J. J. Harris, Phys. Rev. Lett. **72**, 1906 (1994).
[17] H. C. Manoharan, M. Shayegan, and S. J. Klepper, Phys. Rev. Lett. **73**, 3270 (1994).
[18] J. K. Jain, Phys. Rev. Lett. **63**, 199 (1989).
[19] A. Lopez and E. Fradkin, Phys. Rev. B **44**, 5246 (1991).
[20] A. L. Zazunov and D. V. Fil', Fiz. Nizk. Temp. **23**, 1345 (1997) [Low Temp. Phys. **23**, 1010 (1997)].
[21] D. V. Fil', Fiz. Nizk. Temp. **24**, 905 (1998) [Low Temp. Phys. **23**, 681 (1998)].
[22] B. I. Halperin, Helv. Phys. Acta **56**, 75 (1983).
[23] A. Lopez and E. Fradkin, Phys. Rev. B **51**, 4347 (1995).
[24] A. M. Brekhovskikh, *Waves in Layered Media* Academic Press, NY 1960, Moscow (1957); A. M. Brekhovskikh and O. A. Godin, *Acoustics of Layered media* [in Russian], Nauka, Moscow (1989).
[25] G. S. Boebinger, H. W. Jiang, L. W. Pfeiffer, and W. West, Phys. Rev. Lett. **64**, 1793 (1990); J. P. Eisenstein, G. S. Boebinger, L. W. Pfeiffer *et al.*, Phys. Rev. Lett. **68**, 1383 (1992); S. Q. Murphy, J. P. Eisenstein, G. S. Boebinger *et al.*, Phys. Rev. Lett. **72**, 728 (1994).
[26] Y. W. Suen, L. W. Engel, M. B. Santos *et al.*, Phys. Rev. Lett. **68**, 1379 (1992).
[27] S. H. Simon and B. I. Halperin, Phys. Rev. **47**, 17368 (1993).
[28] D. Pines and Ph. Nozière, *The Theory of Quantum Liquids*, New York (1966).
[29] D. Yoshioka, A. H. MacDonald, and S. M. Girvin, Phys. Rev. B **39**, 1932 (1989).

Translated by R. S. Wadhwa

On the spectrum of the Hubbard model with infinite repulsion on anisotropic triangular ladder-type lattice

V. O. Cheranovskii, E. V. Ezerskaya, and M. V. Krikunov

*Kharkov State University, 310077 Kharkov, Ukraine**
(Submitted November 25, 1998)
Fiz. Nizk. Temp. **25**, 384–389 (April 1999)

Low-energy states of the Hubbard model with infinite electron repulsion on an anisotropic triangular strip-type lattice formed by weakly interacting linear segments are studied. The estimates of the stability region boundaries for the ferromagnetic ground state of the lattice are obtained in first order perturbation theory in the interaction between the segments. It is shown that a magnetic transition accompanied by a jumpwise variation of the total spin of the ground state from the minimum to the maximum value is possible for lattices with cyclic boundary conditions and the number of electrons greater than the number of segments by unity.
 [S1063-777X(99)00804-X]

1. INTRODUCTION

The study of possible scenarios of ferromagnetic ordering in the ground state of the Hubbard model is one of the most interesting problems in the physics of many-electron systems.[1,2] The first rigorous proof of the possibility of ferromagnetic ordering in the ground state of the Hubbard model with infinite repulsion was obtained by Nagaoka[3] and Thouless,[4] but it concerns only the case of electron filling with a single hole. It is still unclear whether the ferromagnetic nature of the ground state is preserved for a finite value of hole concentration and/or finite repulsion.

In this research, we study the exact spectrum of low-energy states in the Hubbard model with infinite repulsion on a triangular lattice formed by weakly interacting two-center segments. The interest to such models of strongly correlated electrons is due to a peculiar form of the spectrum and the possibility of ferromagnetic ordering of spins in the ground state for finite concentrations of holes in a half-filled energy band.[5–7] Various many-electron models for lattices of the ladder type (strips) are used for describing high-temperature superconductivity of doped compounds $(VO)_2P_2O_7$ and $SrCu_2O_7$.[6,8] Besides, Hubbard's Hamiltonian for anisotropic strip-type lattices may serve as a simple maniy-electron model for predicting low-temperature properties of stacked crystals formed by various complexes with a charge transfer, including organometallic Miller-type ferromagnets.[9,10]

2. HUBBARD MODEL WITH INFINITE REPULSION FOR LINEAR FRAGMENTS OF A TRIANGULAR LATTICE

Hubbard's Hamiltonian for a triangular lattice of the strip type formed by weakly interacting linear segments (Fig. 1) has the form

$$H=P\sum_{m,\sigma}\{t_1A_1^+(m,\sigma)A_2(m,\sigma)+t_2[A_1^+(m,\sigma)A_1(m+1,\sigma)+A_2^+(m,\sigma)A_2(m+1,\sigma)]+t_3A_1^+(m,\sigma)A_2(m+1,\sigma)+\text{h.c.}\}P. \quad (1)$$

Here P is the projector operator on states without double filling of lattice sites, $A_i^+(m,\sigma)$ the creation operator for electrons with the spin component σ at the ith site of the mth segment $(i=1,2)$, and the parameters t_1 and t_2, t_3 describe electron jumps inside and between segments, respectively $(|t_1|\geqslant|t_2|,|t_3|)$.

The exact diagonalization of the matrix of Hamiltonian (1) for finite lattice fragments gives the ferromagnetic ground state for any electron concentration ρ if $\mu=(t_1t_3)/(|t_1|t_2)>1$. For $-0.5<\mu<1$, ferromagnetic ordering is observed only for $\rho>0.5+\delta$, where δ can be estimated approximately with the help of concepts concerning the emergence of magnetic polarons in the system.[5] Unfortunately, the possibility of direct numerical simulation of the exact spectrum is limited considerably in view of its quasi-degenerate form and the exponential increase in the size of the Hamiltonian matrix.

We shall consider only the occupancy greater than 50% since a simpler case of $\rho\leqslant0.5$ is considered in detail in Ref. 7. For $\rho>0.5$ and in the absence of interaction between the segments, lower energy levels are degenerate in spin and correspond only to single $(n=1)$ and double $(n=2)$ filling of two-center segments (empty segments are absent). Consequently, in accordance with Ref. 7, the interaction between segments with identical occupancies in second order perturbation theory (PT) for $|t_1|\geqslant|t_2|,|t_3|$ is described by the Hamiltonian

$$H(1,2)=\begin{cases}\dfrac{t_2^2}{4|t_1|}[2(1-\mu)P_{12}-(1-\mu)^2-1], & n=1;\\ 0, & n=2,\end{cases} \quad (2)$$

where P_{12} is the operator of transposition of spin variables of the first and second electrons of a pair of interacting segments.

After labelling all N electrons of the lattice consecutively over L segments, we can write the wave function in the form

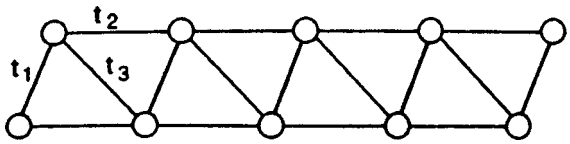

FIG. 1. Triangular strip-type lattice described by Hamiltonian (1).

$$\Psi(L,N,S^z) = \sum_{n_1<n_2<\ldots<n_N} a(n_1,n_2,\ldots,n_{N-L},\sigma_1,\sigma_2,\ldots,\sigma_N) \times B^+(n_1),B^+(n_2),\ldots,B^+(n_{N-L})|0\rangle \times\otimes|\sigma_1,\sigma_2,\ldots,\sigma_N\rangle,$$

$$S^z=\sum_{n=1}^{N}\sigma_n, \tag{3}$$

where $B^+(n_i)$ is the zero-spin operator of creation of an electron pair on the segment with label n_i, and S^z is the z-component of the total spin of the lattice. The interaction of segments with different occupancies in the first order of the PT with such a labelling can be described by a three-electron Hamiltonian of the form

$$H(1,3)=R(1,3)[B^+(2)B(1)+\text{h.c.}],$$

$$R(1,3)=-\frac{t_2}{2}\{P_{12}+P_{23}+\mu\}. \tag{4}$$

For $\rho\sim0.5$ and $\rho\sim1$, we can neglect the terms of the second order of smallness in t_2 for the interaction of segments with different occupancies. In this case, the total lattice Hamiltonian can be written in the form

$$H=\sum_{j=1}^{L} H(j,j+1)[1-B^+(i)B(i)][1-B^+(i+1) \times B(i+1)]+\sum_{i=1}^{L-1} R(j,j+2)[B^+(i+1)B(i) + B^+(i)B(i+1)],$$

$$j=i+\sum_{l=1}^{t-1}\sum_{k=1}^{N-L}\delta(n_k,l). \tag{5}$$

Here $\delta(i,j)$ is the Kronecker delta.

It can easily be seen that the spectrum of the Hamiltonian (5) is independent of the sign of the parameter t_2 in view of the symmetry of the problem. Choosing a positive value of this parameter, we can prove that matrix (5) for $\mu>1$ has only nonnegative elements and is irreducible. Consequently, in accordance with Perron–Frobenius condition, the ground state (5) is nondegenerate and corresponds to an eigenvector with positive components. It can be shown that the spin component of this vector is symmetric relative to transposition of spin variables. For this reason, the ground state (5) for $\mu>1$ corresponds to the maximum value of the total spin of the lattice. The limit of weak interaction between segments ($t_2,t_3\to0$) can be analyzed in a quite similar way. In this case, the sufficient condition for the fulfillment of the conditions for the Perron–Frobenius theorem is $\mu>0$. Thus, the corresponding results of numerical simulation of the spectrum of finite fragments obtained in Ref. 7 are valid for any L. It should be noted that a similar approach was used by Kohno[6] for confirming the ferromagnetic nature of the ground state of a rectangular lattice of the ladder type in the limit of weak interaction of segments for $\rho>0.5$. Since the conditions of the Perron–Frobenius theorem are satisfied in the subspace with any value of S^z, we can easily prove that all the lowermost energy levels $E_0(S)$ of Hamiltonian (5) correspond to the total lattice spin S satisfy the inequality

$$E_0(S_{\min})>E_0(S_{\min}+1)>\ldots>E_0(S_{\max}-1)>E_0(S_{\max}),$$

$$S_{\max}=\frac{L+1}{2}.$$

Consequently, the first excited state (5) for $\mu>0$ is of the one-magnon type.

3. ONE-MAGNON SPECTRUM OF AN INFINITE TRIANGULAR LATTICE OF THE STRIP TYPE

In order to gain information on the stability of the ferromagnetic state of Hamiltonian (5) for negative values of μ, we consider the case $N=L+1$ in the limit of weak interaction between segments, when we can confine an analysis of the total Hamiltonian (5) to only the terms of the first order in t_2 and t_3. In this case, one-magnon states of (5) for $L\to\infty$ can be described by the system of finite-difference equations

$$-\lambda a(m,n)=(2+\mu)[a(m-1,n)+a(m+1,n)], \quad n\neq m,\ m\pm1,\ m+2; \tag{6}$$

$$-\lambda a(m,m)=a(m-1,m-1)+a(m+1,m+1)+a(m-1,m+1)+\mu a(m-1,m)+(1+\mu)a(m+1,m); \tag{7}$$

$$-\lambda a(m,m+1)=a(m-1,m)+a(m+1,m+2)+a(m+1,m)+\mu a(m+1,m+1)+(1+\mu)a(m-1,m+1); \tag{8}$$

$$-\lambda a(m,m-1)=a(m-1,m)+(1+\mu)a(m-1,m-1)+(2+\mu)a(m+1,m-1); \tag{9}$$

$$-\lambda a(m,m+2)=a(m+1,m+1)+(1+\mu)a(m+1,m+2)+(2+\mu)a(m-1,m+2). \tag{10}$$

Here the first argument in $a(m,n)$ corresponds to the number of the segment with double filling, while the second argument corresponds to the number of inverted spin, λ being the energy of the one-magnon state in units of $t_2/2$.

The solution of such a system can be sought in the form

$$a(m,n)=\exp\left(\frac{ik(m+n)}{2}\right)f(n-m), \quad 0\leqslant k<2\pi, \tag{11}$$

where

$$f(l)=\begin{cases}\exp\left(\dfrac{ikl}{2}\right)(A_j x^l+B_j x^{-l}),\ j=1,\ l\geqslant 2;\ j=2,\ l\leqslant -1;\\ f_0,\ l=0;\\ f_1,\ l=1,\end{cases}$$

considering Eqs. (7)–(10) as boundary conditions to Eq. (6). Since x and $1/x$ are simultaneously solutions of the equation

$$\lambda=-(2+\mu)\left(x+\frac{1}{x}\right), \tag{12}$$

connecting the energy λ with the parameter x, this parameter can be either complex-valued with unit modulus, or real-valued. For definiteness, we can assume that real-valued x are modulo smaller than unity. If $|x|=1$ and $x=\exp(ip)$, six coefficients of the wave function (11) are connected by four boundary equations (7)–(10). Such a solution corresponds to the energy band

$$\lambda=-2(2+\mu)\cos p,\quad -\pi<p\leqslant\pi \tag{13}$$

with a ''scattering'' of a magnon by a fragment with double filling. If x is real-valued, we must put $A_1=B_2=0$ in order to ensure a decrease in the wave function (11) for $l\to\pm\infty$. This solution corresponds to bound states. It follows from the boundary equations (7)–(10) that

$$4(1+\mu)x^3\cos k+[\mu^2-4(1+\mu)-4\cos^2 k]x^2$$
$$+4(2+\mu)x\cos k-(2+\mu)^2=0. \tag{14}$$

The ferromagnetic state with the minimum energy equal to $-2(2+\mu)$ is unstable if a one-magnon bound state is formed with an energy $\lambda<-2(2+\mu)$, i.e., Eq. (14) has a solution in the interval $-1<x<0$. It can easily be seen that such a solution of Eq. (14) exists for

$$\mu<-0.5\cos k-1. \tag{15}$$

Thus, the ferromagnetic state is stable for $\mu>-0.5$ since a local energy level cannot exist below the continuous spectrum band.

4. ENERGY SPECTRUM OF A LATTICE WITH CYCLIC BOUNDARY CONDITIONS

Let us consider a lattice in the form of a strip closed as a loop. The Hamiltonian of such a lattice commutes with the operator of a displacement by a unit cell (two-center segment). For this reason, the basis functions on which the Hamiltonian matrix is constructed can be put in correspondence with various irreducible representations of the Abelian group C_L. In such a symmetry-reduced representation, this matrix has a block-diagonal form, which simplified the calculation of its spectrum significantly. In the corresponding reduced form of the Hamiltonian, operators of cyclic permutations of spin variables of all N electrons appear in a natural way.[11,12]

The symmetry reduction for the matrix of the Hamiltonian of an anisotropic triangular lattice can be carried out in the simplest way for $N=L+1$. Without going into details of simple but cumbersome operations with cyclic permutations, which are similar to those considered in Ref. 11 for the Emery model, we can prove that the Hamiltonian of a triangular lattice for $N=L+1$ can be written in the pure spin form:

$$H=\frac{t_2^2}{4|t_1|}\sum_{i=3}^{N}[2(1-\mu)P_{ii+1}-(1-\mu)^2-1]$$
$$+\frac{t_2}{2}\{[P_{12}+P_{1N+1}+\mu I]Q\exp(ik)+\text{h.c.}\},$$
$$k=\frac{2\pi}{L}\nu,\quad \nu=0,1,...,L-1. \tag{16}$$

Here Q is the operator of cyclic permutation of all N spin variables of the lattice and I the unit operator. Various values of k parametrize irreducible representations of the C_L group, and hence describe various types of symmetry of eigenfunctions of the lattice Hamiltonian. It can easily be seen that spectrum (16) for even L does not depend on the sign of t_2. Besides, eigenvalues of (16) do not change as a result of the substitution $\nu\to L-\nu$.

Let us consider the limiting case of weak interaction of segments. In the units of $t_2/2$, the lattice Hamiltonian has the simple form

$$H=(P_{12}+P_{1N+1}+\mu I)Q\exp(ik)+\text{h.c.} \tag{17}$$

The ground-state energy E_0 of this Hamiltonian satisfies the obvious inequality $E_0\geqslant -2\Lambda$, where Λ is the spectral radius of the matrix $(P_{12}+P_{1N+1}+\mu I)$. It will be proved in Ref. 7 that $\Lambda=2+\mu$ for $\mu>-0.5$. On the other hand, the energy of the lower ferromagnetic state of Hamiltonian (17) is equal to $-2(2+\mu)$. Consequently, at least one of states with energy E_0 will be ferromagnetic for $\mu>-0.5$ (the ground state of the lattice can be degenerate).

In order to improve the estimate of the critical value of the parameter μ below which ferromagnetic ordering is violated, we consider the one-magnon spectrum of Hamiltonian (17). In the space of spin configurations (eigenfunctions of the z-component of the total spin of the lattice), one-magnon states are described by the following system of equations:

$$\lambda a_m=(2+\mu)[\exp(ik)a_{m-1}+\exp(-ik)a_{m+1}],$$
$$m=4,...,L,$$
$$\lambda a_3=(2+\mu)\exp(-ik)a_4+[a_1+(1+\mu)a_2]\exp(ik),$$
$$\lambda a_{L+1}=(2+\mu)\exp(ik)a_L+[(1+\mu)a_1+a_2]$$
$$\times\exp(-ik),$$
$$(\lambda-2\cos k)a_1=(\mu a_2+a_3)\exp(-ik)+(1+\mu)$$
$$\times a_{L+1}\exp(ik),$$
$$(\lambda-2\cos k)a_2=(\mu a_1+a_{L+1})\exp(ik)+(1+\mu)a_3$$
$$\times\exp(-ik). \tag{18}$$

In analogy with the linear case, the solution of system (18) will be sought in the form

$$a_m=\exp(ikm)(Ax^m+Bx^{-m}),\quad m=3,...,N. \tag{19}$$

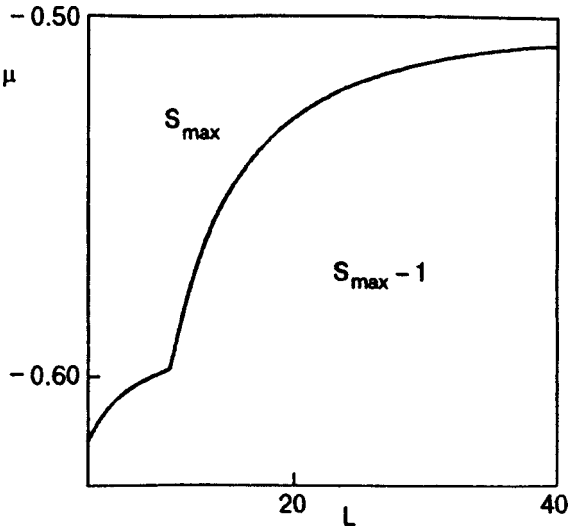

FIG. 2. Dependence of the critical value of parameter μ for which the ferromagnetic state of the strip becomes unstable to the rotation of a single spin on the number of segments L.

After a number of simple but cumbersome calculations similar to those presented above for the linear problem, we obtain the following system of equations for determining the energy λ:

$$\lambda=(2+\mu)(x+1/x);$$

$$(2+\mu)[(\lambda-2\cos k)^2-\mu^2](1-x^{2L})=\mu^2(2+\mu)x^2(1-x^{2(L-2)})+\mu^2[\lambda-(2+\mu)\cos k]x(1+x^L)\times(1-x^{L-2})+(2+\mu)^2[\lambda-(2-\mu)\cos k]x(1+x^{L-2})(1-x^L). \quad (20)$$

This system of equations has the solution $x=\exp(ik)$ with the energy $\lambda=2(2+\mu)\cos k$ for any k from (16). Owing to the scalar form of Hamiltonian (17), the complete set of one-magnon states necessarily includes the states with the maximum total spin $S_{\max}$ and $S^z=S_{\max}-1$. It is such states that are responsible to the solution $x=\exp(ik)$. Consequently, in order to analyze the stability of the ground ferromagnetic state, we must eliminate from (20) the trivial solution $x=-1$ existing for any values of parameters μ.

It can be proved with the help of simple but cumbersome calculations that the lower one-magnon state for a given k has an energy equal to $-2(2+\mu)$ if

$$\mu_c^{(1)}=-2L\left(1-\left(1-\frac{2+\cos k}{2L}\right)^{1/2}\right), \quad k\neq\pi, \quad (21)$$

$$\mu_c^{(2)}=-\frac{2L-\sqrt{2L(L-1)}}{L+1}, \quad k=\pi. \quad (22)$$

The stability boundary of the ferromagnetic state (17) can be determined by considering only the critical states of the parameter μ with the minimum magnitude. It can be proved that this state corresponds to $\mu_c^{(2)}$ for $L<12$. For $L\geqslant 12$, we must use formula (21) for $k=[(L\pm 2)\pi]/L$ (Fig. 2). Thus, one-magnon states with different symmetries intersect in the neighborhood of the point $L=10$. For $L\to\infty$, $\mu_c^{(1)}=-0.5$, which coincides with the estimate for an infinite strip.

TABLE I. Lower energy levels of Hamiltonian (17) for a lattice of ten segments; $m=(N-2S)/2$, $k=(2\pi/L)\nu$.

m	$\mu=-0.500000$	ν	$\mu=-0.520344$	ν	$\mu=-0.598508$	ν
0	−3.00000	5	−2.95931	5	−2.80298	5
1	−2.97206	4	−2.93451	4	−2.80298	5
2	−2.94499	3	−2.91186	3	−2.90250	0
3	−2.91859	2	−2.89168	2	−2.99317	4
4	−2.91279	4	−2.93280	4	−3.02447	4
5	−2.94063	4	−2.95931	4	−3.04500	4

In order to obtain an estimate of the parameter μ corresponding to the boundary of the stability region of the ferromagnetic state of the lattice, it is necessary that its states with several inverted spins lie above the one-magnon states. Unfortunately, we could not obtain analytic formulas for multimagnon energy levels. For this reason, we confined our analysis to numerical simulation of the exact spectrum (17) for finite L. Most typical results of calculations are given in Table I for $L=10$. It can easily be seen that all lower energy levels with the total spin $S<S_{\max}-1$ for the critical value of μ determined from (22) lie below the ferromagnetic state. Consequently, local stability of the ferromagnetic state to the rotation of a single spin does not coincide with global stability. For a lattice with ten segments, the violation of the ferromagnetic state begins at $\mu=0.5203$ through a jumpwise decrease in the total spin to the minimum value without passing through intermediate values (see Table I). Thus, both states with the marginal spin are locally stable in the vicinity of the transition point. It should be noted that a similar transition between the minimum and maximum values of the total spin was observed in the case of weak anisotropy for triangular strip-type lattices for positive μ[7] as well as for the Heisenberg spin model with competing interactions.[13,14]

Formulas (21) and (22) can serve as the lower boundary for the critical value of the parameter μ for which ferromagnetic ordering is violated. On the other hand, the upper boundary of this parameter is equal to -0.5 (see the beginning of this section). Consequently, according to (21), the lower boundary coincides with the upper boundary for $L\to\infty$.

CONCLUSION

The exact spectrum of the Hubbard model with infinite repulsion on an anisotropic triangular strip-type lattice formed by L weakly interacting linear segments has been studied. It is shown that the ground state of the lattice in the limit of weak interaction of segments for positive values of the parameter $\mu=(t_1t_3)/(|t_1|t_2)$ is ferromagnetic for any L. A detailed analysis of the one-magnon spectrum is carried out for the case of lattices with the number of electrons larger by unity than the number of segments. The dependence of the critical value of the parameter μ for which the one-magnon spectrum becomes degenerate on the number of segments L is obtained. It is shown that this dependence for negative μ has a singular point for $L\simeq 10$, at which levels

with different symmetries intersect. The obtained dependence can be used for estimating the stability of the ferromagnetic state of an anisotropic strip-type triangular lattice. Numerical calculations of the exact spectrum of finite fragments with cyclic boundary conditions in the first order of the perturbation theory in interaction between segments are used to demonstrate that the ferromagnetic ordering is violated upon a decrease in the parameter μ through a jumpwise decrease in the ground-state spin to the minimum value bypassing intermediate values.

The authors are grateful to A. A. Zvyagin for fruitful discussions of the results.

*E-mail: cher@spin.univer.kharkov.ua

[1] E. H. Lieb, NATO ASI Ser., Ser. B **343**, 1 (1995).
[2] Yu. A. Izyumov and Yu. N. Skryabin, *Statistical Mechanics of Magnetically Ordered Systems* [in Russian], Nauka, Moscow (1987).
[3] Y. Nagaoka, Phys. Rev. **147**, 392 (1966).
[4] D. J. Thouless, Proc. Phys. Soc. London **86**, 893 (1965).
[5] V. Ya. Krivnov, A. A. Ovchinnikov, and V. O. Cheranovskii, Synth. Met. **33**, 65 (1989).
[6] M. Kohno, Phys. Rev. B **56**, 15015 (1997).
[7] V. O. Cheranovskii, O. Esenturk, and H. O. Pamuk, Phys. Rev. B **58**, 12260 (1998).
[8] E. Dagotto, J. Riera, and D. Scalapino, Phys. Rev. B **45**, 5744 (1992).
[9] A. L. Tchougreeff and I. A. Misurkin, Phys. Rev. B **46**, 5357 (1992).
[10] V. O. Cheranovskii and E. V. Ezerskaya, Phys. Rev. B **55**, 12480 (1997).
[11] V. Ya. Krivnov and V. O. Cheranovskii, Fiz. Tverd. Tela (St. Petersburg) **34**, 3101 (1992) [Sov. Phys. Solid State **34**, 1659 (1992)].
[12] E. V. Ezerskaya and V. O. Cheranovskii, Fiz. Nizk. Temp. **18**, 872 (1992) [Sov. J. Low Temp. Phys. **18**, 614 (1992)].
[13] D. V. Dmitriev, V. Ya. Krivnov, and A. A. Ovchinnikov, Phys. Lett. A **207**, 385 (1995).
[14] D. V. Dmitriev, V. Ya. Krivnov, and A. A. Ovchinnikov, Phys. Rev. B **55**, 3620 (1997).

Translated by R. S. Wadhwa

LATTICE DYNAMICS

Low-temperature lattice instability in SnTe

O. N. Nashchekina, E. I. Rogacheva, and A. I. Fedorenko

Kharkov State Polytechnical University, 310002 Kharkov, Ukraine)*

A. P. Isakina and A. I. Prokhvatilov

B. Verkin Institute for Low Temperature Physics and Engineering, National Academy of Sciences of the Ukraine, 310164 Kharkov, Ukraine

(Submitted July 3, 1998; revised December 3, 1998)
Fiz. Nizk. Temp. **25**, 390–395 (April 1999)

The temperature dependences of the unit cell parameter $a(T)$ of tin telluride with different extents of deviation from stoichiometry are obtained during heating from 80 to 290 K. The $a(T)$ dependence for a sample with the stoichiometric composition (50 at.%Te) displays an anomaly in the temperature range 90–100 K, which is attributed to the well-known ferroelectric phase transition (PT). Well-pronounced jumps in the unit cell parameter ($\Delta a/a \approx 0.015$) observed for 50.4 at.%Te in the intervals 135– 150 K and 200-215 K correspond to a negative thermal expansion coefficient. Upon a further increase in the deviation from stoichiometry (50.8 at.%Te) these effects become less pronounced. The instability in the crystal lattice in certain temperature intervals is attributed to phase transitions in the subsystem of intrinsic defects (nonstoichiometric vacancies) associated with their redistribution over the cation sublattice upon a change in the temperature and composition. The role of relaxation phenomena in the rearrangement of crystal defect subsystem is determined.
[S1063-777X(99)00904-4]

INTRODUCTION

Considerable deviation from stoichiometry in the semiconducting compound SnTe with a broad homogeneity region ($\approx$1 at.%) on the side of excess tellurium determines a high concentration of intrinsic defects (mainly cation vacancies) and *p*-type charge carriers ($p_{77}=10^{20}-10^{21}\,\mathrm{cm}^{-3}$) in this compound.[1–3] Within the homogeneity region of SnTe, the unit cell parameter *a* decreases linearly with increasing Te concentration.[1–3] It is well known that SnTe undergoes a ferroelectric phase transition (FPT) of the displacement type from a cubic structure of the NaCl type to the rhombohedral $A7$-structure at a temperature T_c close to 100 K.[4–6] It was found that the value of T_c decreases upon an increase in the charge carrier concentration, and FPT is not observed for $p_{77}=(7-10)\cdot 10^{20}\,\mathrm{cm}^{-3}$.[7–11] Some authors[12–14] report a much higher value of T_c (160 K,[12] and 140–145 K[13,14]) and presume the existence of at least two phase transitions (PT) in SnTe.[8,12,13] The possibility of two consecutive (in temperature) structural PT in SnTe from the cubic to the rhombohedral phase and from the rhombohedral to the rhombic phase is considered.[12] Structural instability of SnTe as well as other semiconductors belonging to IV–VI groups is usually attributed to the softening of the transverse optical mode with zero momentum as a result of the interband electron–phonon interaction.[15,16] It is assumed that the interaction of electrons from two adjacent (filled and empty) bands with one of optical vibrations results in band ''mixing'' leading to anharmonism and instability of the optical vibration being ''mixed,'' and hence to a PT. The existence of two interacting normal phonon modes experiencing softening and determining the existence of several PT is possible in compounds of this type.[17] It is proposed that not only the electron subsystem, but also intrinsic crystal lattice defects play a certain role in the mechanism of structural transformations during PT. Khandozhko *et al.*[18] discovered steps at $T_n=376/n$ (where $n=1-6$) on the temperature dependences of resonant fields of ^{119}Sn nuclei in NMR experiments. These anomalies cannot be described by the model of softening of the phonon spectrum as a result of the electron–phonon interaction. The authors of Ref. 18 suggested that the observed effects are associated with the movement of crystal lattice defects affecting the local distribution of electron density upon a change in temperature. This is confirmed by the long-term instability and hysteresis phenomena observed in experiments. However, the physical nature of high- temperature transitions observed in Ref. 18 is not clear. Balagurova *et al.*[19] pointed out a large number of temperature anomalies in compounds of IV–VI groups as well as in other narrow-band materials, attributing these anomalies to nonstoichiometry, peculiarities of band structure, and other factors.

On the one hand, an increase in the deviation from stoichiometry leads to a decrease in T_c or disappearance of FPT, while on the other hand an increase in the concentration of nonstoichiometry defects (charged cation vacancies) inevitably leads to the interaction between the defects (Coulomb, deformation-induced, etc. interaction). As a result, the

probability of the rearrangement of the defect subsystem leading to the decomposition of the homogeneous phase into a mixture of phases with different stoichiometries or to the emergence of ordering in defect arrangement increases at quite low temperatures with the deviation from the stoichiometric composition. A short-range order is possible when ordered regions (clusters) with a composition slightly differing from the average composition of the crystal are formed. A regular distribution of defects can spread over the entire crystal (long-range order), leading to the formation of a superstructure existing in a certain interval of temperatures and concentrations. Finally, the excess of point defects can be eliminated due to partial lattice rearrangement as a result of crystallographic shift for a considerable concentration of nonstoichiometric defects.[20] What has been said above indicates the possibility of phase transitions in SnTe due to redistribution of nonstoichiometric defects.

This research aims at an analysis of temperature dependences of the unit cell parameter of SnTe with different extent of deviation from stoichiometry.

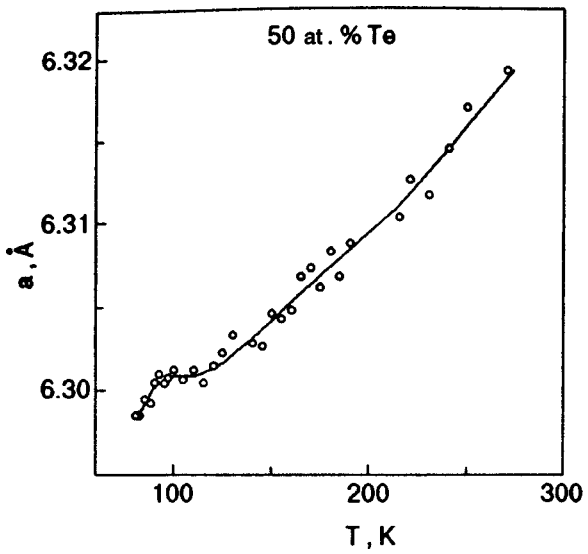

FIG. 1. Temperature dependence of the lattice parameter a of SnTe with the stoichiometric composition (50 at.%Te).

MATERIALS AND METHODS OF INVESTIGATION

The composition of the samples under investigation corresponded to Te concentrations of 50, 50.4, and 50.8 at.%, which corresponds to hole concentrations $p_{77}=1.7\times10^{20}$, 8×10^{20}, and $1.5\times10^{21}\,\mathrm{cm}^{-3}$ (samples 1, 2, and 3 respectively). The samples were synthesized in quartz ampules evacuated to 10^{-2} Pa at 1200 K for 5–6 h under vibrational mixing of the melt. Homogenizing annealing was then carried out for 200 h at $T=820$ K, followed by cooling with the switched-off furnace (at a rate ~1 K/min). After such a thermal treatment, the homogeneity range for SnTe lies between 50.1 and 50.8 at.%Te.[2,3]The unit cell parameter a was measured in the temperature range 80–290 K on the x-ray diffractometer DRON-3M equipped with a special helium cryostat. The original ingots comprising large-size crystals were crushed into powder and annealed in vacuum at 500 K for 2 h. During the recording of x-ray diffraction patterns, the temperature of the samples was stabilized at each point to within ±0.05 K. The error in determining a did not exceed 0.02%. The values of a obtained at room temperature for samples 1–3 correspond to the available data.[2,3]

EXPERIMENTAL RESULTS

Figures 1 and 2 show the temperature dependences of the lattice parameter a for samples 1–3. Sample 1 displays an anomaly in the temperature range 90–100 K, that can be naturally attributed to the known FPT. The estimate of the variation of the thermal expansion coefficient (TEC) in this temperature range by using the graphic differentiation method shows that the inflection on the $a(T)$ curve corresponds to an λ-type anomaly on the temperature dependence of the TEC typical of the second- order PT. This is in accord with the results obtained in Ref. 25, where the TEC was determined dilatometrically.

The $a(T)$ dependence for sample 2 displays two clearly manifested anomalous regions in the temperature intervals 135–150 K and 200–215 K, in which the value of a decreases upon heating, which corresponds to a negative thermal expansion coefficient. The jumps in the value of a in these regions are significant, amounting to ~0.01 Å, i.e., $\sim1.5\%$ in both cases. It should also be noted that the value of a for sample 2 at 80 K virtually coincides with the value of a for sample 1 with the stoichiometric composition and even exceeds this value in the region of anomalies. The values of $a(T)$ for sample 1 at $T>215$ K (Fig. 1) are higher than for sample 2 (Fig. 2), which corresponds to the normally observed variation of a within the homogeneity region for SnTe at room temperature.[1–3]

For sample 3, the anomaly in the temperature range 135–150 K is less pronounced, and instead of a clearly

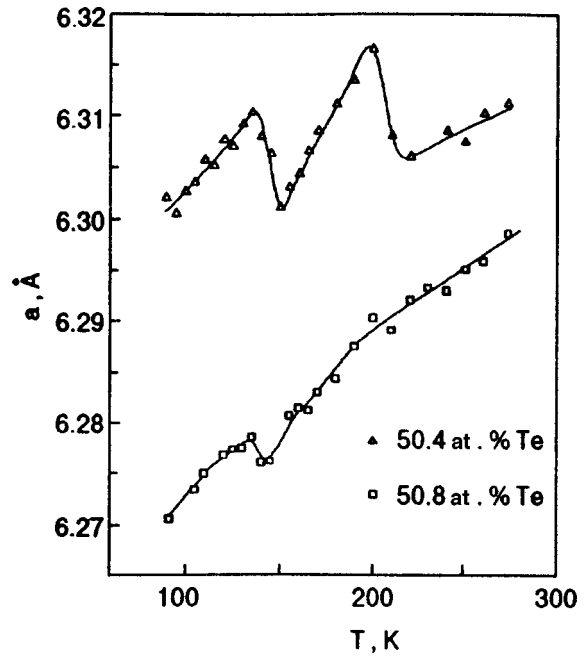

FIG. 2. Lattice parameter a of SnTe with the nonstoichiometric composition (50.4 and 50.8 at.%Te as a function of temperature.

manifested anomaly at 200 K, we observe a bend beyond which the rate of variation of a with temperature becomes constant.

Thus, lattice instability effects accompanied with a transition of the TEC to the range of negative values are manifested most clearly in sample 2.

DISCUSSION OF RESULTS

The presence of pronounced anomalies on the $a(T)$ curve for sample 2 indicates the instability of the crystal lattice in certain temperature intervals. Taking into account the high concentration of intrinsic defects in this sample ($\sim$1.6% of vacancies in the cation sublattice), it is natural to assume that the emergence of new PT in SnTe upon an increase in the extent of deviation from stoichiometry can be due to a change in the conditions of thermodynamic equilibrium and the type of polymorphism in the presence of vacancies as well as due to redistribution of intrinsic defects as a result of their interaction. Naturally, both these factors are interrelated, and the influence of defects on the electron spectrum and dynamics of the crystal lattice might be most significant just as a result of a redistribution of defects with the formation of configurations corresponding to the free energy minimum. Moreover, the formation of such configurations may become a necessary condition for the emergence of new PT. The time of realization of a PT depends on temperature as well as on the mechanism of PT (diffusion, martensite, electronic, etc.).

It is well known at present that in the case of strongly nonstoichiometric phases, broad homogeneity regions often split into a number of ordered phases with a more restricted nonstoichiometry.[20] Due to a considerable contribution of the ionic component of the chemical bond in IV–VI group compounds and electrical activity of nonstoichiometric defects, an ordered arrangement of the latter is stimulated by a noticeable energy gain.[21] The probabilities of the formation of commensurate superstructures with periods multiple to the period of the initial lattice and of the emergence of a set of discrete structural states are quite high.[22] A microdomain state can be formed, in which a crystal contains regions of various compositions with different types of ordering.[23] This can be a reason behind a large number of temperature anomalies observed in group IV–VI compounds and solid solutions on their basis.

It should be noted that the composition of sample 2 (50.4 at.%Te) corresponds to the peak on the liquidus and solidus curves of the Sn–Te system, which is displaced relative to the stoichiometric composition.[1–3] Besides, estimates of the optimal compositions of ordering in the homogeneity regions of SnTe[2,3] show that the composition with 50.4 at.%Te corresponds to the formation of a fcc lattice of vacancies with the parameter $a=4a_0$, where a_0 is the unit cell parameter of SnTe. The fact that this composition corresponds to the peak on melting curves and the presence of singular points on the concentration dependences of some parameters[2,3,24,25] indicate that such a possibility can be realized. Thus, the anomalies observed on the $a(T)$ curve for sample 2 can probably be a consequence of redistribution of nonstoichiometric defects up to the formation of a superstructure of vacancies.

The redistribution of defects resulting in the formation of ordered configurations is usually associated with migration of atoms and follows the diffusion mechanism. The rate of diffusion in normal crystals at temperatures from 80 to 300 K is low, and such transition must be hampered. It should be noted, however, that if diffusion occurs according to the vacancion mechanism (which is most probable in the given case), the self-diffusion coefficient D and the vacancy diffusion coefficient D_i are connected through the relation $D=fAD_i$, where f is the correlation factor and A the relative fraction of vacancies.[26,27] It follows hence that an increase in the vacancy concentration leads to an increase in the self-diffusion rate. Such a sharp increase in the diffusion coefficient upon the introduction of structural vacancies associated with deviations from stoichiometry is confirmed experimentally.[27] Since the concentration of structural vacancies in SnTe crystals (2–3%) at low temperatures is much higher than the concentration of thermal vacancies ensuring the vacancion mechanism of diffusion in most crystals (10^{-14}–10^{-18}% at 300 K if we assume that the energy of vacancy formation is $E_v=1-1.5$ eV), we can expect that the diffusion rate in SnTe is much higher than in stoichiometric crystals. The presence of nonequilibrium point defects of various types formed as a result of rapid cooling also stimulates the increase in the rate of diffusion processes.[26] In order to estimate the time required to complete diffusion in SnTe samples at low temperatures, we must know the activation energy of vacancy diffusion or activation energy of self-diffusion as well as their dependence on the vacancy concentration. To our knowledge, no information has been obtained in this field.

It should also be borne in mind that the samples under investigation were subjected to a prolonged (200 h) homogenizing annealing at 820 K, resulting in a high degree of crystal homogeneity and a quite uniform distribution of vacancies over the volume. Under such conditions, displacements of atoms by small distances are sufficient for the formation of a long-range order, which facilitates the formation of a superstructure of vacancies at low temperatures.

On the other hand, the possibility of defect ordering at temperatures above 300 K, when the diffusion rate is still significant, and the PT observed at 80–300 K are nondiffusive should not be ruled out.

The observed anomalies are characterized by a considerable variation of the unit cell parameter for the same symmetry (the NaCl-type structure is preserved) and by the negative sign of the TEC. This suggests that such a strong manifestation of PT is determined not only by thermodynamic, but also by kinetic factors. It was mentioned above that the $a(T)$ curves were recorded during heating of the samples cooled preliminarily to 80 K at a rate of $\sim$20 K/min. It can be assumed in this connection that a certain nonequilibrium state with a parameter a higher than in the equilibrium state sets in in sample 2 as a result of an abrupt decrease in its temperature from room to liquid nitrogen temperature and incompleteness of diffusion processes whose rate is extremely small at such low temperatures.

A considerable rate in the increase in a for sample 2 in the temperature range 80–135 K indicates a higher value of the TEC than near the room temperature, indicating a lower thermal stability of the alloy. The latter effect is apparently due to a high degree of disordering determining the high concentration of defects. The heating of such a nonequilibrium system increases the diffusion rate and must lead to complex processes associated with equilibrium phase transformations (if these occur) on one hand and the relaxation of the system to the equilibrium state on the other hand. As a result, the manifestation of equilibrium PT accompanied by relaxation processes can become anomalous. Such a situation is probably observed in sample 2: excess defects are ''cast away,'' the defect system is rearranged, and the value of a decreases in the temperature intervals corresponding to equilibrium PT (135–150 K and 200–215 K). Finally, starting from ~215 K, the unit cell parameter corresponds to the equilibrium value. on the other hand, the rearrangement of the defect subsystem at 135–150 K and 200–215 K can be a purely relaxation process corresponding to nonequilibrium PT: the system returns to its equilibrium state via a number of intermediate states corresponding to metastable equilibrium at each temperature.

The following question arises in this connection: why are the jumps in the lattice parameter manifested most clearly for the composition with 50.4 at.%Te rather than for the composition with 50.8 at.%Te. A possible reason behind this effect can be determined by kinetic factors. As a matter of fact, sample 3 contains twice as many nonstoichiometric vacancies in the cation sublattice (3.2 at.%) as in sample 2 (1.6 at.%). For this reason, the diffusion rate in sample 3 can be much higher than in sample 2, and the structure formed in sample 3 after rapid cooling is less disordered. In other words, the structure formed in the samples with a higher vacancy concentration for identical conditions of preparation and thermal processing is closer to the equilibrium state at a given temperature. It is probably for this reason that the values of a for sample 3 virtually coincide with equilibrium values, and the jumps in a upon an increase in temperature are much smaller.

Thus, the concentration of vacancies in sample 2 is high enough to stimulate the processes of their redistribution. However, this concentration is insufficient for the completion of diffusion processes in the case of rapid cooling, and the structure formed is far from equilibrium. The sample returns to equilibrium through a number of intermediate states.

Thus, structural instability of samples 2 and 3 in certain temperature intervals can be due to the following factors.

(1) The presence of equilibrium PT associated with a redistribution of nonstoichiometric defects. The sharp change in the unit cell parameter accompanying these PT during sample heating is apparently due to the nonequilibrium nature of the initial structure obtained as a result of rapid cooling from room temperature. The diffusion rate increases as a result of heating, and the system abruptly goes over to the equilibrium state corresponding to a given temperature at the point where an equilibrium PT (e.g., vacancy ordering) must take place. These processes lead to giant instability of the lattice, resembling the crystallization of a supercooled liquid or the heating of the amorphous phase capable of crystallization. It should be noted that Fukui et al.[28] obtained amorphous SnTe films during condensation on substrates at $T=4.2$ and 77 K. The resistivity of such films drops jumpwise upon heating at 180 K, i.e., at a temperature close to the jump in the unit cell parameter on the $a(T)$ curve (see Fig. 2).

(2) The existence of intermediate metastable states through which the system passes on its way to the equilibrium state during heating.

It should be noted that the positions of two steps on the temperature dependence of the resonant field of ^{119}Sn nucleus[17] coincide with the positions of steps on the $a(T)$ curve obtained by us, which indicates that the PT was detected by two different methods and confirms their existence.

CONCLUSIONS

Tin telluride with various degrees of deviation from stoichiometry (50.0, 50.4, and 50.8 at.%Te) has been studied by using x-ray diffraction analysis during heating in the temperature range 80–290 K. The temperature dependence of the unit cell parameter for a sample of the stoichiometric composition displays an anomaly in the range 90–100 K, which is apparently associated with the known ferroelectric PT. Two phase transitions observed in samples of nonstoichiometric tin telluride in the temperature intervals 135–150 K and 200–215 K are pronounced most clearly for the sample with 50.4 at.% Te, in which they are accompanied by considerable (~1.5%) jumps in the unit cell parameter and a transition in the thermal expansion coefficient in the range of negative values. It is assumed that these PT are due to redistribution of nonstoichiometric vacancies over the cation sublattice and the formation of configurations corresponding to the free energy minimum at a given temperature. A considerable magnitude of effects accompanying a PT in the sample with 50.4 at.%Te and the negative sign of the TEC are apparently the results of action of kinetic factors, i.e., the nonequilibrium nature of the initial state as a result of rapid cooling to 80 K and relaxation processes occurring during heating. An increase in the concentration of cation vacancies leads to an increase in the rate of diffusion processes owing to which the effects occurring during phase transition are suppressed. The possibility of purely relaxation nature of the observed phase transitions cannot be ruled out when the system returning to the equilibrium state passes through a number of intermediate metastable states.

*)E-mail: nashon@kpi.kharkov.ua

[1] N. Kh. Abrikosov and L. E. Shelimova, *Semiconducting Materials Based on $A^{IV}B^{IV}$* [in Russian], Nauka, Moscow (1975).
[2] E. I. Rogacheva, G. V. Gorne, N. K. Zhigareva, and A. B. Ivanova, Izv. Akad. Nauk SSSR, Neorg. Mater. **27**, 267 (1991).
[3] E. I. Rogacheva, G. V. Gorne, and S. A. Laptev, Izv. Akad. Nauk SSSR, Neorg. Mater. **22**, 41 (1986).
[4] H. B. Littlewood, Lect. Notes Phys. **152**, 238 (1982).

[5] A. Bussmann-Holder, H. Bilz, and W. Kress, J. Phys. Soc. Jpn. **49**, Suppl. A, 737 (1980).
[6] T. Suski, Mater. Sci. **11**, 3 (1985).
[7] L. Muldawer, J. Nonmet. **1**, 117 (1973).
[8] L. J. Brillson, E. Burstein, and L. Muldawer, Phys. Rev. B **B9**, 1551 (1974).
[9] M. Iizumi, Y. Hamaguchi, K. F. Komatsubara, and Y. Kato, J. Phys. Soc. Jpn. **38**, 443 (1975).
[10] K. L. I. Kobayashi, Y. Kato, Y. Katayama, and K. F. Komatsubara, Phys. Rev. Lett. **37**, 772 (1976).
[11] S. Sugai, K. Murase, S. Katayama *et al.*, Solid State Commun. **24**, 407 (1977).
[12] V. Fano, G. Fedeli, and I. Ortalli, Solid State Commun. **22**, 467 (1977).
[13] Sh. Sh. Bashkirov, I. A. Dobryakov, A. B. Liberman, and S. S. Tsarevskii, Sov. Phys. Crystallogr. **30**, 1016 (1985).
[14] A. D. C. Grassie, J. B. Agapito, and P. Gonzalez, J. Phys. C **C12**, L925 (1979).
[15] P. I. Konsin, Fiz. Tverd. Tela (Leningrad) **18**, 701 (1976) [Sov. Phys. Solid State **18**, 404 (1976)].
[16] N. N. Kristoffel and P. Konsin, Ferroelectrics **6**, 3 (1973).
[17] Y. Lepine, Solid State Commun. **44**, 1269 (1982).
[18] A. G. Khandozhko, E. I. Slyn'ko, S. D. Letyuchenko, and K. D. Tovstyuk, Ukr. Fiz. Zh. **23**, 1747 (1978).
[19] E. A. Balagurova, Yu. B. Grekov, N. A. Semikolenova, and Yu. S. Kharitonovskii, in *Systems of Special Temperature Points in Solids* [in Russian], Nauka, Moscow (1986).
[20] R. Collongues, *La non-stoechiomètrie*, Masson, Paris (1971).
[21] J. Mycielski, Solid State Commun. **60**, 165 (1986).
[22] V. A. Golovko and A. P. Levanyuk, Fiz. Tverd. Tela (Leningrad) **23**, 3170 (1991) [Sov. Phys. Solid State **23**, 1844 (1981).
[23] S. M. Ariya and M. P. Morozova, Zh. Obshch. Khim. **28**, 2617 (1958).
[24] D. I. Baltrunas, S. V. Motiejunas, and E. I. Rogacheva, Phys. Status Solidi A **A97**, K131 (1986).
[25] E. I. Rogacheva, N. A. Sinelnik, and O. N. Nashchekina, Acta Phys. Pol. A **A84**, 733 (1993).
[26] B. S. Bokstein, S. Z. Bokstein, and A. A. Zhukhovitskii, *Thermodynamics and Kinetics of Diffusion in Solids* [in Russian], Metallurgiya, Moscow (1974).
[27] D. Show (Ed.), *Atomic Diffusion in Semiconductors*, Plenum Press, London–New York (1973).
[28] K. Fukui, K. Inoguchi, S. Kondo, and T. Tatsukawa, Jpn. J. Appl. Phys., Part 1 **23**, 1141 (1984).

Translated by R. S. Wadhwa

CHRONICLE

31st Conference on Low Temperature Physics, Moscow, December 2–3, 1998

V. G. Peschansky

*B. Verkin Institute for Low Temperature Physics and Engineering, National Academy of Sciences of the Ukraine, 310164 Kharkov, Ukraine**

(Submitted December 15, 1988)
Fiz. Nizk. Temp. 25, 396–399 (April 1999)

 [S1063-777X(99)01004-X]

The 31st Conference on Low Temperature Physics was held in Moscow on December 2–3, 1998. The conference was organized by the Scientific council of the Russian Academy of Sciences on the problem of ''Low Temperature Physics,'' P. L. Kapitza Institute for Physical Problems, Moscow, and M. V. Lomonosov State University, Moscow. It was a continuation of the regular All-Union conferences held previously in the USSR. The first two conferences were held in Kharkov even before the II World war, and the third conference was also held in Kharkov in 1954. In 1955, Academician Petr Leonidovich Kapitza became the head of the Scientific council on low temperature physics and a permanent chairman of All-Union conferences on cryogenics, which were held annually at various centers of low-temperature studies. In 1957, P. L. Kapitza invited two groups of physicists from Cambridge and Oxford headed by A. B. Pippard and K. Mendelson, who took an active part in the work of the conference. Ties with foreign cryogenic physicists became even closer after the International Conference on Low-Temperature Physics (LT-10) held in Moscow (1966) under the aegis of the International Union of Pure and Applied Physics (IUPAP, UNESCO). In 1969, the Soviet–Japanese Conference on Low-Temperature Physics was organized in Novosibirsk. Since 1970, All-Union conferences on low-temperature physics have been carried out biannually with regular participation of physicists from Comecon countries, thus acquiring the status of an international conference. The scope latest (31st) Conference also extended beyond the Russian regions since more than 30 reports were presented by Ukrainian science centers, and approximately 20% of papers contained results of joint studies with scientists from the USA, Canada, Japan, Great Britain, France, Germany, Denmark, Netherlands, Belgium, Sweden, Finland, Switzerland, Macedonia, and Poland.

The Organizing Committee headed by A. F. Andreev, Vice President of the Russian Academy of Sciences, included six 45-minutes long plenary papers and 128 reports at four sections of the conference, viz., quantum liquids and crystals (section G), fundamental problems in superconductivity (section S), low-temperature solid-state physics (section T), and electron phenomena at low temperatures (section E).

The plenary sessions were held in the mornings in the Conference Hall of the Institute of Physical Problems, while meetings in sections were conducted in the afternoons in various buildings of the MSU and Institute of Physical Problems. Plenary papers by A. F. Andreev, I. M. Suslov, V. L. Gurevich, V. F. Gantmakher, A. N. Vasil'ev, and N. A. Babushkina were devoted to current problems in the physics of condensed state at low temperatures.

In his report ''Mesoscopy and Fundamental Properties of Space,'' A. F. Andreev (Institute of Physical Problems, Russian Academy of Sciences, Moscow) paid attention to the important role of low-temperature physics in the development of modern concepts concerning fundamental properties of physical space. This is due to high accuracy of measurements at low temperatures and the possibility to attain quite low temperatures ~ 1 mK at which the energy difference between an excited and the ground state is much larger than temperature. Under such conditions, conventional degrees of freedom are ''frozen out,'' and the space is characterized only by additional degrees of freedom in the form of a nonrelativistic version of Grassman spinor coordinates. The contribution made by Andreev to this field is quite profound, and his report aroused a considerable interest. He proposed a correct description of mesoscopic superconductivity for which the invariance of the gauge transformations is violated as well as low-temperature experiments for studying the geometry of the superspace.

The report made by I. M. Suslov (Institute of Physical Problems, Russian Academy of Sciences, Moscow) was devoted to an analysis of the density of states in the vicinity of Anderson's transition in the $(4-\varepsilon)$-dimensional space. A consistent fluctuational analysis of the problem leads to the emergence of a singularity for the dimension $d=4$ of the space, which was eliminated by the author for $d<4$ with the help of ε- expansion used for the summation of diagrams and Lipatov's method for calculating long- range interaction approximations.

In the report made by V. L. Gurevich (''Photomagnetism of Metals and Generation of Electron Current by Illumination,'' V. L. Gurevich and R. Laino), the results of theoretical and experimental investigations of photomagnetic phenomena in normal metals were considered. Illumination induced a magnetic flux in a sample made of a nonmagnetic metal (Cu, Al, or Zn) of a special shape. At 4 K, it was equal

to approximately one flux quantum for an incident light intensity of $0.04\,W/cm^2$. The emergence of a surface current as a result of transfer of the momentum of light quanta to electrons or due to anisotropy in the probabilities of interband electron transitions was considered as a possible mechanism of the effect. The existence of the effect makes it possible to use optical spectroscopy at a high frequency of light for studying the relaxation mechanisms of charge carriers with an energy higher than the Fermi energy. In his report ''Quantum Superconductor–Insulator Transitions,'' V. F. Gantmakher presented the results of experimental investigations of magnetoresistance of amorphous In_2O_x films at low temperatures (down to 30 mK), which were carried out together with V. T. Dolgopolov, M. V. Golubkov, G. E. Tsyndynzhapov, and A. A. Shashkin at the Institute of Solid State Physics, Russian Academy of Sciences (Chernogolovka). A sharp increase in resistance was observed in samples with $x<3$ in magnetic fields B stronger than the critical field B_c; the resistance attained its maximum value and then decreased with increasing field. The transition to the insulator state observed at $B=B_c$ is apparently associated with localization of Cooper electron pairs, which is replaced by their delocalization in a strong magnetic field and a transition to the normal metallic state.

The report ''Charge Splitting and Spin Gap in NaV_2O_3 by A. N. Vasil'ev (Moscow State University) contained a brief review of experimental and theoretical investigations of a specific phase transition in this compound, during which the formation of charge density waves in the crystal is accompanied by the emergence of a gap in the magnetic excitation spectrum. Sodium divanadate is the first inorganic compound in which these two cooperative quantum effects are combined in such a peculiar form. Doubling of the crystal lattice period in NaV_2O_3 is accompanied by a redistribution of charge between vanadium ions. The degree of oxidation of the ions is four and five since nine electrons are distributed between two identical vanadium ions. As a result V^{4+} and V^{5+} ions form spin ''ladders'' in vanadium–oxygen layers. A long-range magnetic order cannot be established in the spin chain along the generatrix of such a ladder, and a decrease in temperature leads to a redistribution of the charge between vanadium ions, resulting in the formation of new zigzag chains of V^{4+} and V^{5+}. As a charge subsystem, these chains are charge density waves, while as a spin subsystem they are dimerized and display an energy gap.

The report by N. A. Babushkina (''Giant Isotopic Effect and Other Low-Temperature Phenomena in Rare-Earth Manganites,'' N. A. Babushkina, L. M. Belov, O. Yu. Gorbenko, A. R. Kaul. K. I. Kugel, and D. I. Khomskii) was devoted to experimental investigations of the influence of isotopic effect on the resistance of the $(La_{1-x}Pr_x)_{0.7}Ca_{0.3}MnO_3$ system close to structural instability. By varying the concentration of La and Pr in such compounds, different states from the ferromagnetic metal $La_{0.7}Ca_{0.3}MnO_3$ to the charge-ordered antiferromagnetic insulator $Pr_{0.7}Ca_{0.3}MnO_3$ can be realized. A noticeable distortion of crystal lattice takes place in this case. The electrical resistance of ceramics and thin films of this system in the temperature range 4.2–300 K was very sensitive to the replacement of ^{16}O by ^{18}O. The influence of a magnetic field on the metal–insulator transition temperature in these systems with varying composition was also analyzed. A theoretical interpretation of the observed phenomena was proposed by Khomskii (Gröningen University).

The results of investigation of various physical properties of manganites were considered in detail during meetings in sections (section T). In most of the reports presented to this section, low-temperature magnetism in various compounds including quasi-two-dimensional and quasi- one-dimensional magnets was discussed. Due attention was paid to phase transitions and structural features of fullerene crystals.

New data obtained in x-ray diffraction experiments on deformation of the RbC_{60} molecule and the known experimental results were analyzed in the report by V. L. Aksenov (Joint Institute for Nuclear Research, Dubna) on the basis of the symmetry theory of orientational phase transitions in fullerene crystals, which was developed by the author together with Yu. A. Ossipyan and V. S. Shakhmatov. New experiments were proposed for detecting and studying the predicted structural peculiarities, including those with Raman scattering involving polarization analysis. An analysis of experiments on infrared absorption and scattering of neutrons in uranium dioxide was carried out by Yu. G. Pashkevich (Physicotechnical Institute, National Academy of Sciences of the Ukraine, Donetsk) and A. V. Eremenko (B. Verkin Institute for Low temperature Physics and Engineering, National Academy of Sciences of the Ukraine, Kharkov).

The dynamics of nano- and microclusters adsorbed on the atomically clean surface of a crystal was considered in the report by I. A. Gospodarev, A. M. Kosevich, and S. B. Feodos'ev (B. Verkin Institute for Low temperature Physics and Engineering, National Academy of Sciences of the Ukraine, Kharkov).

L. A. Boyarskii (Institute of Inorganic Chemistry, Siberian Branch of the Russian Academy of Sciences, Novosibirsk) reported on the possibility of using the NMR technique in strong magnetic fields exceeding 1.5 T for studying fine effects associated with chemical and structural inequivalence of the positions of vanadium atoms in vanadium dioxide.

L. A. Fal'kovskii (Landau Institute of Theoretical Physics, Russian Academy of Sciences, Chernogolovka) indicated the possibility of ''cold'' destruction of metals with the help of short light pulses allowing electrons to acquire an energy exceeding the Fermi energy. The destruction occurs due to the deformation of the cold lattice as a result of direct electron– phonon interaction and requires much smaller energy expenditures than for the equilibrium melting of the crystal.

In section G, reports from the Moscow region and Kharkov were presented (approximately in equal proportions) as well as a report from the Physical Research Institute at the Rostov University. Main attention was paid to the properties of liquid and solid helium isotopes and their mixtures. E. Ya. Rudavskii and V. A. Maidanov (B. Verkin Institute for Low temperature Physics and Engineering, National Academy of Sciences of the Ukraine, Kharkov)

presented basically new results of experimental investigations of kinetics and nuclear magnetic relaxation of a quantum system in the form of solid or liquid inclusions of ^{3}He in the crystal matrix of ^{4}He. A. Ya. Parshin (Institute of Physical Problems, Russian Academy of Sciences, Moscow) reported on optical studies of equilibrium and kinetic properties of the faces of helium crystals at ultralow temperatures, carried out at the Institute of Physical Problems and Helsinki University of Technology. I. N. Adamenko (Kharkov State University) presented the results of fruitful cooperation of theoretical physicists from Kharkov and the experimental group headed by A. Wyatt (University of Exeter, UK), leading to the identification of a new effect, viz., generation of ''hot'' phonons by a cold phonon beam in superfluid helium. Experimental studies of spin dynamics in ^{3}He$-B$ were considered in the paper by V. V. Dmitriev, I. V. Kosarev, and D. V. Ponarin (Institute of Physical Problems, Russian Academy of Sciences, Moscow) devoted to the observation of fractional NMR harmonic and in the theoretical work by I. A. Fomin (Institute of Physical Problems, Russian Academy of Sciences, Moscow) ''Localized Precessing Spin Structures in ^{3}He$-B$.''

A magnetic field does not remove completely the degeneracy in spin rotation during pairing with spin in ^{3}He$-B$, and the magnetization can be directed either along the field, or against it. As a result, domains with a domain wall (DW) at which magnetization rotation takes place can be formed. Fomin proved that a precessing DW can exist along with a static DW. He found the solution of spin dynamics equation describing a precessing DW whose lifetime increases upon cooling, thus making its experimental observation quite possible.

The largest number of papers presented to the Conference belonged to the section of superconductivity, including two 30-minute reports by Yu. V. Kopaev (Institute of Physics, Russian Academy of Sciences, Moscow) and Y. G. Ponomarev (Moscow State University) and 37 reports lasting 15 minutes each. More than 30 reports contained the results of investigation of physical properties of high-T_c superconductors, and traditional problems of superconductivity were discussed only in a few communications.

A. M. Troyanovskii (Institute of High Pressure Physics, Russian Academy of Sciences, Troitsk) studied the vortex system in a layered type II superconductor $NbSe_2$ by using a scanning tunnel microscope. The vortex structure in $LuNi_2B_2C$ was investigated by L. Ya. Vinnikov and F. L. Barkov (Institute of Solid State Physics, Russian Academy of Sciences, Chernogolovka) and K. O. Cheon, P. C.

Canfield, and V. G. Kogan (Iowa State University, USA) by using the decoration technique. The emission of electromagnetic radiation induced by Sweahart waves was considered in the report by A. S. Malishevskii, V. P. Silin, and S. A. Uryupin (Institute of Physics, Russian Academy of Sciences, Moscow) in the case of a Josephson junction in a thin superconducting film whose thickness is much smaller than the London length. Peculiarities of the resistive state of superconducting nanostructures were considered in the report by K. Yu. Arutyunov, D. E. Presnov, S. V. Lotkhov, and A. B. Pavolotskii (Moscow State University) and D. Rinderer (University of Lausanne, Switzerland).

The reports devoted to high-temperature superconductivity contained interesting results that cannot be described in detail in a brief communication. A quite unexpected view on high-T_c superconductor of the $La_{1-x}Sr_xCuO_4$ type was proposed by V. V. Kopaev and Yu. V. Kopaev, who treated them as natural heterostructures in which $2D$ electron states of CuO_2 layers in a unit cell play the role of quantum wells, while $2D$ states of the reservoir behave as quantum barriers.

The quasi-two-dimensional nature of conductivity is manifested still more clearly in $Nd_{2-x}Ce_xCuO_4$ compounds in which anisotropy of electrical conductivity can attain values of the order of 10^{-4}. The results of systematic analysis of resistivity and Hall effect in $Nd_{2-x}Ce_xCuO_4$ monocrystalline films of thickness $\sim$5000 Å at low temperatures down to 0.2 K in magnetic fields up to 12 T were presented in the paper by A. N. Ignatenkov, V. N. Neverov, A. I. Ponomarev, L. D. Sabirzanova, G. I. Kharus, N. G. Shelushina, and T. B. Charikova (Institute of Metal Physics, Ural Branch if the Russian Academy of Sciences, Ekaterinburg), N. A. Babushkina (Russian Science Center ''Kurchatov Institute,'' Moscow) and G. A. Emel'chenko and A. A. Zhokhova (Institute of Solid State Physics, Russian Academy of Sciences, Chernogolovka).

A considerable part of papers presented to section E was devoted to investigation of various properties of low-dimensional structures at low temperatures, which were mainly carried out in Moscow region and in St. Petersburg. Considerable interest was aroused by the report ''Origin of Low-Temperature Anomalies in Oscillatory Parameters of Quasi-two-dimensional Organometals Based on BEDT-TTF Molecule'' delivered by S. V. Demishev (Institute of General Physics, Russian Academy of Sciences, Moscow) and V. V. Moshchalkov (K. U. Leuven, Belgium). The amplitude of quantum oscillations of magnetization and magnetoresistance begins to decrease with temperature at $T \leqslant 1$ in layered conductors $(BEDT\text{-}TTF)_2XHg(SCN)_4$, where X = (K, Tl), in fields stronger than 20 T. The authors were able to find a convincing explanation for these anomalies by associating them with the renormalization of the g-factor. S. V. Demichev also emphasized the unusual behavior of high-frequency characteristics of this complex with charge transfer: the observed cyclotron resonance frequencies were found to be weakly sensitive to the magnetic field orientation relative to the layers.

In his report entitled ''Hybridization of Electron Subbands of a Double Quantum Well in a Quantizing Magnetic Field,'' V. T. Dolgopolov reported on quite subtle experimental and theoretical investigations of the electron energy spectrum of the compound $Al_xGa_{1-x}As$ by magnetocapacitive measurements and far-infrared spectroscopy. V. I. Okulov, E. A. Pamyatnykh, V. V. Slovikovskaya, and V. V. Ustinov (Institute of Metal Physics, Ural Branch of the Russian Academy of Sciences, Ural University, Ekaterinburg) pointed towards the possibility of gathering vital information about the electron states in Fe/Cr type superlattices with the help of ultrasonic measurements.

The Scientific council on the problem of ''Low Tem-

perature Physics'' met on December 2, 1998. Earlier, the Scientific council used to organize during the period between the cryogenic conferences a symposium on superconductivity and superfluidity in Bakuriani (Georgia), a seminar on nonlinear effects in condensed media in Novosibirsk, and a seminar on low- temperature metal physics in the town of Stary Karavan between Donetsk and Kharkov. International Schools on electronic effects at low temperatures were organized regularly for young scientists. However, in the four years that had elapsed since the 30th Low-Temperature Conference, the Scientific council was engaged only in preparation for the 31st Conference. Hence there was no need for chairmen of sections to present any reports. The participants reiterated their desire to continue the tradition, and the 32nd Conference will also be held probably in Moscow in the year 2000.

*)E-mail: vpeschansky@ilt.kharkov.ua

Translated by R. S. Wadhwa

Lev Samoilovich Palatnik (1909–1994): To his 90th Birth Anniversary

Fiz. Nizk. Temp. **25**, 400 (April 1999)
[S1063-777X(99)01104-4]

The 90th birth anniversary of Prof. Lev Samoilovich Palatnik, a leading physicist during his lifetime, falls on April 26, 1999.

Prof. Palatnik made a significant contribution to the physics of phase transitions, crystalline and amorphous materials, superconductivity and magnetism. He was the founder of the famous school on the physics of thin films and thin-film materials science. The fundamental studies carried out by Prof. Palatnik and his school received a logical continuation and culminated in the development of several new applied fields including research materials used in space science, radiation physics, electronic technology, space technology, and the development of first microstructures in the USSR.

Dr. Palatnik was a talented teacher and organizer of scientific activity. For many years, he was the head of the Department of metal and semiconductor physics, as well as the laboratory founded by him for studying the problems of microfilm technology. Together with Academician B. I. Verkin, he was responsible for founding and organizing the physics and engineering faculty at the Kharkov Polytechnical Institute, and for opening the new specialization ''Cryogenic technology.''

The polished manners and personal charm of Lev Samoilovich invariably attracted talented young scientists. About 350 Ph.D's and 40 D.Sc's passed out from the scientific school set up by Prof. Palatnik. His excellent monographs are being used by students, postgraduates and research workers specializing in the field of solid state physics. Prof.
Palatnik continued to participate actively in the research and teaching activity, preserved a sharp instinct for discerning new effects and the ability to detect prospective trends until his last days, inspiring his colleagues and pupils to new scientific achievements.

Editorial Board

